RÉPUBLIQUE ALGÉRIENNE DÉMOCRATIQUE ET POPULAIRE
MINISTÈRE DE L'ENSEIGNEMENT SUPÉRIEUR ET DE LA RECHERCHE SCIENTIFIQUE

ÉCOLE NATIONALE POLYTECHNIQUE

المدرسة الوطنية المتعددة التقنيات
Ecole Nationale Polytechnique

Département de Génie Civil

Final Year Project Thesis

In partial fulfillment of the requirements for the degree of State Engineer in Civil Engineering

---

Artificial neural networks for predicting the maximum surface settlement induced by EPB-TBM: The Algiers Metro Case

---

AYARI Ilies & DERBAL Yacine

Supervised by **Dr. SEBAI Souad**, ENP

Presented and publicly defended on (01/07/2025)

Jury Members:

President:	Prof. BOURZAM Abdelkrim	ENP
Examiner:	Prof. BOURAHLA Nouredine	ENP
Guest:	Miss. ZEGHMAR Racha	ENP

ENP 2025

Département de Génie Civil / ENP, 10 Rue des Frères OUDEK, El Harrach 16200 Alger, Algérie.

RÉPUBLIQUE ALGÉRIENNE DÉMOCRATIQUE ET POPULAIRE
MINISTÈRE DE L'ENSEIGNEMENT SUPÉRIEUR ET DE LA RECHERCHE SCIENTIFIQUE

ÉCOLE NATIONALE POLYTECHNIQUE

المدرسة الوطنية المتعددة التقنيات
Ecole Nationale Polytechnique

Département de Génie Civil

Final Year Project Thesis

In partial fulfillment of the requirements for the degree of State Engineer in Civil Engineering

---

Artificial neural networks for predicting the maximum surface settlement induced by EPB-TBM: The Algiers Metro Case

---

AYARI Ilies & DERBAL Yacine

Supervised by **Dr. SEBAI Souad**, ENP

Presented and publicly defended on (01/07/2025)

Jury Members:

President:	Prof. BOURZAM Abdelkrim	ENP
Examiner:	Prof. BOURAHLA Nouredine	ENP
Guest:	Miss. ZEGHMAR Racha	ENP

ENP 2025

Département de Génie Civil / ENP, 10 Rue des Frères OUDEK, El Harrach 16200 Alger, Algérie.

RÉPUBLIQUE ALGÉRIENNE DÉMOCRATIQUE ET POPULAIRE
MINISTÈRE DE L'ENSEIGNEMENT SUPÉRIEUR ET DE LA RECHERCHE SCIENTIFIQUE

ÉCOLE NATIONALE POLYTECHNIQUE

المدرسة الوطنية المتعددة التقنيات
Ecole Nationale Polytechnique

Département de Génie Civil

Mémoire de projet de fin d'études

Pour l'obtention du diplôme d'ingénieur d'État en Génie Civil

---

Réseaux de Neurones Artificiels pour la prédiction du tassement maximal en surface induit par le TBM-EPB : Cas du métro d'Alger

---

AYARI Ilies & DERBAL Yacine

Sous la direction de **Dr. SEBAI Souad**, ENP

Présenté et soutenu publiquement le (01/07/2025)

Composition du jury:

Président:	Pr. BOURZAM Abdelkrim	ENP
Examinateur:	Pr. BOURAHLA Nouredine	ENP
Invitée:	Mlle. ZEGHMAR Racha	ENP

ENP 2025

Département de Génie Civil / ENP, 10 Rue des Frères OUDEK, El Harrach 16200 Alger, Algérie.

ملخص

تهدف هذه الأطروحة إلى تقديم منهجية لربط تشوهات سطح الأرض (الهبوط) بمعطيات تشغيل آلة حفر الأنفاق (TBM)، إضافةً إلى هندسة النفق والمعطيات الجيوتقنية، وذلك بالاعتماد على نموذج شبكات العصبونية الاصطناعية (ANN) من أجل التنبؤ بقيمة الهبوط الأقصى على سطح الأرض. تم تحليل البيانات المستخرجة من أعمال حفر امتداد خط المترو رقم "1" بمدينة الجزائر (من محطة الحراش إلى مطار هواري بومدين الدولي)، والتي نُفذت باستعمال آلة TBM ذات درع واقٍ. وقد تمكن النموذج المقترح من إعادة إنتاج قيم الهبوط المسجلة على طول مسار النفق (العقد 1-9) بدقة مرضية. كما تم اعتماد خطوات تمهيدية مُخصصة لمعالجة البيانات بهدف تعزيز دقة النموذج، تلتها دراسة تحليلية لحساسية النموذج بهدف تقييم الأثر الفردي لكل عامل من العوامل المدخلة.

الكلمات المفتاحية :الشبكات العصبونية الاصطناعية – آلة الحفر ذات الضغط الترابي (EPB-TBM) – التعلم الآلي – التنبؤ بهبوط السطح.

Résumé

Ce mémoire présente une méthodologie permettant de corréler les tassements du sol en surface avec les paramètres de fonctionnement du tunnelier (TBM), la géométrie du tunnel et les paramètres géotechniques, en utilisant un modèle de réseau de neurones artificiel, qui est ensuite utilisé pour prédire le tassement maximal en surface. Les données analysées proviennent du creusement du tunnel de l'extension de la ligne «1» du métro d'Alger (El-Harrach – Aéroport international Houari-Boumediene), réalisé principalement à l'aide d'un tunnelier à bouclier. Les tassements en surface observés sur l'ensemble du tracé du projet d'extension du métro d'Alger (Contrat 1-9) ont été reproduits de manière «satisfaisante» par le modèle RNA proposé. Une procédure de pré-traitement dédiée a été nécessaire pour améliorer la capacité prédictive du modèle, suivie d'une analyse de sensibilité permettant d'évaluer la contribution individuelle de chaque variable.

Mots clés : Réseau de neurones artificiel - Execution au EPB-TBM - Apprentissage automatique- Prédiction du tassement en surface.

Abstract

This thesis presents a methodology to correlate ground surface movements (settlement) with tunnel boring machine (TBM) operation parameters , Tunnel geometry and Geotechnical parameters using an Artificial neural network model to predict maximum ground surface settlement. Data analyzed were selected from the excavation of the extension of Algiers subway line "1" (El-Harrach to H.B. Int. Airport) tunnel, which was performed by a shield TBM. The surface settlements observed along the entire tunnel section of the project (Contract 1-9) were satisfactorily reproduced by the proposed ANN model. A dedicated pre-processing procedure was necessary to enhance the model's predictive capability, followed by a sensitivity analysis to assess the individual contribution of each feature.

Keywords : Artificial neural network - EPB-TBM Tunneling - Prediction of surface settlement - Machine learning.

Acknowledgements

First and foremost, we thank Almighty Allah for granting us the health, strength, and determination to begin and complete this thesis.

We would like to express our deepest gratitude to our supervisor, Dr. SEBAI Souad, for her invaluable guidance, constructive remarks, and constant support throughout this work. Her expertise and availability were essential to the progress and successful completion of our study.

We are particularly grateful to COSIDER TP for providing the data and resources essential to this research. We extend our sincere thanks to Mr. AZZI Ameziane for offering us the opportunity to complete our internship within the company, and to Mr. HANNACH Hocine and Mr. BENHAMICHE Mazigh for their valuable assistance in providing and clarifying the technical data.

We also express our sincere gratitude to the National Polytechnic School of Algiers for the quality of the education we received and the continuous support provided by its faculty and staff throughout our academic career.

Our heartfelt thanks go as well to the members of the jury for the attention they have given to our work and for the honor of reviewing and evaluating it.

We warmly thank all those who contributed to the successful completion of this work. In particular, we are sincerely grateful to Mr. Abdellatif HANNACHI for his valuable help with the Python implementation and code development, and to Mr. Yacine HASNAOUI for his insightful advice and thoughtful guidance.

Finally, we would like to express our deepest gratitude to our families, who have always supported us with love and patience, as well as to all those who helped us—whether directly or indirectly—throughout this journey.

AYARI Ilies and DERBAL Yacine.

Dedication

I dedicate this work first and foremost to my dear mother, for her love, her prayers, her patience, and her countless sacrifices.

To my father, who left us too soon but is never forgotten. May Allah grant him His mercy and surround him with His light.

To my two sisters, Mayssa and Melissa, for their constant support, kindness, and affection.

To my entire civil engineering class, with whom I shared years of study, projects, challenges, and achievements.

Special thanks to my close friends: Boudjerda Anis, Ayari Ilies, Mohamed Mounsif Benmdjennah, Akram Khenfous, and Boukharouba Mohamed, for their sincere friendship, their attentive support, and their motivating presence during difficult times.

To my lifelong friends, those I grew up and studied with from childhood to the present day I send you all my affection and warmest regards.

To my thesis partner, Ilies, for his serious collaboration, constant commitment, and the team spirit we maintained throughout this project.

I would also like to thank all the teachers who contributed to my education, for their dedication, their teaching, and their high standards.

A special acknowledgment to my supervisor, Dr. Souad Sebai, for her attentive support, valuable advice, and high-quality supervision throughout this work.

Finally, to all the people who supported, helped, or encouraged me, directly or indirectly, I express my deepest gratitude.

Thank you all.

Yacine Derbal.

Dedication

I dedicate this thesis, with all my heart, to my parents. To my mother, whose endless care, gentle attention, and unconditional love have carried me through every stage. To my father, who has supported me in every possible way. His generosity, sacrifices, and constant presence have profoundly shaped the person I am. I am deeply and endlessly grateful for all that he has done for me. Everything I am today is the result of their love, strength, and unwavering support.

I also dedicate this work to my dear family. To my brothers, Chaouki and Fares, for always standing by me, pushing me forward, and never letting me give up. To my sisters, Houda and Sara, who have been incredibly supportive, deeply encouraging, and endlessly caring. Your presence in my life means more than words can express. To all of your families, I wish nothing but good health, lasting happiness, and a future as bright as your hearts.

To my second mother, Mama Zohra, may health and serenity gently accompany you in every day to come. To my aunts, Nadia and Dounia, whose presence has always been a quiet source of strength and comfort. To my uncle Azziz, and to my dear Tata, whose affection and support I carry with me always. To all of your families, I send my deepest gratitude, and I wish you lives filled with peace, dignity, and the gentle light of lasting love.

To my dearest friends, Anis, Yacine, Moncef, Mohamed, and Akram, it has been a true pleasure to share this journey with you. Your friendship has added light and laughter to these years. A special thanks to my thesis partner, Yacine. Working with you has been a great experience, and I'm grateful for every step we took together.

And finally, I want to thank everyone I have met along this journey, whether from up close or afar. Each encounter, no matter how brief, has left a mark, and I carry a part of it with me as I move forward.

Ilies AYARI.

Table of Contents

List of Tables

List of Figures

List of Acronyms

- **FEM**: Finite Elements Method
- **FDM**: Finite Difference Method
- **PK**: Kilometric Point
- **TBM**: Tunnel Boring Machine
- **EPB**: Earth Pressure Balance
- **EMA**: Entreprise Metro D'Alger
- **WSW**: West-Southwest
- **ENE**: East-Northeast
- **MPBX**: Multi-Point Borehole Extensometer
- **ABS**: Acrylonirtile Butadiene Styrene
- **PVC**: Polyvinyl Cholride
- **GSS**: Ground Surface Settlement
- **ANN**: Artificial Neural Network
- **MLP**: Multi-layer Perceptron
- **ReLU**: Rectified Linear Unit
- **FF**: Feed Forward
- **NN**: Neural Network
- **MSE**: Mean Square Error
- **MAE**: Mean Absolute Error
- **RMSE**: Root Mean Square Error
- **DistS**: Distance From Station
- **ECV**: Equivalent Cover Depth

General Introduction

In recent decades, the accelerated growth of cities particularly in metropolitan areas with limited surface availability has introduced numerous challenges especially in transportation and logistics, thus increasing the demand for underground infrastructure such as rapid transit systems.

Metro tunnel construction has emerged as a strategic solution to address traffic congestion and enhance urban mobility. While some tunnels are built in stable rock to minimize ground deformation as is the case in the Moscow Metro (>80m depth) [19] and the Washington D.C. Metro (50–60m) [20]. Most metro tunnels are constructed at shallow depths of 20–30m. At these depths, ground settlement becomes a major concern for surface structures and infrastructure, posing significant geotechnical and engineering challenges.

The Algiers Metro project highlights these challenges, built in a dense and historically rich urban environment where the metro alignment runs at shallow depths and passes through heterogeneous soil conditions. This setting complicates efforts to control ground movements and ensure the safety of existing buildings and infrastructure. One notable example is Place des Martyrs station, which was built in an area of major archaeological significance. Excavations during its construction in 2013 revealed Roman, Byzantine, Ottoman, and colonial remains dating back 2,000 years that made the construction more complex. To protect these discoveries, the station's design was subsequently modified to minimize damage to the archaeological site and to integrate a museum component for public display [21].

Figure 0.1: Archaeological remains at Place des Martyrs [2].

Tunnel excavation involves numerous interacting parameters, whether natural such as soil geology, groundwater level or operational like the TBM settings, all of which influence ground deformation. These interactions are not always fully understood and are often difficult to model using traditional analytical or numerical methods [15]. In recent years, advanced construction methods were introduced on work sites using multifunction machines such as shield tunnel boring machines (TBMs). These machines, which apply face support pressure via air, slurry, or earth, allow for a safer and more efficient construction of shallow tunnels in urban environments with challenging geological conditions. However, even with such equipment, ground movements especially vertical surface settlements are inevitable and can propagate to the surface, potentially impacting nearby structures.

If not properly predicted and managed, surface settlement can cause severe damage to infrastructure. Numerous global case studies have reported structural issues such as wall cracking, slab deflection, tilting, and utility damage resulting from tunneling-induced settlement. In sensitive urban areas, even millimeter-scale differential settlements can trigger visible and costly structural damage, particularly in rigid masonry buildings.

Figure 0.2: Damage caused by twin tunnel excavations along the Esenler–Başakşehir subway line (Turkey) [3].

Table 0.1 summarizes the most common types of damage associated with tunnel-induced settlement.

Table 0.1: Common Types of Damage Caused by Tunnel-Induced Settlement

Damage Mechanism	**Description**
Cracking in structural elements	Cracks appear in masonry and concrete walls, often perpendicular to the direction of settlement. Columns may crack in plaster, and beams may lose shear capacity.
Differential settlement and tilt	Uneven ground loss leads to tilting or steps. Floor slabs may deflect or sag, showing hairline cracks, especially under load.
Hogging vs. sagging	Structures may bend upward (hogging) or downward (sagging). Hogging façades are typically more prone to damage.
Infrastructure and utilities	Roads, pipelines, and tracks can subside or become misaligned.
Adjacent tunnels and structures	Older tunnels and nearby underground structures may deform due to nearby excavation or dewatering.

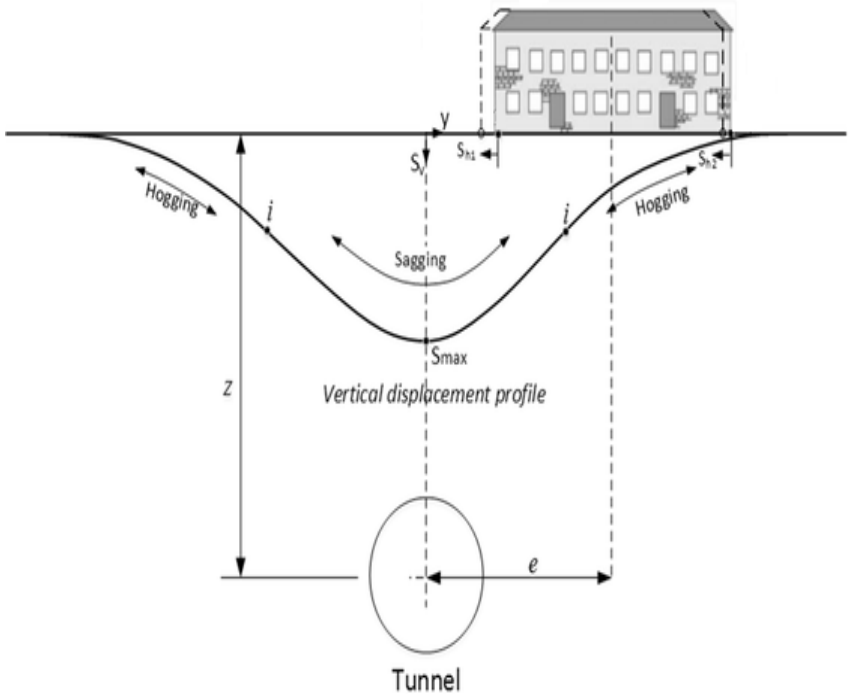

Figure 0.3: Sagging and Hogging phenomenon (Modified from [4]).

Given these risks, accurate prediction of settlement is essential to ensure safety and efficiency. Traditional modeling methods, such as *limit equilibrium analysis*, *cavity expansion theory*, and *numerical simulations* (e.g., FEM, FDM, 3D modeling), have been used to study TBM-induced settlement. Several studies have employed three-dimensional numerical modeling to investigate these effects: for instance, Emilios et al. [22] simulated EPB-induced subsidence and adjacent building deformation, while Wu et al. [23] analyzed TBM–ground interaction mechanisms and

their influence on surface structures. These approaches, while insightful, are computationally intensive and require significant calibration to capture complex coupled behaviors.

In this context, Artificial Neural Networks (ANNs) have emerged as a powerful alternative, especially in geotechnical engineering. ANNs are well suited for nonlinear, data-driven problems like predicting tunneling-induced settlement. Suwansawat and Einstein [24] , for instance, used an ANN to predict settlement from EPB tunneling and found no single operational parameter could fully explain surface response, underlining the complexity of the problem. Compared to conventional methods, ANNs can handle large datasets and extract hidden relationships between multiple variables.

Objectives of the Study

The purpose of the present thesis is to develop and evaluate a methodology for predicting maximum ground surface settlement using an Artificial Neural Network (ANN) model, and to identify the most influential tunneling factors. The approach is applied to vertical ground movement data collected during the extension of Algiers Subway Line 1 (El-Harrach to Houari Boumediene Airport), specifically from tunnel sections 1 to 9 (spanning 8.8km) excavated by an Earth Pressure Balanced (EPB) Tunnel Boring Machine (TBM).

Prior to training, TBM operational, geometrical and geotechnical data undergo a pre-processing phase to minimize noise and inconsistencies. Once a robust ANN model is established, sensitivity analysis is conducted to determine the most critical input factors influencing settlement.

The ultimate goal is to support proactive risk management. By anticipating conditions that may lead to excessive settlement, engineers can adjust tunneling strategies accordingly. The ANN thus serves as a decision-support tool, capturing the combined effects of soil parameters, groundwater levels, cover depth, and TBM parameters on surface response.

This thesis highlights the practical importance of predictive modeling. Accurate settlement forecasting is essential for safeguarding surface infrastructure and minimizing economic impact. The findings are expected to contribute to safer, more efficient tunneling practices in Algeria and other densely built urban environments.

This thesis is structured into five chapters as follows:

Chapter 1 : Provides an overview of the studied project, highlighting the use of an Earth Pressure Balance Tunnel Boring Machine (EPB-TBM), its characteristics, the construction process, and the general geological and hydrological context.

Chapter 2 : Introduces the concept of ground settlement, detailing its types and the key factors that influence its occurrence during tunnel construction. It also presents the instrumentation and monitoring systems employed to measure and record settlement, along with the data acquisition methodology and frequency applied throughout the project.

Chapter 3 : Discusses Artificial Neural Networks (ANNs), covering their inspiration and historical development, evolution over time, various types, and the fundamental principles behind their operation.

Chapter 4 : Focuses on the construction of the database and the preprocessing phase.

Chapter 5 : Presents the implementation of the Artificial Neural Network (ANN), the search for the optimal model, the assessment of its performance, and concludes with a sensitivity analysis and discussion.

In conclusion, the thesis presents the main findings, offers recommendations, and outlines perspectives for future research.

Chapter 1

Project Overview and Site Context

1.1 Introduction

This chapter provides an overview of the studied project, with a particular focus on the use of an Earth Pressure Balance Tunnel Boring Machine (EPB-TBM). It outlines the main characteristics of the TBM employed, details the construction process adopted for the Algiers Metro Line 1 extension, and presents the general geological and hydrogeological conditions encountered along the tunnel alignment. This contextual background is essential for understanding the operational environment of the TBM and the factors influencing ground behavior during excavation.

1.2 General description of Algiers Metro

1.2.1 History

The metro of Algiers is a rapid transit system serving the city of Algiers, envisioned in the 1970s and officially inaugurated in 1982 the project was then delayed due to economic reasons until 1994 when the first 450m long section was delivered. Aiming to modernize the public transport system and to establish a long term solution for transportation related problems responding to the rapid growth of the metropolis.

1.2.2 Algiers metro line “1”

Line "1" is extending from Martyr’s square to El-Harrach center and Ain-Naa’dja branching from Hai-Elbadr with a total route length of 13.5km and containing 19 stations (Figure 1.1). It was constructed via 3 different phases finishing with the expansion from "Haï el Badr" to "El Harrach Centre".

Figure 1.1: Line 1 of Algiers Metro [5].

1.2.3 Extension of Algiers Metro Line 1

The extension project of the Algiers metro is a very important project and represents a strategic step for the city of Algiers. It aims to solve the problems related to traffic congestion suffered by the Algiers province as the capital of the country. This extension will help enhance the efficiency of the urban transport network and respond to the growing demand for mobility.

This large-scale project, which connects the El Harrach Centre station to the Houari Boumédiène International Airport, constitutes a development and extension of the public transport network in Algeria. It includes 9 new stations and ten ventilation shafts with a total excavated length of 9,565 meters (Figure 1.2).

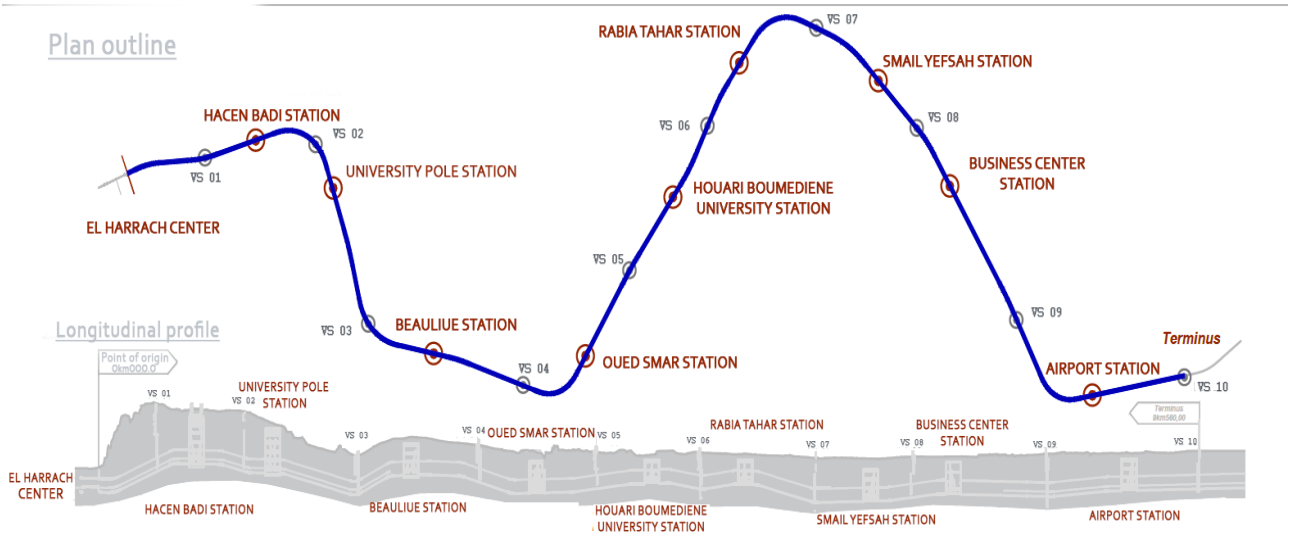

Figure 1.2: Plan outline for the extension of Algiers metro line "1"

The route of this extension stands out for its complexity, notably due to the presence of five curves with very small radii (Around 198 meters), which can affect TBM operations and the tunnel design (Figure 1.3).

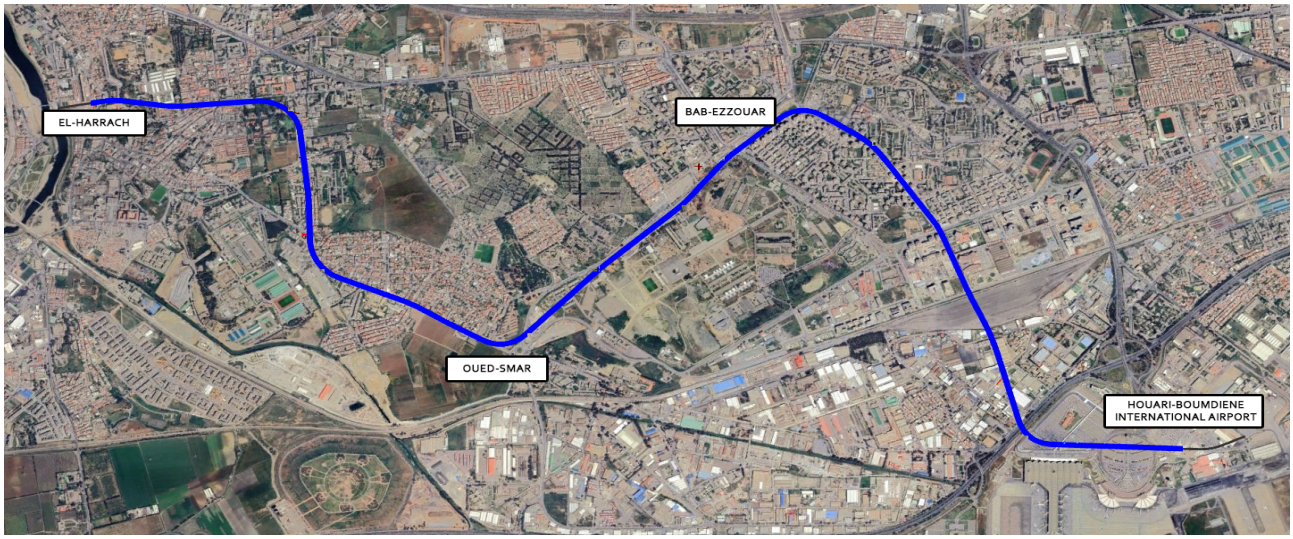

Figure 1.3: Algiers metro line "1" extension (Google-earth)

To successfully carry out this project, the Algiers Metro Company (EMA), as the delegated project owner, entrusted the execution of the works to the construction company COSIDER TP, a key player in the execution of large-scale infrastructure projects, recognized for its expertise and experience in this field. The latter subcontracted SELI-overseas a specialized company in underground works and in mechanised TBM tunnel excavation.

1.3 Execution

This section outlines the execution methodology adopted for the construction of the Algiers Metro Line 1 extension, with particular emphasis on the tunneling technique employed and the technical characteristics of the TBM used on site.

1.3.1 Tunnel boring machine (TBM)

The tunnel boring machine (TBM) used for the excavation is an Earth-pressure balance TBM (EPB-TBM) with a diameter of 10.5 meters, model C665, developed by the company CREG-WIRTH, bearing the serial number CTE10470E-3500 (Figure 1.4). It was designed by taking into consideration the geological, hydrogeological and geometric conditions of the project.

Figure 1.4: TBM “CREC665” Also known as KAHINA used for this project [6].

1.3.2 Working principle of the EPB-TBM

An EPB-TBM is a specialized type of tunnel boring machine designed for excavating tunnels in soft, cohesive, or mixed ground conditions, particularly where maintaining face stability is critical such as in urban environments or areas with high groundwater levels. Figure 1.5 Shows the general assembly on an EPB-TBM.

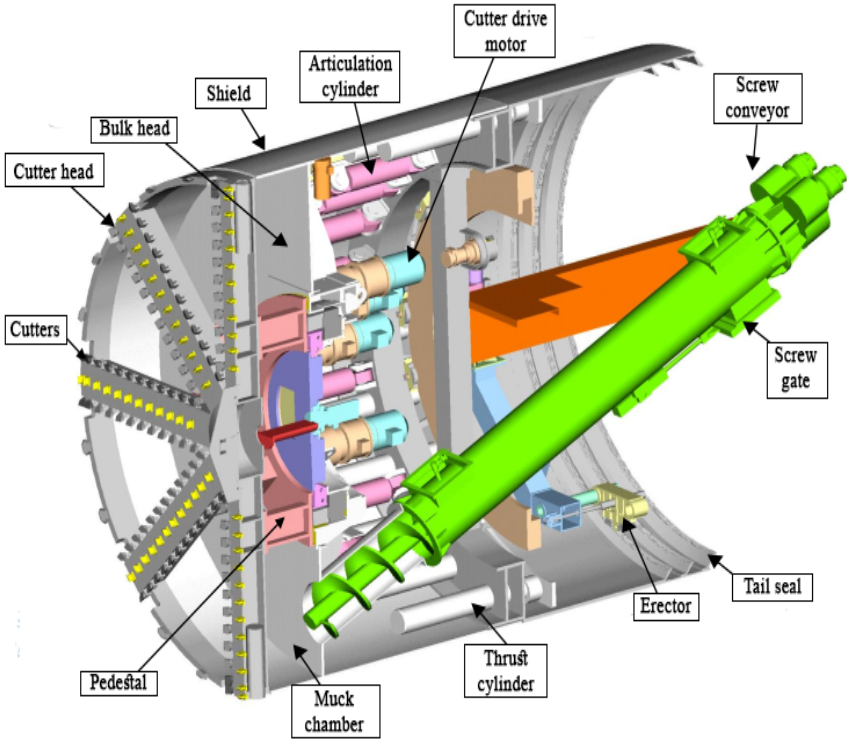

Figure 1.5: General assembly on an EPB-TBM(Modified from [7]).

The core concept of an Earth Pressure Balance Tunnel Boring Machine (EPB-TBM) is to use the excavated soil itself to support the tunnel face, ensuring stability throughout the excavation process. As the machine advances, soil is excavated by the rotating cutterhead and enters a pressurized excavation chamber (Muck chamber) through openings at the front. In this chamber, the incoming soil mixes with previously excavated material to form a paste-like consistency. This paste helps balance the external pressures from the surrounding soil and groundwater. Optimal performance of the EPB-TBM is typically achieved in cohesive soils with a consistency index (IC) between 0.5 and 0.75 [25].

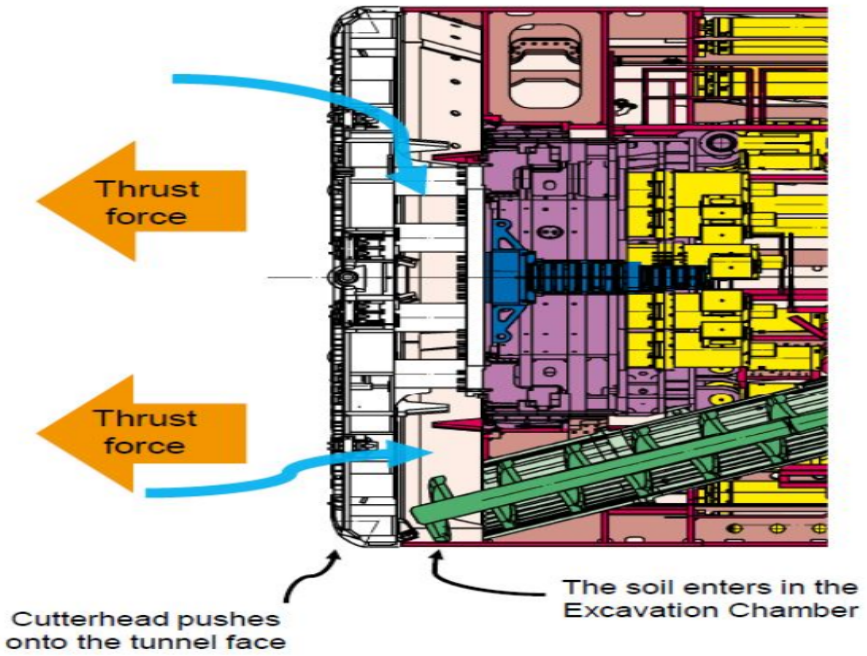

Figure 1.6: Muck chamber mechanism [8].

The rotating speed and direction of the cutterhead is in most cases changed during the excavation to accomplish the best mixing and conditioning of the ground and to counter a rolling of the shield. Inside the excavation chamber, between the cutterhead rear and the fixed elements of the pressure wall, the excavated material is kneaded into a plastic mash with the support of the mixing blades. If the muck is too dry or sticky conditioning agents like foam or bentonite are added to the mix to help obtain a plastic consistency [26].

Pressure balance is maintained when the internal pressure of the soil paste matches the surrounding earth and groundwater pressures.A screw conveyor positioned at the back of the chamber (Figure 1.6) continuously removes the conditioned material at a controlled rate. This regulation of the outflow is critical for maintaining consistent pressure at the face. The excavated material is then transferred onto a conveyor belt system and transported out of the tunnel.

As the TBM advances, an annular void forms between the excavated ground and the segmental lining, which must be filled immediately to prevent ground loss and surface settlement. This is achieved through simultaneous grouting, injected under pressure via dedicated nozzles located around the tail shield. The tail seal system, equipped with multiple sealing brushes and often lubricated with grease, prevents the infiltration of groundwater and grout during ring installation. Thrust cylinders then push the TBM forward by reacting against the completed segment rings, ensuring a continuous cycle of excavation, muck removal, ring assembly, and grouting.

1.3.3 TBM “KAHINA” Characteristics

This section outlines the main technical features of the EPB-TBM “KAHINA”

Cutterhead: In addition to clayey soils, the cutterhead is also designed to ensure a good flow ability of sandy cobble stratum ground condition, with an opening ratio of 39%. Injection nozzles foreseen 12 pipelines, each one has an independent pump, and they are connected with the cutterhead via centre rotary joints. The 12-foam line also has 8 injection points, 6 going to the excavation chamber and 2 connected to the screw conveyor.

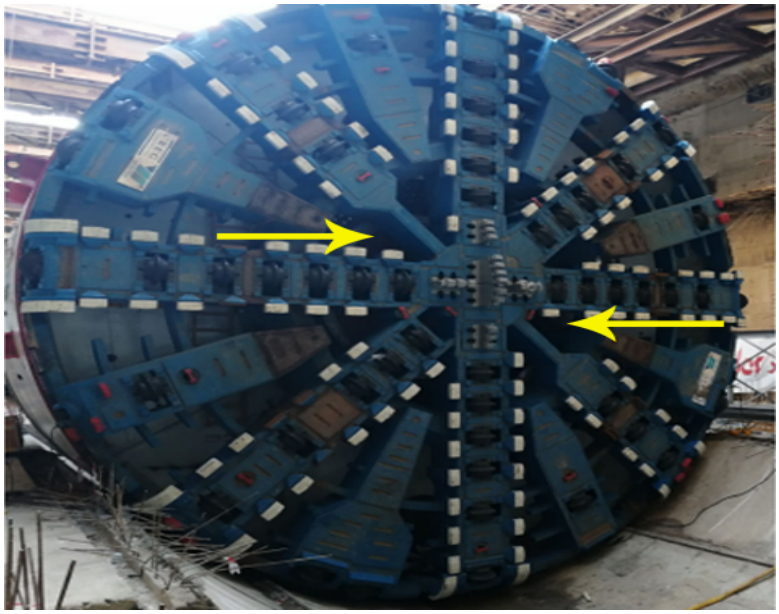

Figure 1.7: KAHINA’s cutter head and its opening, highlighted with yellow arrows (Modified from [1]).

Thrust cylinders : There are 38 thrust cylinders in total which are divided in 6 groups.

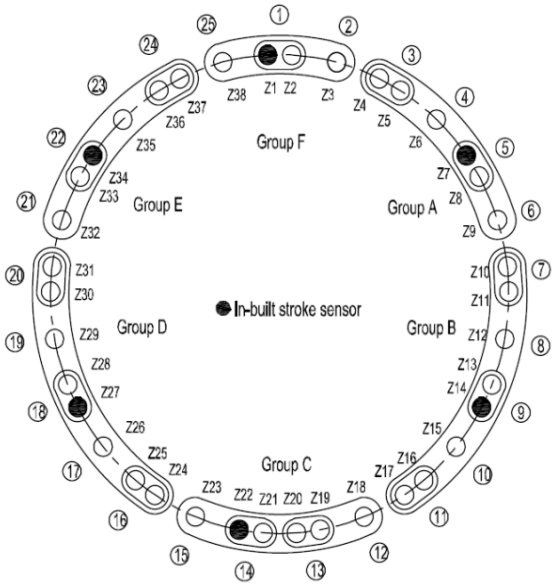

Figure 1.8: Thrust cylinders distribution [1].

Each thrust group is equipped with a built-in stroke sensor to determine the TBM direction's attitude during advancing. Thrust cylinders can produce a maximum thrust force of 106,910 kN at maximum hydraulic pressure of 350 bar.

Articulation cylinder system : There are in total 18 cylinders divided in 4 groups (Figure 1.9) equipped with displacement sensors embedded in four different articulation cylinder groups to detect the stroke.

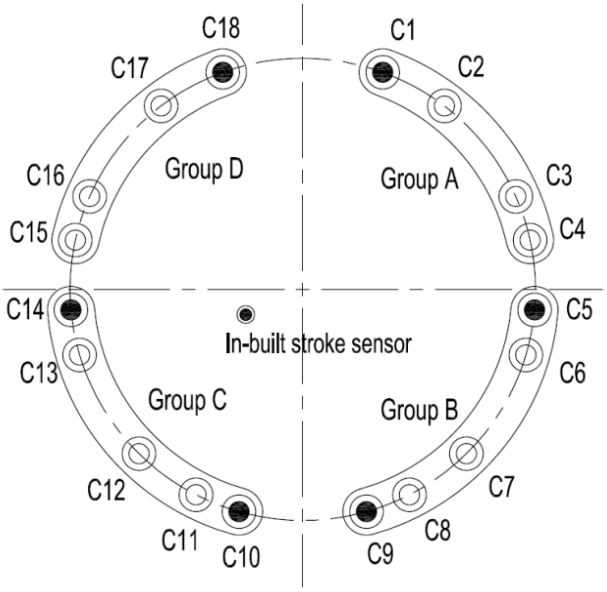

Figure 1.9: Articulation cylinders distribution [1]

Tail void Grouting: A bi-component grout is used, composed of components A (grout) and B (accelerator), is injected at the rear of the shield through six grouting lines, where the two components are mixed at the nozzles. Each grouting line is equipped with a dedicated grouting pump and a spare line to be used in case of clogging.

Table 1.1 below highlights the main characteristics of the TBM, including general dimensions, operating capacities, and other key parameters such as thrust and power systems.

Table 1.1: Principal characteristics of the TBM [1] .

Characteristics	**Unit**
Estimated total length (including back up)	85 (m)
Estimated shield length	10.5 (m)
Exit speed: (geology related)	90 (mm/min)
Maximum head rotation	2.73 (rpm)
Operating pressure	5 (bar)
Type of motors	Electric
Installed motors	10
Free positions for motors	3
Motor power	350
Nominal Thrust	130.000 (KN)
Number of thrust cylinders	38

1.3.4 Sequence of tunnel execution

This metro line extension project will be carried out in two main phases of work (Figure 1.10). With Oued-Smar as a Launching and supply section.

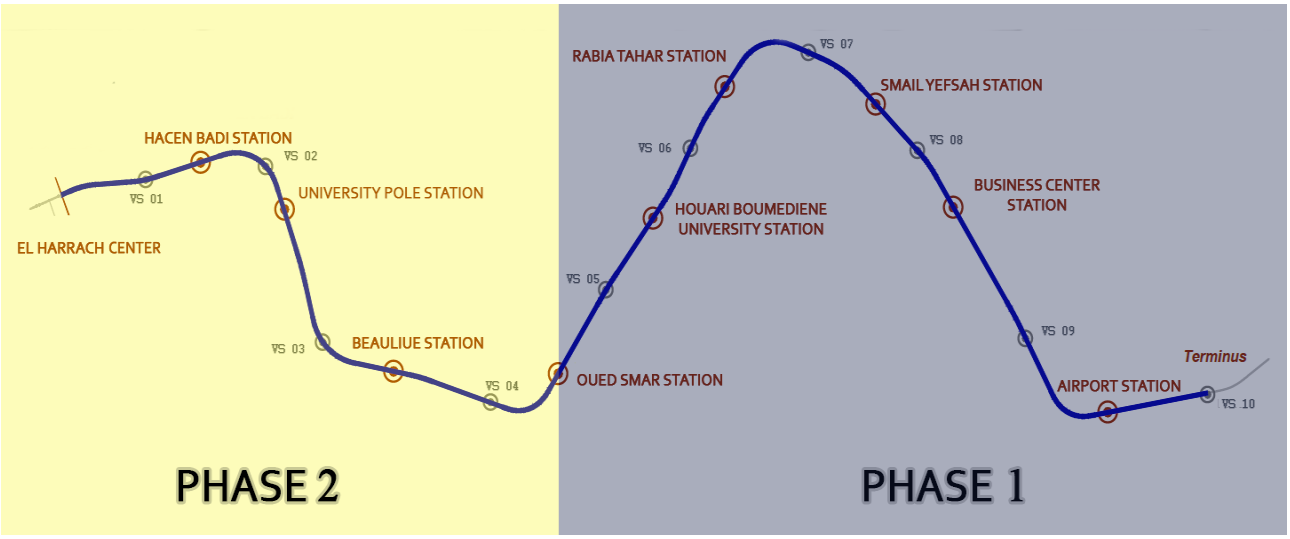

Figure 1.10: Construction phases of the tunnel project

Phase 1: This first phase consists of the realization of 6 tunnel sections from Oued-Smar station to Hourai-Boumediene Int. Airport station and extended to the ventilation shaft N°10, with a linear distance of 5,768 m, this first phase consists of the realization of the following 06 tunnels:

Table 1.2: Phase 1 of the extension (Modified from [1]).

№ of Tunnel Section	**Starting point**	**Arriving point**	**Length (m)**
5	Oued-Smar Station	USTHB University Station	869
6	USTHB station	Rabia Tahar station	656
7	Rabia Tahar station	Smail Yefsah	965
8	Smail Yefsah	Business Center station	586
9	Business Center Station	Airport Station	1368
10	Algiers International Airport	Ventilation shaft 10	566

Once it reaches the ventilation shaft N°10, the tunnel boring machine will be disassembled, transported to Oued Smar, and then reassembled to begin the second excavation phase towards El Harrach Centre.

This Phase of the construction will be addressed as "Zone 1" In the upcoming sections.

Phase 2: This second phase consists of the realization of 4 tunnel sections over a length of 3807m from Oued Smar station to El Harrach downtown

Table 1.3: Phase 2 of the extension (Modified from [1]).

№ of Tunnel Section	**Starting point**	**Arriving point**	**Length (m)**
1	Oued-Smar Station	Beaulieu station	904
2	Beaulieu station	Pôle Universitaire station	1138
3	Pôle Universitaire station	Hassan Badi station	529
4	Hassan Badi station	El Harrach Centre station	751

This Phase of the construction will be addressed as "Zone 2" In the upcoming sections.

The work sequencing for the tunnel construction is shown in Figure 1.11 .

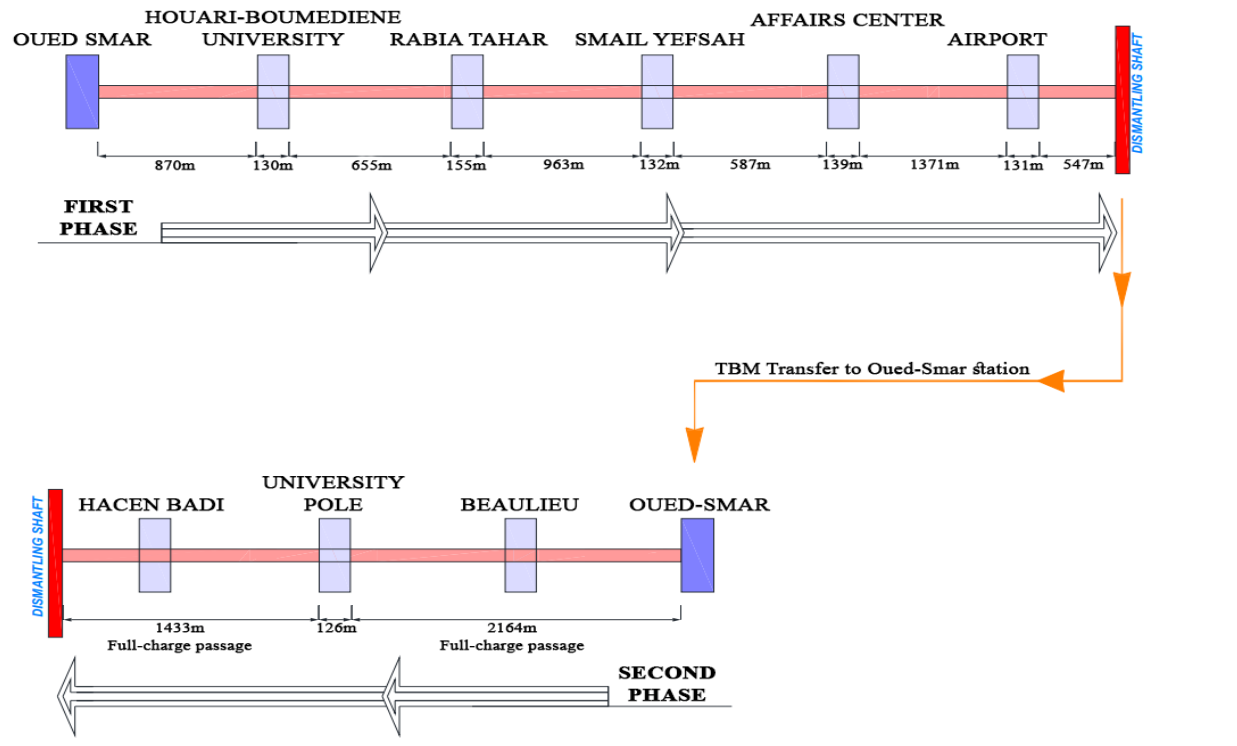

Figure 1.11: Work sequencing scheme (Modified from [1]).

1.3.5 Characteristics of the Studied area

Table 1.4 provides a summary of some technical parameters of this alignment :

Table 1.4: Technical Specifications of the Tunnel

Length of the tunnel	9,565 meters
Internal Diameter	9,3 meters
External Diameter	10,2 meters
Excavation Diameter	10,5 meters
Number of stations to be crossed	8 stations
Average tunnel Depth	An Average Depth of approximately 15 to 20 meters below the ground surface
Excavation Method	Full-face Excavation Method
Support Method	Precast Concrete Segments
Average Ring Length	Two types of rings were used to ensure they follow the alignment and avoid issues related to stresses, which could cause deformations, misalignment of segments or cracks in the concrete. Type 01: with an average length of 1,8m. Type 02: with an average length of 1,4m.

1.4 Geological Context

This extension of Algiers metro line "1" is located in the eastern part of the plain of Mitidja which extends over an area of 1300 km2 or 100 km long and a width that varies between 8-18 km, it is an elongated depression from west to east, from Hadjout to Blida and curves in direction WSW-ENE from Blida to the Oued-ElHamiz and the sea. This plain, bounded on the west by the Oued-Nador and on the east by the Oued-Boudouaou, is bounded to the north by the anticline of the Sahel and to the south by the Atlas blidéen.

1.4.1 The plain of the Mitidja

The plain of the Mitidja is formed by Tertiary land and filled by Quaternary. In the extract of the geological maps at scale 1:50,000, sheet 21 from Algiers and sheet 42 from Arba, the study route has been implanted (Figure1.12) in plan, the study area is mainly constituted by recent alluvial deposits, where it is possible to differentiate two formations: a3 - Alluvions marshes and flood areas; a2 - Silty alluvium and p2q – Maison Carrée Marl (Late and Quaternary Pliocene former)

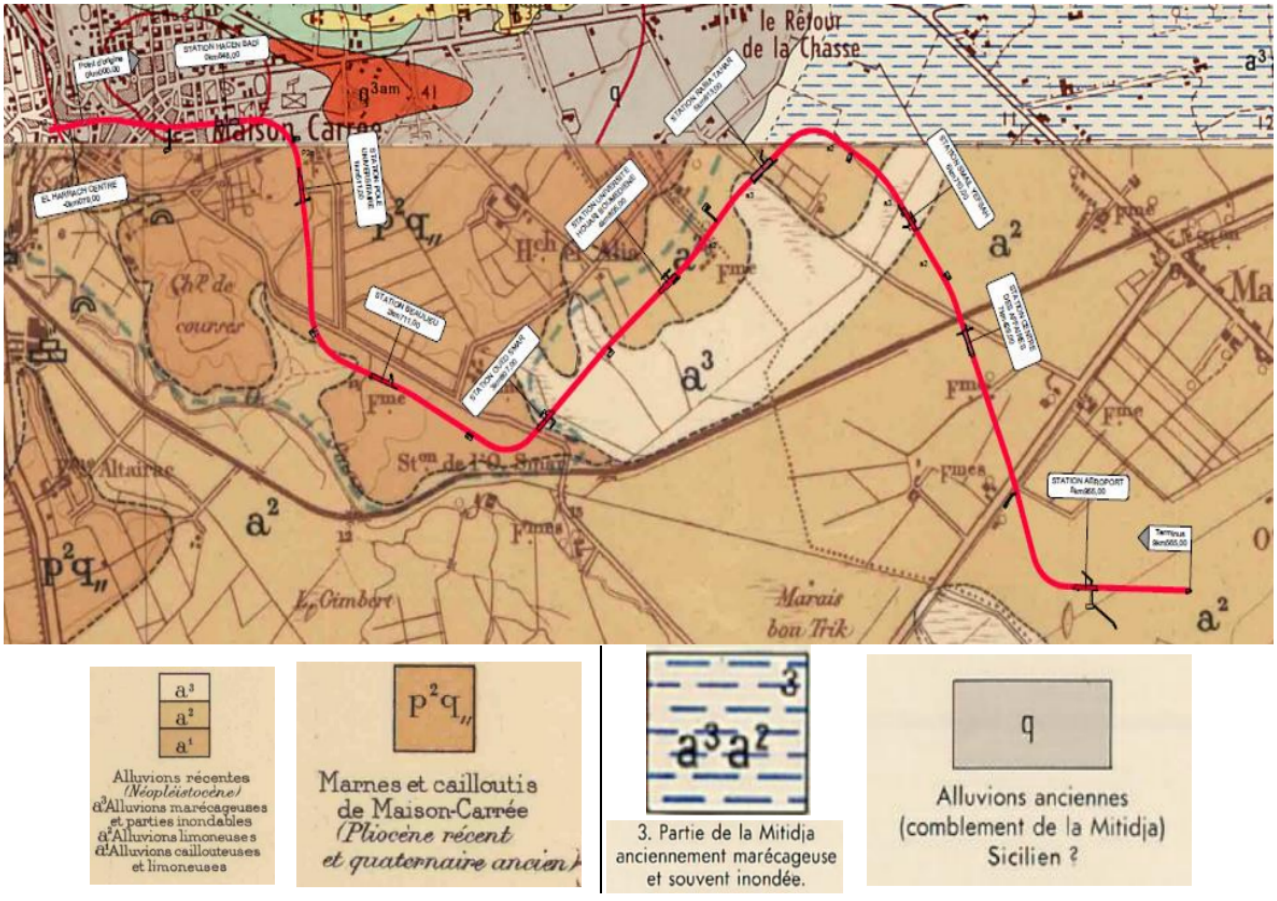

Figure 1.12: Extract from the Geological Maps sheet no21 of Algiers and sheet no 42. (The Extension Alignment implemented)

1.4.2 Lithology

The differentiated lithological units present in the underground of the studied area are, in chronological order from the oldest to the most recent:

Tertiary - Astien

It is characterized by shallow marine deposits, represented by a lithological succession that generally includes, from bottom to top, the following facies: marly-sandy, calcareous-sandy, molassic, and sandy-clayey, collectively referred to as the Astian Molasse. These facies show intercalations and frequent lateral variations. They were identified during the geological study of the tunnel extension line as Units TS, TG, and TM.

- **Unit TS**: This unit represents fine, medium to coarse, sand with sandstone fragments, these formations appear only in depth, particularly in Section 1 (pk 0+000 to pk 0+782.50), Section 2 (pk 0+912.00 to pk 1+445.80) and Section 3 (pk 1+576.20 to pk 2+646.30);
- **Unit TG**: This unit represents unweathered to cracked sandstone, these formations appear only in depth, particularly in Section 2 (pk 0+912.00 to pk 1+445.80);
- **Unit TM**: This unit represents marly clay to marl. These formations appear only in depth, particularly in Section 1 (pk 0+000 to pk 0+782.50), Section 2 (pk 0+912.00 to pk 1+445.80)

Quaternary

After the sedimentation of the Astian, erosion of the Tellian Atlas led to the deposition of Quaternary sediments in low-lying areas and along the marine coast. These deposits include a wide range of facies, mainly detrital in nature, and lie over older layers. The main facies were identified during the geological study of the tunnel underground as Units QM, QS, and QA.

- **Unit QM**: This unit represents a deposition of Clays and Marls, known as those of El Harrach. It also includes cross-stratified sandstones, occasionally containing levels of pebbles and lumachelles, which testify to an agitated coastal environment before the sea resumed its general regression.
- **Unit QS**: This unit consists of a detrital deposit resulting from the dismantling of uplifting reliefs, it is mainly composed of clayey, sandy, and pebbly facies.
- **Unit QA**: This unit consists of a detrital depost corresponding to significant fluvio-continental sedimentation, occuring across the alluvial plains in continuity with previous depositional events. It is composed of clayey facies formed of clays and sandy clays with pebbles.

Table1.5 summarizes the main lithostratigraphic units encountered along the tunnel alignment.

Table 1.5: Main lithostratigraphic units intersected along the tunnel alignment

Stratigraphy	**Symbology**	**Lithology**	**Observations**
Recent	R	Fill	Layer of no importance for excavation, very superficial
Quaternary	QA	Silty clay with low sand content	Important layer for excavation in sections 7–10
	QG	Pebbles with a clayey or sandy-clayey matrix	Important in section 9
	QS	Silty-clayey sands with pebbles, sandstone and conglomerates	Important layer thickness in sections 5–9
Upper Pliocene – Early Quaternary	QM	Marly clays and marls with sandstones and conglomerates	Important in sections 1–6, 9–10
	QM_{sg}	Silty-clayey sands with pebbles	Present as lenses in QM: sections 1, 3–5, 9
	QM_s	Fine to medium silty sand	Present as lenses in QM: sections 1, 4, 10
Tertiary Astien	TS	Fine to coarse sand with sandstone fragments	Important in sections 1–3
	TG	Fractured sandstone with lumachelle	Important in section 2
	TM	Marly clay and marl	Very deep; not relevant in sections 1–2

1.4.3 Subsurface Conditions throughout the Tunnel Alignment

The main units excavated inside the tunnel along the extension El-Harrach - Bab-Ezzouar - Algiers International Airport are presented in Table 1.6 below, including the length and depth of the cover along the sections and the units above the tunnel crown.

Table 1.6: Geological units encountered along each tunnel segment

Tunnel	**Pk start**	**Pk end**	**Length (m)**	**Depth (m)**	**Units inside the tunnel**	**Units at the tunnel's crown**
T1	0+000,00	0+782,50	782.50	[7–41]	QS / QM / QM_{sg} / QM_s / TS / TM	QA / QS / QM / QM_{sg} / QM_s
T2	0+912,00	1+445,80	533.80	[23–32]	QS / QM / TG / TS	QA / QS / QM / QM_{sg} / TG / TS
T3	1+576,20	2+646,30	1070.10	[13–26]	QM / QM_{sg} / TS	QG / QM / QM_{sg}
T4	2+775,70	3+741,95	966.20	[13–20]	QM / QM_{sg} / QM_s	QA / QS / QM / QM_{sg} / QM_s
T5	3+872,00	4+740,50	868.50	[10–25]	QS / QM / QM_{sg}	QA / QS / QM / QM_{sg}
T6	4+869,90	5+527,50	657.60	[10–15]	QS only	QA / QS / QM
T7	5+677,65	6+644,96	967.30	[10–21]	QA / QS	QA / QS
T8	6+774,97	7+363,13	588.20	[13–16]	QA / QS	QA / QAs / QS
T9	7+501,13	8+873,10	1372.00	[15–17]	QA / QG / QM / QM_{sg}	QA / QG / QM
T10	9+002,90	9+575,00	572.10	[15–16]	QA / QM / QM_s	QA / QM / QM_s

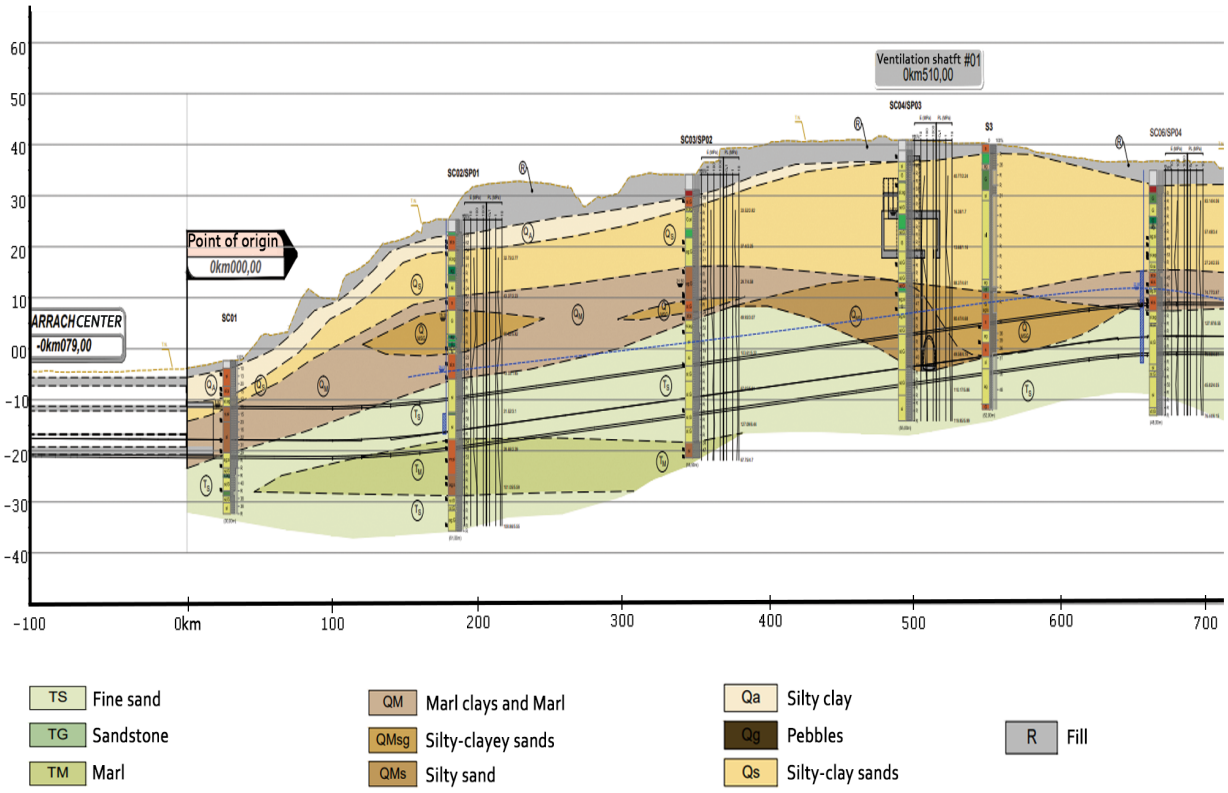

Figure 1.13: Longitudinal profile showcasing units distributions in tunnel Section 1 (pk+0.000,00 to pk+0.700,00). (Details in Appendix A)

1.5 General Hydrology

The route of the entire extension of the Algiers Metro line between El-Harrach –Algiers International Airport, currently under construction, develops in the eastern part of the vast Mitidja Plain, limited between the Oued El-Harrach and the Oued El-Hamiz. According to the bibliography, the eastern part of the Mitidja Plain, in northern Algeria, covers about 575 km². It is bounded by the Mediterranean Sea to the north, the Atlas Mountains (1200–1600 m elevation) to the south, the Oued El-Harrach to the west, the Oued Réghaia to the east, and the "Petit Sahel" (200 to 250 m elevation) to the northeast. The general elevation of the plain varies from 20 to 50 m. The main watercourses are the Oued El-Harrach (West), Oued El-Hamiz (Center), and Oued El-Réghaia (East). The most important water catchment areas are Bouréah, Hamiz, Haouch Félit, and Baraki. In the eastern part of the Mitidja Plain, from top to bottom, there are two main aquifers:

The Quaternary alluvium:

- This aquifer is located in more or less consolidated gravels and sands, inter-stratified with clay. It is recharged by:
  - Precipitation;
  - Infiltration from Oued El-Harrach and Oued El-Hamiz;
  - Drainage from the Astien reservoir.

- It is separated from the Astien aquifer by the El Harrach Formation, except to the east of El Hamiz, where the two are in direct contact.
- The unconfined aquifer extends along the entire Mitidja basin.

The Astien reservoir

- It is confined beneath the marls of “Maison-carrée”, currently called the “El Harrach marl,” in which clayey elements dominate in an alternation comprising sticky marls, gravelly clays, and some beds of sand and gravel—except in the eastern part where it is in direct contact with the Mitidja aquifer.

In plan view, the route under study crosses several geological formations, which can be classified into two hydrogeological categories of terrains (As shown in the excerpt from the hydrogeological map of the Algiers region, at a scale of 1:200,000, Figure 1.14);

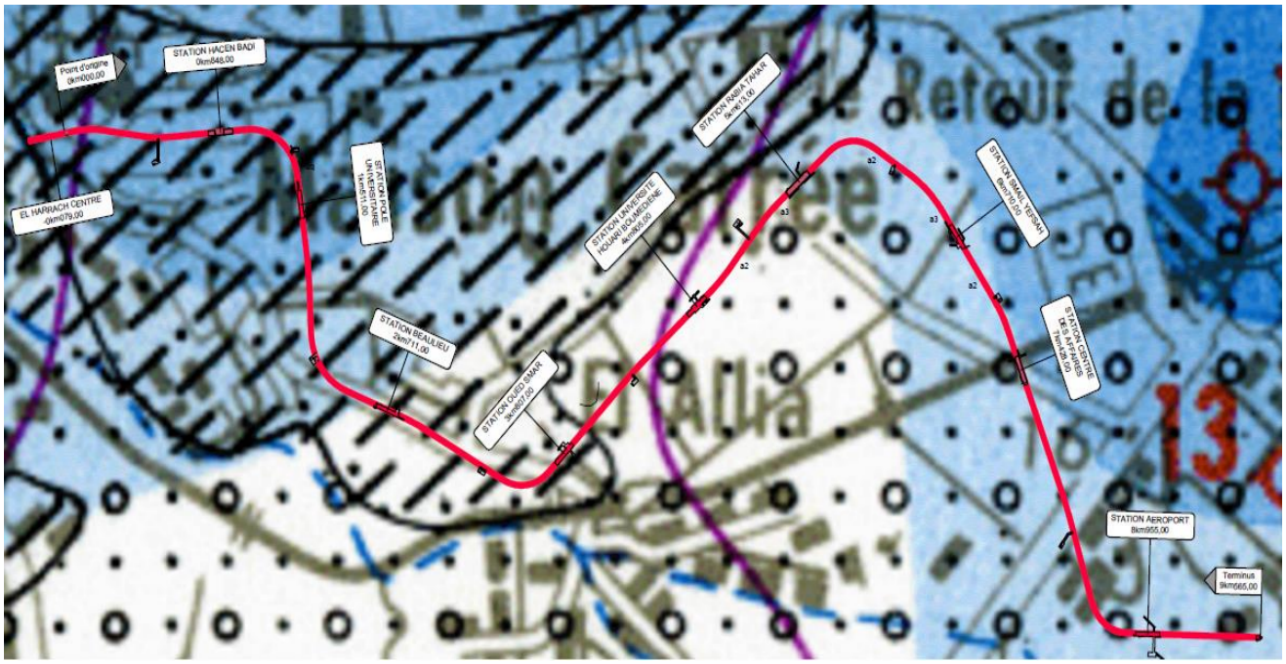

Figure 1.14: Excerpt from the Hydrogeological Map of the Algiers Region (Alignment implemented).

Table 1.7: Hydrogeological Classification of the Mitidja Formations

Class	Stratigraphy	Symbology	Lithology	Hydrogeology
I	Quaternary		Alternation of clays and gravel (Mitidja)	Permeability generally high. Water resources important
II	Quaternary		Clay and pebbles from Villafranchien (Mitidja)	Low permeability. Substrate of the water table of the alluvions in the Mitidja

- **Class I**: Highly permeable soils. Water resources generally significant..
- **Class II**: Soils with medium permeability. Water resources variable.

In plan view along the route, the permeability is characterized as shown in Table 1.8

Table 1.8: Permeability in plan along the route based on the Hydrogeological Map of the Algiers region.

Tunnel (Section)	**Pki**	**Pkf**	**Extension (m)**	**Hydrogeology**
T1	0+000,00	0+782,50	782,50	Medium Permeability
T2	0+912,00	1+445,80	533,8	Medium Permeability
T3	1+576,20	2+646,30	1070,1	Medium Permeability
T4	2+775,70	3+741,95	966,2	Medium Permeability
T5	3+872,00	4+740,50	868,5	Medium to High Permeability
T6	4+869,90	5+527,50	657,6	High Permeability
T7	5+677,65	6+644,96	967,3	High Permeability
T8	6+774,97	7+363,13	588,2	High Permeability
T9	7+501,13	8+873,10	1372	High Permeability
T10	9+002,90	9+575,00	572,1	High Permeability

1.6 Conclusion

The extension of Algiers Metro Line 1 between El Harrach Centre and Houari Boumédiène International Airport is a key infrastructure project intended to improve urban mobility and reduce congestion in the capital. With a length of 9.5 km and 9 new stations, the project is was executed in two main phases using an Earth Pressure Balance Tunnel Boring Machine (EPB-TBM) adapted to the local geological and hydrogeological conditions.

The tunnel alignment crosses complex terrain within the Mitidja plain, requiring careful consideration of soil behavior, groundwater conditions, and construction techniques. In summary, the main units that govern the tunnel excavation are Units QM (marly clays), QS (silty-clayey sands), and TS (Sands), which represent the dominant lithologies encountered along the tunnel route.

Chapter 2

Ground Surface Settlement and Monitoring

2.1 Introduction

Soil settlement is defined as a vertical deformation of the ground caused by the application of an external load (structural load, embankments, the soil's own weight, etc.). It results from the rearrangement of soil grains, dissipation of pore water, and progressive soil consolidation. This phenomenon is particularly pronounced in saturated fine soils (clays, silts), where low permeability causes slower and more prolonged settlement.

Three types of settlement are distinguished:

- **Uniform settlement**, which affects an entire structure evenly and is generally not critical.
- **Tilting**, a form of nonuniform settlement that typically occurs without visible cracks. It often results from soil liquefaction, causing the entire structure to tilt without necessarily damaging its integrity [9].
- **Differential settlement**, which is more dangerous as it causes uneven subsidence that can lead to cracks or structural deformations.

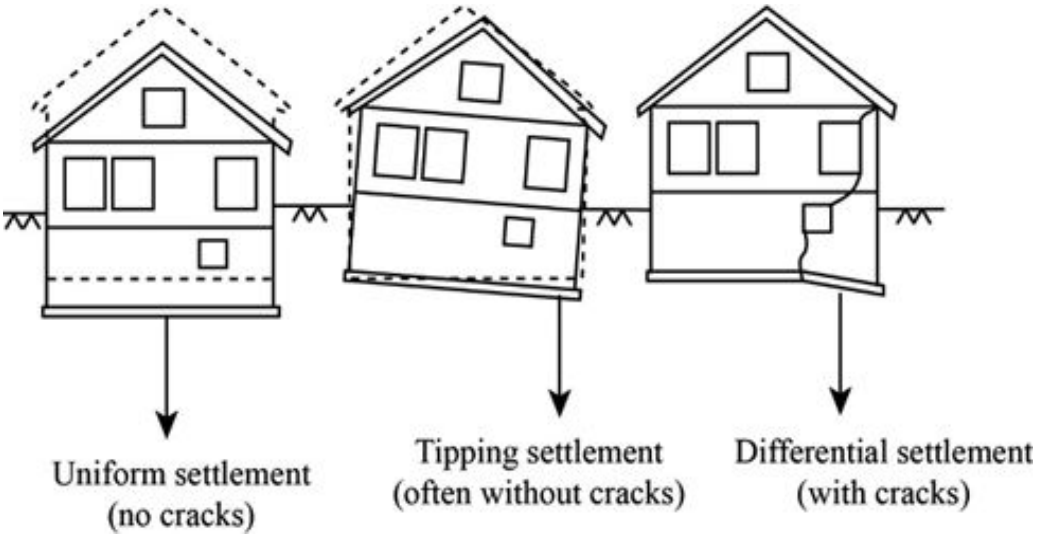

Figure 2.1: Different types of settlement [9].

Consolidation lies at the heart of the phenomenon, and Terzaghi's one-dimensional theory explains its time evolution: initially *immediate settlement*, then *primary consolidation* (due to pore water dissipation), and finally *secondary consolidation* (particle creep).

The main causes of settlement include:

- Natural consolidation under constant loads (e.g., weight of structures or embankments)
- Groundwater pumping
- Resource extraction (e.g., mining, groundwater)
- Civil engineering activities, including soil compaction and mechanized tunneling (e.g., with Earth Pressure Balance Tunnel Boring Machines), which can induce ground settlement due to excavation-related disturbances.

In this study, we focus specifically on ground settlement induced by EPB-TBM excavation.

2.2 Surface Settlements Induced by EPB-TBM Tunneling

The excavation of tunnels using Earth Pressure Balance Tunnel Boring Machines (EPB-TBMs) inevitably induces ground deformations that may result in surface settlements. The extent and characteristics of these settlements are governed by a combination of factors, generally classified into three main categories:

- **Tunnel geometry** including tunnel diameter, depth, and alignment.
- **Geological and hydrogeological conditions** such as soil permeability, groundwater level and soil resistance.
- **TBM operational parameters** such as face pressure, advance rate, and volume loss.

This chapter analyzes the influence of each category on the occurrence and magnitude of surface settlements during shield tunneling.

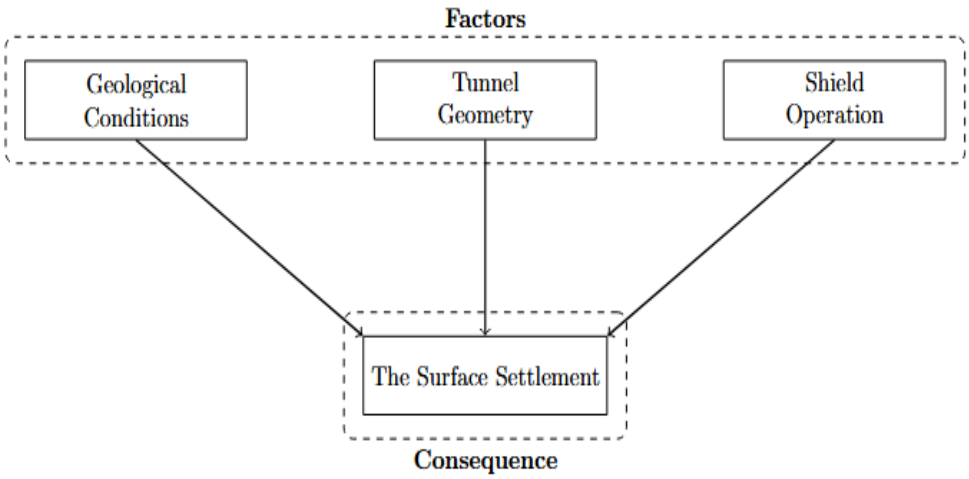

Figure 2.2: Main Factors Influencing Surface Settlement in EPB-TBM Tunneling

2.3 Factors Influencing Surface Settlement in EPB-TBM Tunneling

2.3.1 Tunnel Geometry

In this subsection, the factors taken into account and having a significant influence on the magnitude of settlement are three: tunnel diameter, cover depth and distance from station.

2.3.1.1 Tunnel Diameter

The tunnel diameter is a very important factor that strongly influences surface settlement. It corresponds to the outer diameter of the shield (i.e., the excavation diameter). An increase in tunnel diameter leads to an extension of the vault (crown) length, which increases the temporary loads that the surrounding ground must bear. Moreover, this increase expands the influence zone around the tunnel face, covering an area with a diameter equal to that of the tunnel. This region experiences a higher typically maximum convergence rate compared to other parts of the tunnel. As a result, controlling convergence becomes more difficult, especially in loose or low-cohesif soils. Furthermore, a larger diameter means a wider cross-sectional area, which, under constant soil conditions, causes a greater volume of ground to move toward the tunnel. This situation further complicates the effective installation of a temporary support system due to the increased stresses and the larger surfaces that need to be stabilized. Since this tunnel was excavated using the same shield throughout the entire alignment, the diameter remains constant (10.5m); therefore, its influence can be neglected in this case.

2.3.1.2 Cover Depth

The cover depth, defined as the thickness of soil above the tunnel, plays a key role in the behavior of the soil during shield excavation. In shield tunneling, the arching phenomenon refers to the structural formation that redistributes pressure around an excavated opening, redirecting some of the vertical overburden stress laterally into an arch above the tunnel. The Arching effect was developped in 1943 by K.Terzaghi [27].

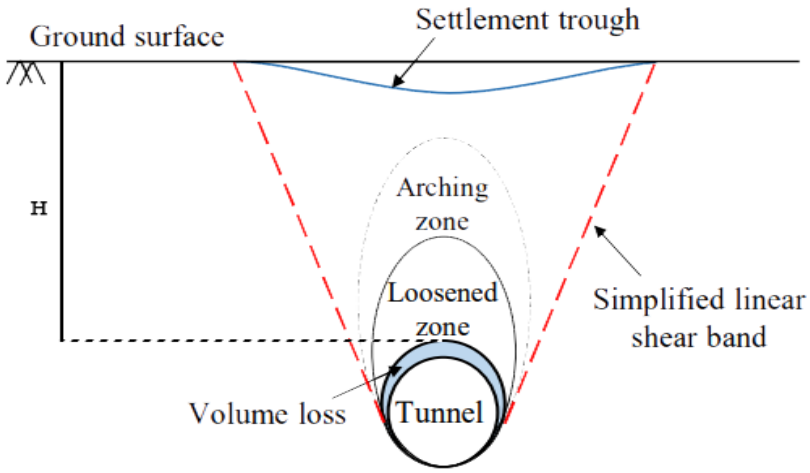

Figure 2.3: Scheme illustrating Arching zone (Modified from [10]).

- **Effect of shallow cover depth**: When the tunnel depth is shallow, the soil's ability to behave like an arch is limited. This results in greater vertical deformation of the soil above the tunnel, thus increasing surface settlement. Studies have shown that for low depth-to-diameter ratios (H/D), the maximum settlement is higher and the affected area is larger [28], this phenomenon is clearly represented in Figure 2.4 for a tunnel section in Zone 1. [11]

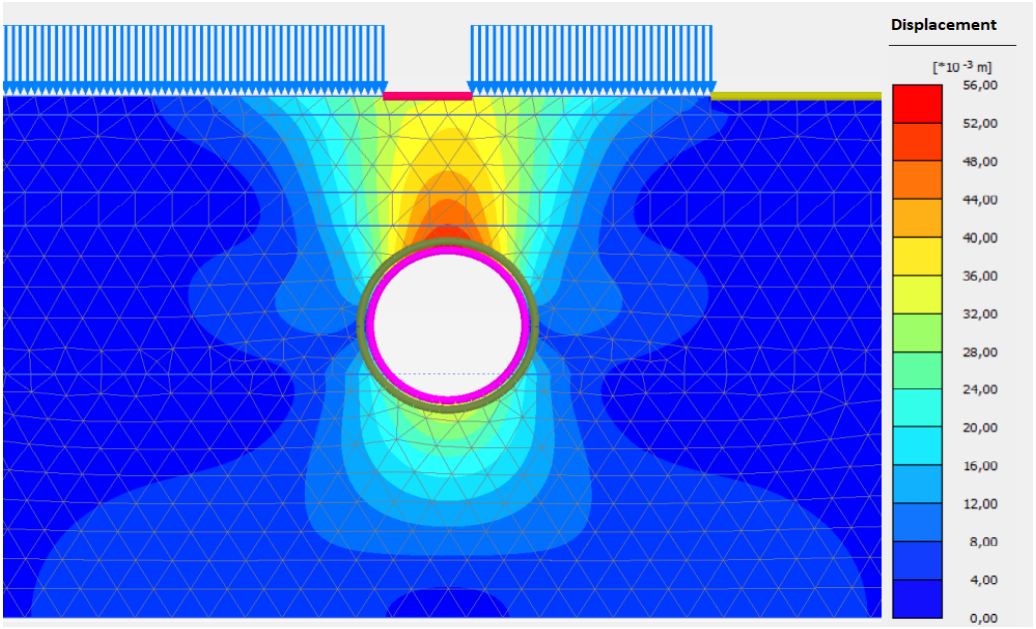

Figure 2.4: Simulation under Plaxis 2D software showing the arching zone for a tunnel depth of 20m (Extension line 1). [11]

The efficiency of that arch and thus the reduction in settlement at the tunnel crown and surface is a strong function of the cover depth.

- **Effect of deep cover depth**: As the cover depth increases, the arching effect becomes more pronounced. This allows the soil above the tunnel to deform less, thus reducing surface settlement. A greater cover depth generally reduces surface settlement by promoting the arching effect. However, even a significant cover depth may not be sufficient to limit settlement if other factors, such as soil properties and tunnel diameter, are not optimized.

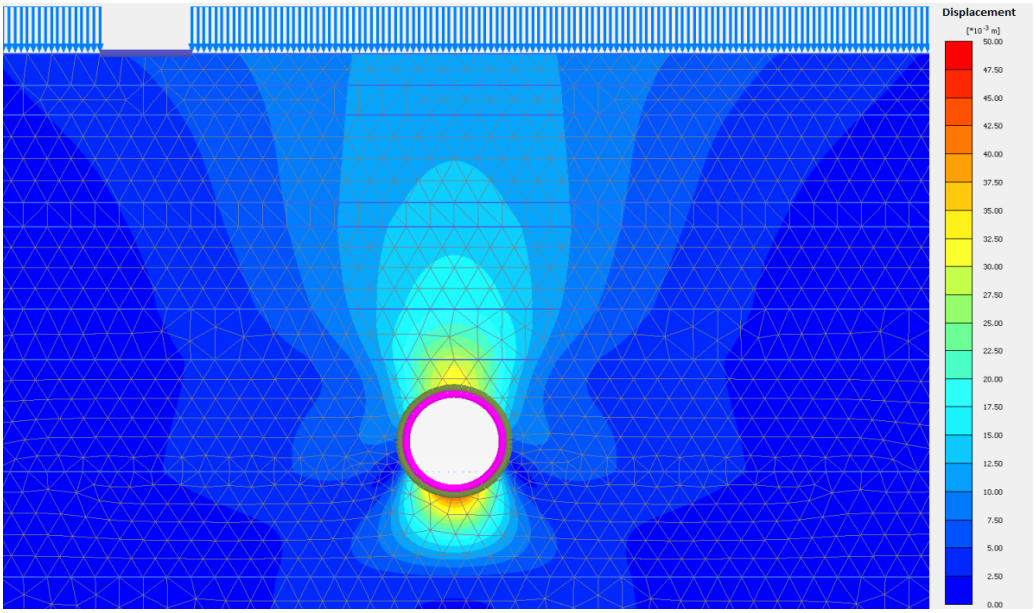

Figure 2.5: Simulation under Plaxis 2D software showing the arching zone for a tunnel depth of 66m (Extension line 1). [11]

An illustration of the relationship between the tunnel depth-to-diameter ratio (H/D) and the observed ground surface settlement, for the case of extension of line 1, is provided in Figure 2.6.

In the present study, given the tunnel diameter of 10,5m and friction angle of 20°, and according to Terzaghi theory, the arching effect becomes significant only when H/D ratio exceeds 3,5. As shown in Figure 2.6, only 14 settlement measurement points, for which H/D is greater than 3,5, were recorded along the tunnel section N°1. we can see that surface settlements in this tunnel section are very small (less than 8mm).

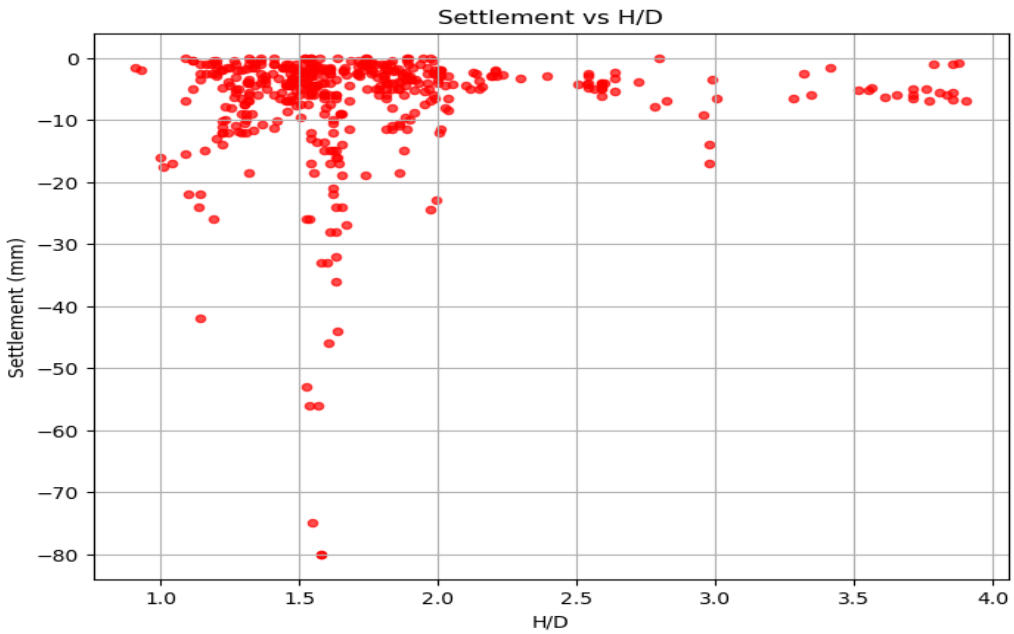

Figure 2.6: Settlement vs H/D Scatter plot (Extension of line 1-Algiers metro).

2.3.1.3 Distance from station

The distance from station or distance from the launching shaft plays an important role in the development of surface settlement during tunnel excavation using an Earth Pressure Balance (EPB) shield. Generally, the most significant ground deformations are observed near the starting point of the tunnel. This is because, in the early stages, the machine is not yet fully stabilized: excavation parameters such as pressure, foam injection rate, and advance speed are still being adjusted, and the temporary support system is not yet working at full efficiency. As tunneling progresses, these parameters become more stable, allowing for better control of ground loss and, consequently, surface settlement. Therefore, the further the machine advances from the launch shaft, the more consistent the excavation becomes, often leading to a gradual reduction in surface settlement.

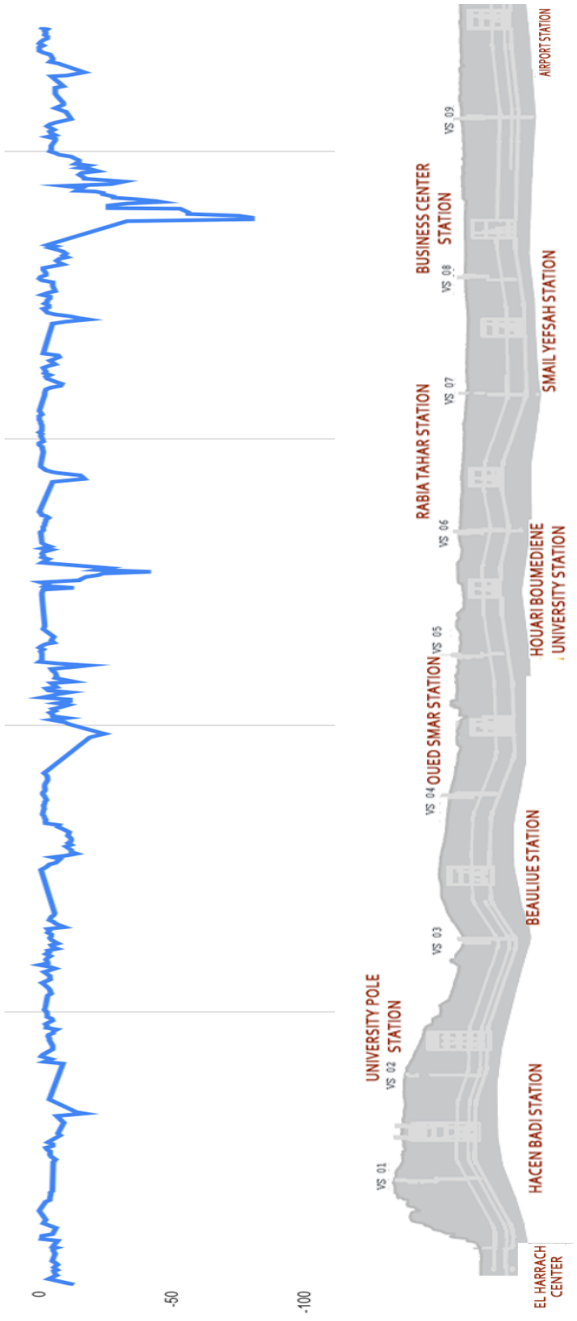

Figure 2.7: Recorded settlement along the tunnel drive from Tunnel section 1 to 9

2.3.2 Geological Conditions

Several geological parameters are known to significantly influence ground surface settlement during tunnel excavation. These include the nature of the soil (geological profile), groundwater table level, internal friction angle, soil permeability, soil cohesion, the elastic modulus, and the compression modulus. In the following sections, some of these factors are discussed in more detail to highlight their contribution to surface deformation.

2.3.2.1 Soil permeability

Soil permeability is a key factor in the behavior of soil under load. It expresses the soil's ability to allow water to flow through it under the effect of a pressure gradient or gravity. The more permeable a material is, the faster water drains out, which allows settlement to occur over a relatively short period of time, as is often the case with sandy or gravelly soils. In contrast, in fine-grained soils with low permeability, such as clays, water drainage is very slow, leading to gradual settlement over several months or even years. The coefficient of consolidation C_v is used to quantify this phenomenon, taking into account permeability, compressibility, and soil structure.

2.3.2.2 Groundwater table level

Groundwater table level has a significant influence on the effective stress in the soil, which is the actual force supported by the soil grain structure. Effective stress is defined by the equation:

$$\sigma' = \sigma_{\text{total}} - u$$

Where u is the pore water pressure. Therefore, a drop in the groundwater level results in a decrease in pore pressure, which increases effective stress and causes soil settlement through consolidation. Conversely, a rise in the groundwater level reduces effective stress, which can slow down or temporarily prevent settlement, and in some clayey soils, it may even cause temporary swelling.

2.3.2.3 Soil Cohesion

Soil cohesion is as decisive a factor as the other parameters influencing the magnitude of surface settlement. It reflects the ability of soil particles to resist separation and remain bonded together under the effect of interparticle forces (electrostatic, capillary, or suction forces). This cohesion helps reduce deformations, contributes to the stability of the soil structure, and enhances its resistance to applied loads. A soil with high cohesion (such as cohesive clays) generally exhibits better resistance to deformation and, consequently, reduced settlement under load.

Conversely, in the case of low cohesion, particularly in dry, very loose, or reworked soils, the soil is more likely to deform under stress, leading to greater settlements.

It is also important to emphasize that cohesion is strongly influenced by water content. In fact, increasing moisture reduces the cohesion forces between particles (especially in clayey soils), which can weaken the soil structure and increase its compressibility, leading to more significant settlement.

2.3.3 Operational parameters of the EPB-TBM (Tunnel Boring Machine)

Among the many operational parameters of the Earth Pressure Balance (EPB) shield that influence ground surface settlement, we can mention: Face Pressure, Penetration rate , Mass Loss, Tail Void Grouting , Thrust cylinder , Pitching angle.

In this section, we will focus on most of these parameters, particularly those that are likely to have a significant influence [24] on settlement generation.

2.3.3.1 Face Pressure

Face pressure plays a crucial role during the excavation of a tunnel using an Earth Pressure Balance (EPB) shield. It corresponds to the pressure exerted by the excavation chamber on the tunnel face and aims to balance the forces exerted by the soil and pore water. This pressure allows for the temporary support of the ground at the face, ensuring stability during shield advancement and preventing collapses that could lead to the formation of voids and, consequently, surface settlements.

The variation in face pressure has a direct impact on soil behavior and the resulting settlements.

Table 2.1 presents the possible scenarios based on the face pressure conditions.

Table 2.1: Effects of Face Pressure Variations on Tunnel Stability and Ground Settlement

Face Pressure Condition	**Effect on Stability**	**Consequence on Surface Settlement**
Insufficient face pressure	Fails to counterbalance the forces exerted by the soil and pore water	Instability at the face, inflow of soil into the chamber, and thus the formation of voids at the tunnel face, resulting in significant surface settlements
Optimal face pressure	Provides mechanical equilibrium at the face, enables precise control of the excavated soil volume	Reduces settlements.
Excessive face pressure	Can lead to overpressure in the excavation chamber, forcing the soil outward	Potentially causing surface heave, especially in fine and saturated soils.

An illustration of the relationship between the Face Pressure and the observed ground surface settlement is provided in Figure 2.8.

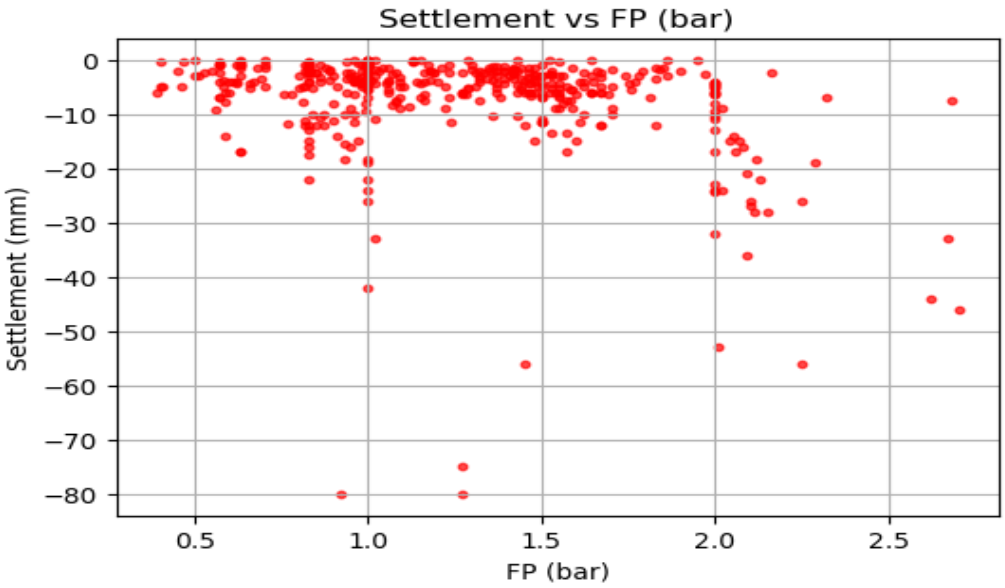

Figure 2.8: Settlement vs Face pressure Scatter plot (Extension of line 1-Algiers metro).

2.3.3.2 Penetration Rate

The penetration rate of tunnel boring machines (TBMs) is commonly used as a performance indicator during excavation works and serves as a key parameter for estimating the construction duration and associated costs.

It represents the ratio between the excavated distance and the time required for excavation, excluding pauses or operational stoppages. Generally expressed in millimeters per minute (mm/min) or meters per hour (m/h).

To maintain a balanced earth pressure during excavation, it is crucial for operators to adjust the muck extraction rate based on the penetration rate. If the muck extraction rate is too high compared to the TBM's advancement, too much soil is removed, which can lead to an imbalance and cause ground loss. On the other hand, if the extraction rate is too low compared to the penetration rate, the volume of excavated soil is less than the volume replaced by the shield's advance, which can result in excessive face pressure. Meaning that the spoil removal rate must be adjusted accordingly to maintain optimal face pressure.

An illustration of the relationship between the Penetration-rate and the observed ground surface settlement is provided in Figure 2.9.

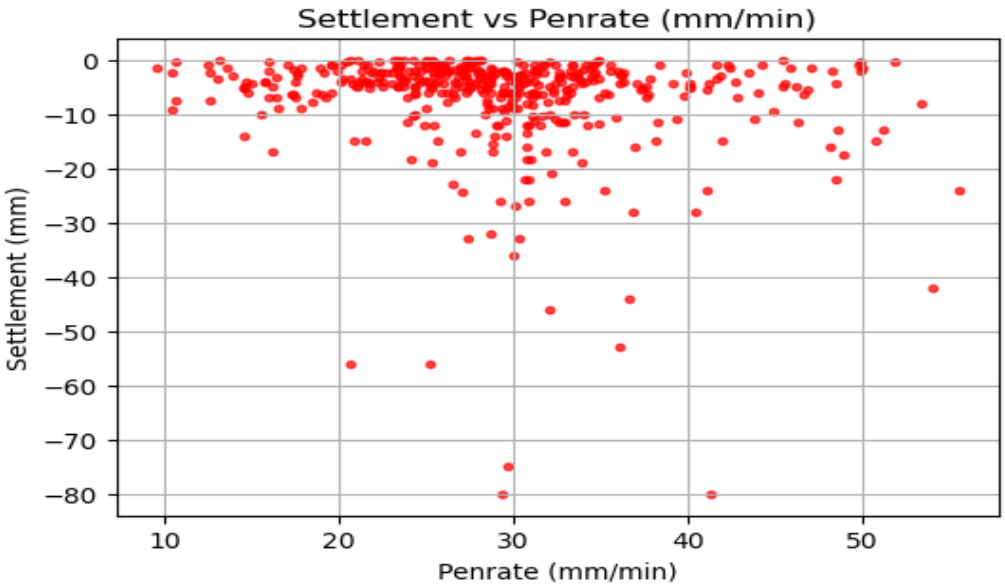

Figure 2.9: Settlement vs Penetration-rate Scatter plot (Extension of line 1-Algiers metro).

2.3.3.3 Mass Loss

Mass loss represents the difference between the theoretical mass of soil to be excavated (calculated as the product of soil density and the excavated volume) and the actual mass of soil removed during TBM operation. This discrepancy is an important indicator that can be directly linked to ground surface deformations. A negative mass loss value means that more soil was excavated than anticipated, which may indicate over-excavation, loss of confinement, or ground loosening. Such conditions can create voids around the tunnel lining, resulting in ground surface settlement. On the other hand, a positive mass loss value indicates that less soil was excavated than expected which may suggest under-excavation or face clogging. This can lead to a build-up of pressure at the tunnel face or along the shield, potentially causing ground uplift, also known as heave.

An illustration of the relationship between the Mass loss and the observed ground surface settlement is provided in Figure 2.10.

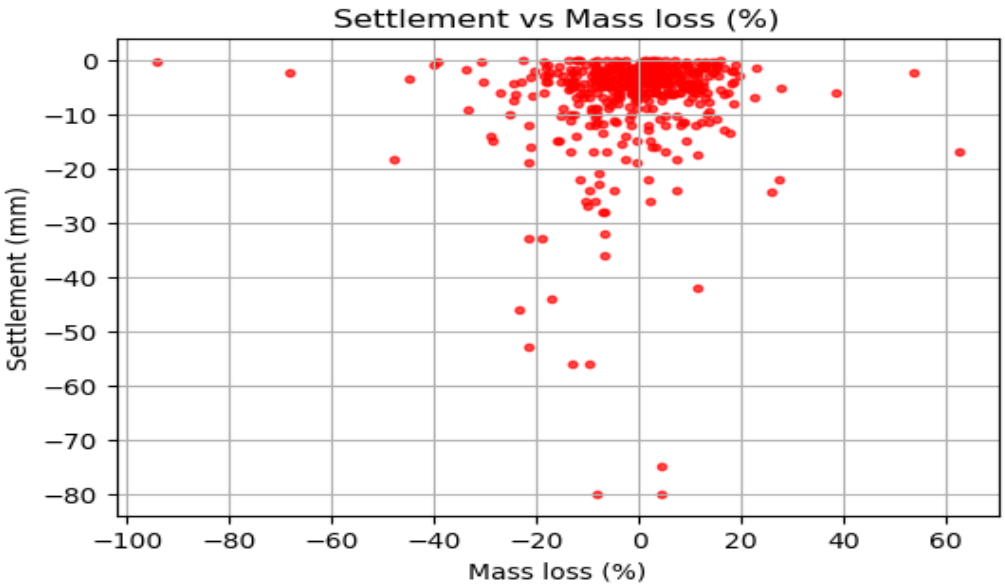

Figure 2.10: Settlement vs Mass Loss Scatter plot (Extension of line 1-Algiers metro).

2.3.3.4 Thrust Cylinder

Thrust is the axial force applied by a TBM's hydraulic jacks to advance the shield against the tunnel face. In EPB-TBMs, this thrust also contributes to maintaining face pressure, ensuring stability at the tunnel face and preventing collapse or over-excavation of the cavity created during excavation.

Although thrust itself does not directly cause ground settlement, it has a critical indirect effect by influencing key mechanisms such as face pressure control, mass loss, and face stability [29]. Therefore, analyzing thrust in isolation is insufficient, as its effect is intrinsically linked to other operational parameters. Table 2.2 summarizes the influence of different thrust regimes on ground behavior.

Table 2.2: Effects of Different Thrust Regimes During Excavation

Thrust regime	**Mechanism**	**Mass loss**	**Result**
Excessive thrust	-Cutter over-penetration -Soil over-excavation in the chamber -Temporary face heave	Gradual mass loss as face heave relaxes	Delayed settlement
Insufficient thrust	-Cutter stalls against ground -Chamber under-filled Face pressure drop	Sudden Mass loss at face	Immediate surface settlement

An illustration of the relationship between the Thrust and the observed ground surface settlement is provided in Figure 2.11.

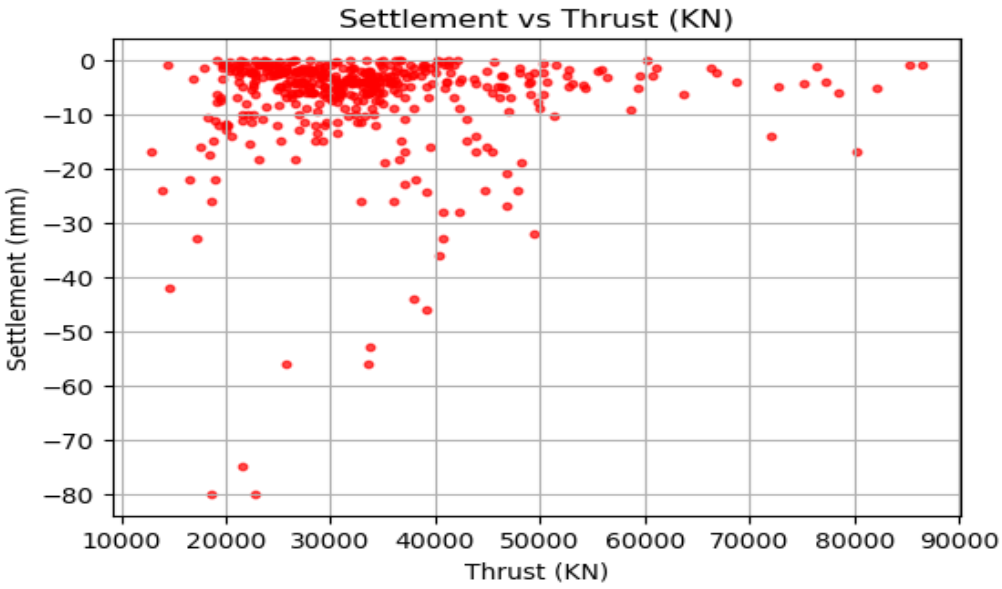

Figure 2.11: Settlement vs Thrust cylinder Scatter plot (Extension of line 1-Algiers metro).

2.3.3.5 Tail Void Grouting

The advancement of the shield (TBM) results in the formation of an annular void between the excavated ground and the installed tunnel lining. If left unfilled or inadequately filled, this void allows the surrounding soil to migrate toward the tunnel, leading to ground subsidence and surface settlements. Grouting is essential to fill this gap and counteract soil movement, thereby limiting ground deformations.

The performance of the grouting process is primarily influenced by parameters such as injection pressure and grout volume. An optimal balance between these factors is critical to ensure effective backfilling and structural integrity. The effects of various injection pressure scenarios on ground stability are summarized in Table 2.3.

Table 2.3: Effects of Injection Pressure on Backfilling Grout Performance

Injection Pressure	**Potential Consequences**	**Impact on Stability**
Sufficient / Optimal	- Homogeneous grout distribution in the annular void - Soil movements toward the tunnel prevented	- Ensures structural stability - Minimizes settlement risk
Excessive	- Ground heave - Possible damage to tunnel lining	- Overstressing of surrounding ground - Potential structural damage
Insufficient	- Incomplete void filling - Potential for water ingress	- Increased risk of differential settlements - Compromised tunnel durability

An illustration of the relationship between the Tail void Grouting and the observed ground surface settlement is provided in Figure 2.12.

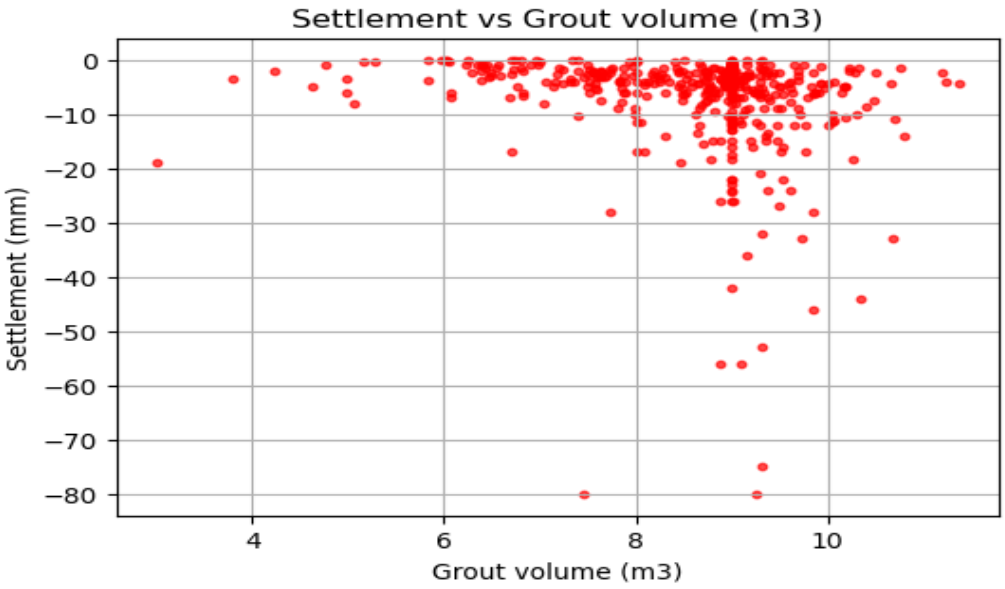

Figure 2.12: Settlement vs Tail void Grouting Scatter plot (Extension of line 1-Algiers metro).

2.3.4 Summary

Table 2.4 summarizes the various factors influencing settlement, that have been considered in the present study.

Table 2.4: Categories and associated influencing factors

Category	**Factors**
Tunnel Geometry	Cover depth (m) Tunnel Diameter (m) Distance from Station (m)
Geological Conditions	Soil permeability (m/s) Groundwater table level (m) Soil cohesion (kpa)
Shield Operation Factors	Face pressure (bar) Penetration rate (mm/min) Mass loss (%) Thrust cylinder (KN) Tail void Grouting (m^3)

2.4 Settlement Monitoring Instruments

Surface settlement during EPB–TBM tunneling is monitored using surface markers (leveling benchmarks and survey targets), while multi-point borehole extensometers (settlement meters) (MPBX) are used for subsurface settlement. These instruments are installed along the tunnel axis and referenced to stable control points outside the zone of influence, with data collected periodically. [30, 31].

2.4.1 Surface markers and settlement arrays

For the of the Extension of Algiers metro ligne "1" a large number of surface settlement markers and settlement arrays were installed along the entire tunnel alignment to measure and record surface settlements. Typically, surface settlement markers were installed on the tunnel axis approximately every 12.5 or 25 meters intervals and settlement arrays were installed in groups of 3 every 50 meters: one positioned on the tunnel axis, and the other two placed 10 meters on either side of the axis (Figure 2.13).

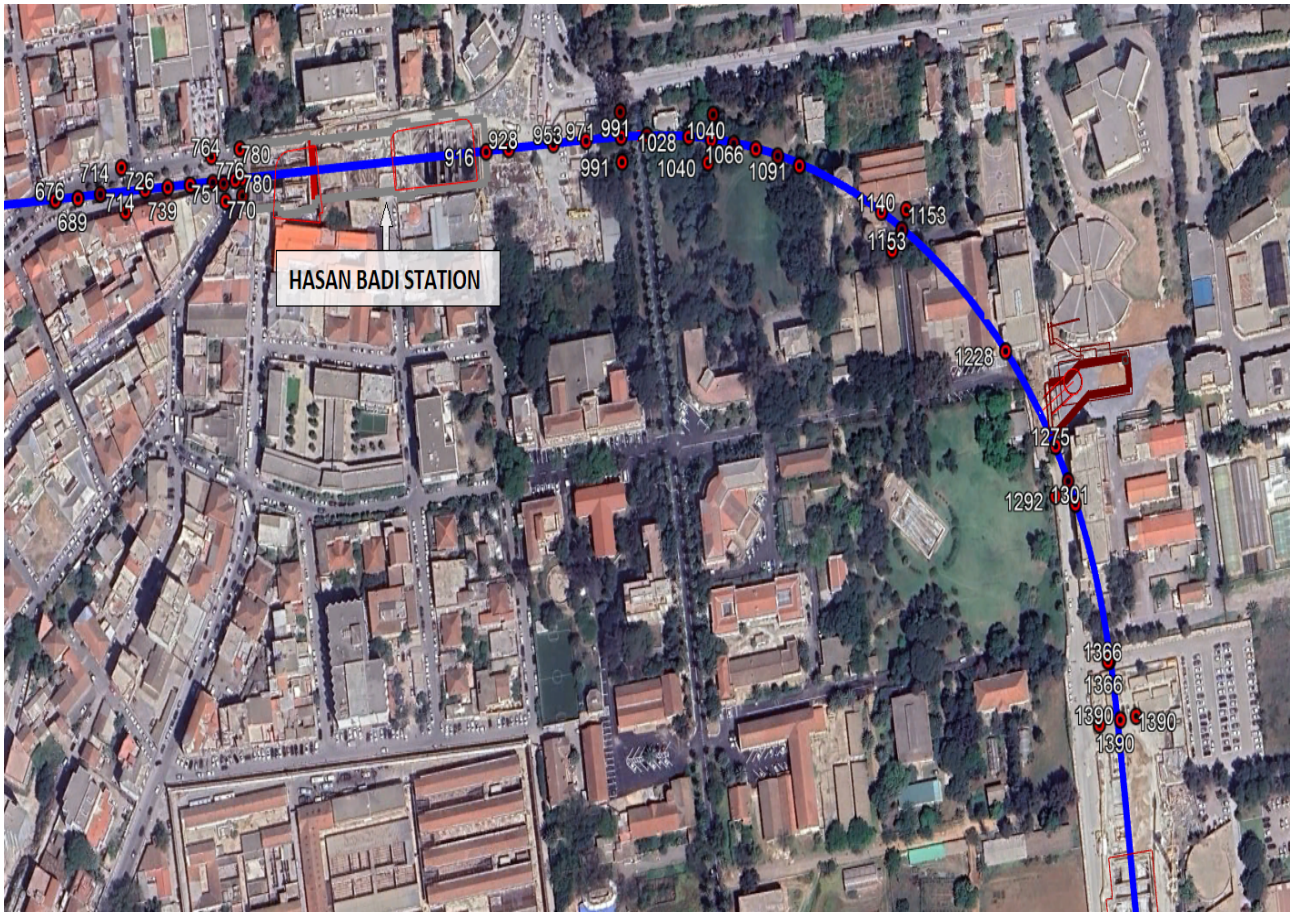

Figure 2.13: Distribution of settlement markers and arrays of settlement markers in tunnel section 2.

In cases where surface obstacles, such as buildings or other infrastructure, prevent the precise installation of measurement equipment, the layout of the points is adjusted accordingly, and the monitoring plan is updated to reflect these changes.

2.4.1.1 Execution

Surface settlement along the tunnel alignment is monitored using conventional measurement rods. These consist of 1-meter-long steel bars that are anchored into a non-deformable structure (such as a concrete block). At the bottom end, each bar is welded or fixed to a 20×20cm metallic plate, which ensures a stable connection to the underlying support.

The free (upper) end of the rod is exposed at the surface, where precise leveling measurements can be taken using standard surveying instruments. This exposed tip serves as the reference point for vertical displacement monitoring.

The Z-coordinate (elevation) of this point is recorded periodically, before, during, and after tunnel excavation. Any decrease in Z indicates vertical ground settlement. By installing a series of such rods along the tunnel alignment, a detailed settlement profile can be developed over time.

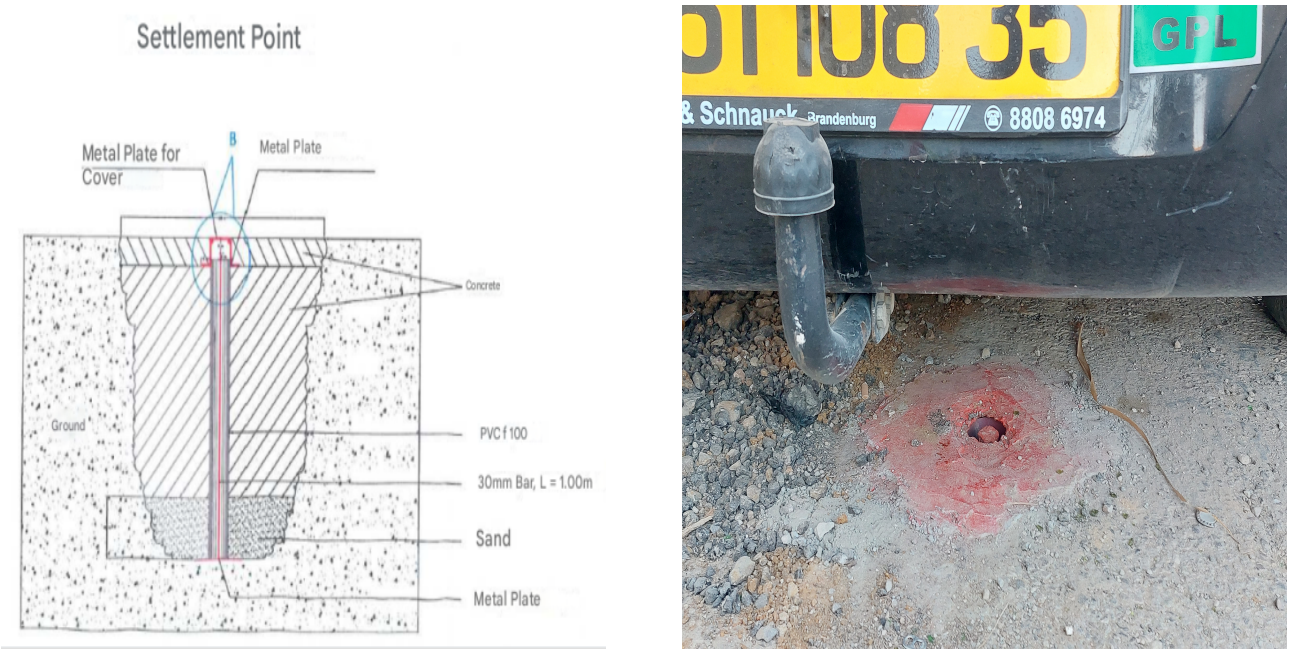

(a) Settlement marker schematic

(b) Settlement marker at pk1+315.00

Figure 2.14: Settlement marker

2.4.1.2 Reading frequency

The reading frequency is linked to the progress of the excavation by the TBM.

Surface settlement measurements are taken once per day (daily) for points located within the range of (-50 m; +50 m) along the tunnel axis relative to the TBM's excavation face, and once every two (2) days for points within the range of (-100 m; +100 m). Outside the (-100 m; +100 m) zone, the frequency becomes monthly and is eventually stopped if stability is confirmed.

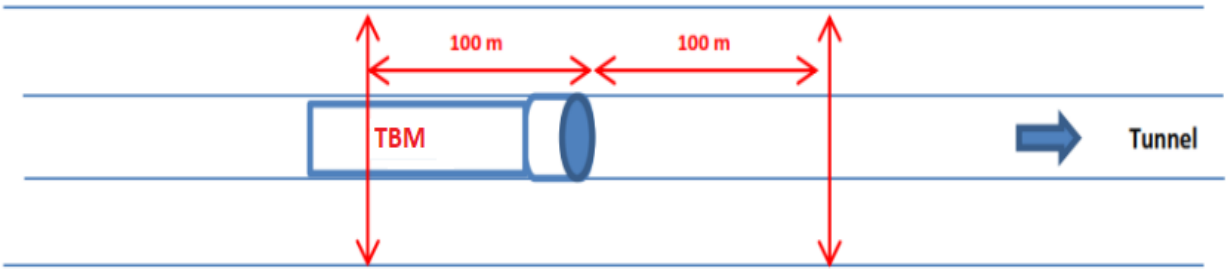

Figure 2.15: Reading zone for settlement marker and settlement arrays

Once relative settlement stability over time is observed, readings will be spaced out to once a week, then once a month, until they are fully discontinued. If an alert threshold is exceeded during measurements, a second exceptional reading may be carried out for the affected settlement points, continuing until stabilization is achieved.

2.4.2 Inclinometric monitoring

To assess deformation within the soil mass, inclinometers are installed to measure horizontal ground movements, particularly in areas affected by construction activities.

2.4.2.1 Execution

Inclinometer monitoring involves installing 55 mm diameter, 3-meter-long ABS tubes (Figure 2.16) into a borehole of project-specified diameter and depth. Each tube is equipped with four internal grooves forming two perpendicular axes; one groove is aligned perpendicular to the tunnel axis to measure horizontal displacements induced by tunneling.

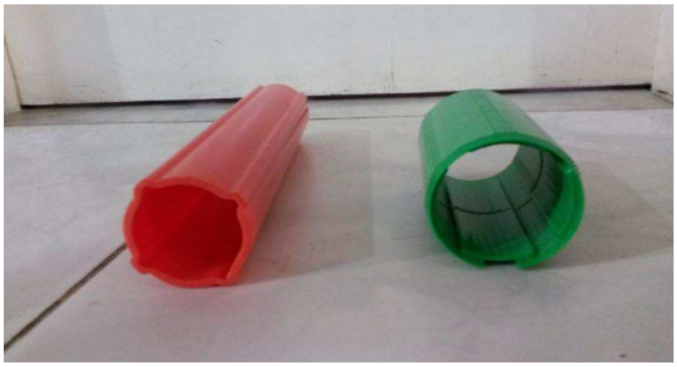

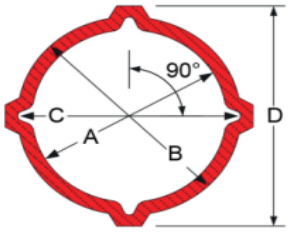

Type	A	B	C	D
2"	47 mm	55 mm	54 mm	60 mm

Figure 2.16: Inclinometer tubes

The tubes are interlocked at machined ends for precise alignment, with joints secured using rivets, sealing tape, and adhesive to ensure watertightness. A bottom cap protects the first tube from clogging, and the entire assembly is grouted in place using cement grout similar to the surrounding soil, poured from the bottom up to avoid voids. At the surface, the tubes are covered by metal protection caps.

Inclinometers measure horizontal ground deformation by recording tilt angles along the depth of a borehole using a biaxial probe guided within grooved ABS tubes. The inclinometer probe is lowered at regular depth intervals (e.g., every 0.5m or 1m) and measures the inclination relative to the vertical axis. The recorded tilt angles θ at each depth are then converted into cumulative horizontal displacements using numerical integration. This is expressed as:

$$u(z) = \int_{z_0}^{z} \tan(\theta(s))\, ds$$

where $u(z)$ is the horizontal displacement at depth z, $\theta(s)$ is the tilt angle at point s, and z_0 is the reference depth (typically the bottom of the borehole). By processing the tilt data in this manner, engineers can reconstruct the lateral deformation profile of the ground and monitor potential movements toward or away from the tunnel axis with high precision.

Inclinometer installations are typically spaced at two per special section, with depth depending on ground cover and tunnel alignment.

2.4.2.2 Reading frequency

After the initial reading is established, 3 readings will be taken following the passage of the TBM for each section. Additional measurements were carried out when necessary.

2.4.3 Settlement Meters

Settlement meters or settlement gauges, are simple and robust measuring instruments used to monitor underground settlements and uplift (Heaves). They were installed in locations defined by the project (areas where settlement is to be monitored and at depths where movement is likely to occur).

Settlement is transferred to the surface by transfer rods and is measured either through precision leveling or by topographic methods. The instrument is widely used to monitor the surface stability of underground excavations.

2.4.3.1 Execution

The instrument consists of a galvanized tubular rod inserted into a hole drilled by rotary methods. The lower end of the rod is anchored in a cement grout, while the upper part is protected by a PVC sleeve and terminates with either a leveling sphere or a target prism for measurement. Optional protective elements, such as galvanized tubes or concrete boxes, may also be installed around the top for added durability.

Leveling and reverse-leveling readings were taken from a stable benchmark located outside the tunnel's zone of influence. Vertical ground movements at the anchored depth are directly transferred to the surface via the rod, allowing for reliable monitoring with minimal instrumentation complexity.

Triple settlement meters can be installed in the same borehole, provided that the borehole diameter is compatible.

The settlement meters are located in the special sections, with 3 series of settlement meters installed at different depths as follows:

- Above the tunnel axis
- At both ends of the tunnel, approximately 8.00 m away (Tunnel diameter is 10 m) from the tunnel axis

Figure 2.17: An array of settlement meters above the tunnel axis at pk2+654,00.

2.4.3.2 Reading frequency

The frequency of readings is also linked to the progress of the TBM excavation. Settlement measurements are taken once per day (daily) for points within the range of (-50 m; +50 m) along the tunnel axis and relative to the TBM's excavation front, and once every two (02) days for points within the range of (-100 m; +100 m).

When the excavation front is more than 100 meters away from the special section, if stability is observed in the measurements, readings will be scheduled once a month (01/month) for 3 months, after which measurements will be suspended until further notice (in the case of buildings).

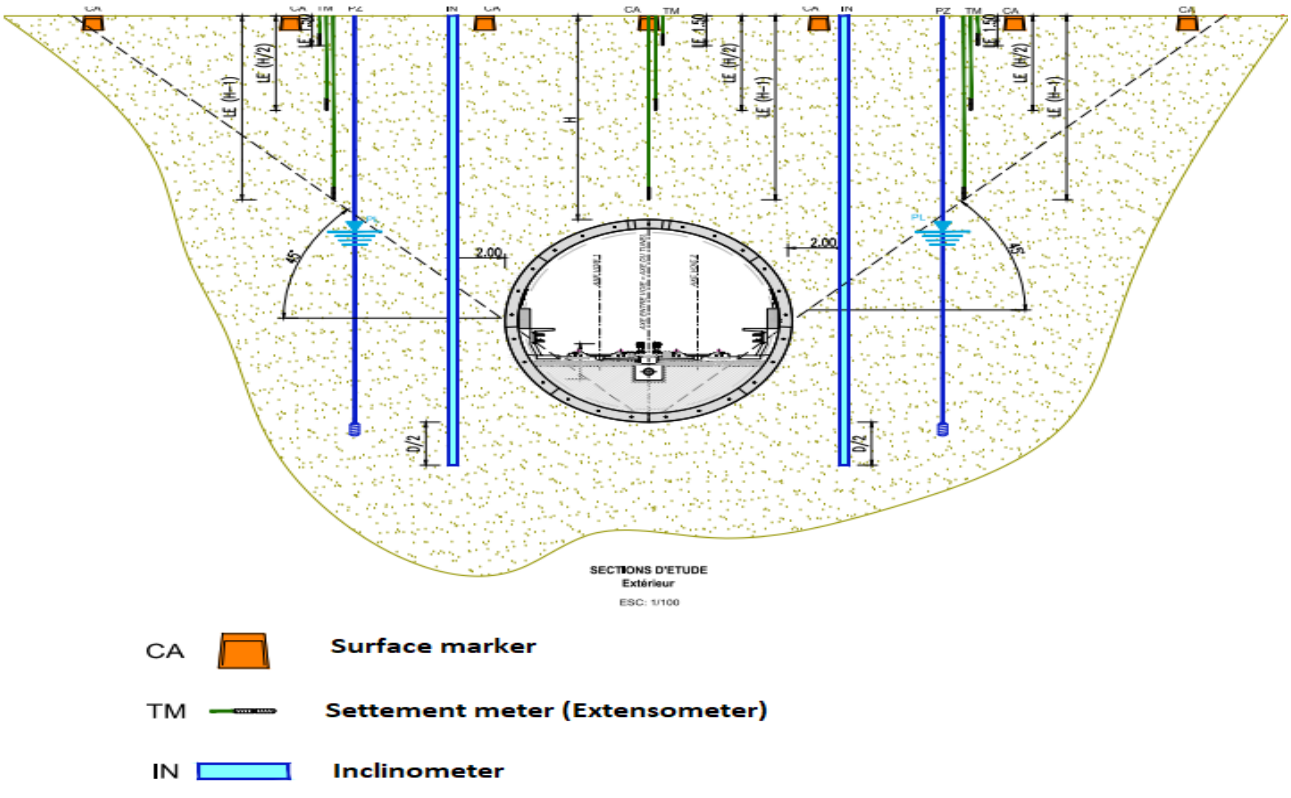

Figure 2.18: Instrument used to measure and record settlement.

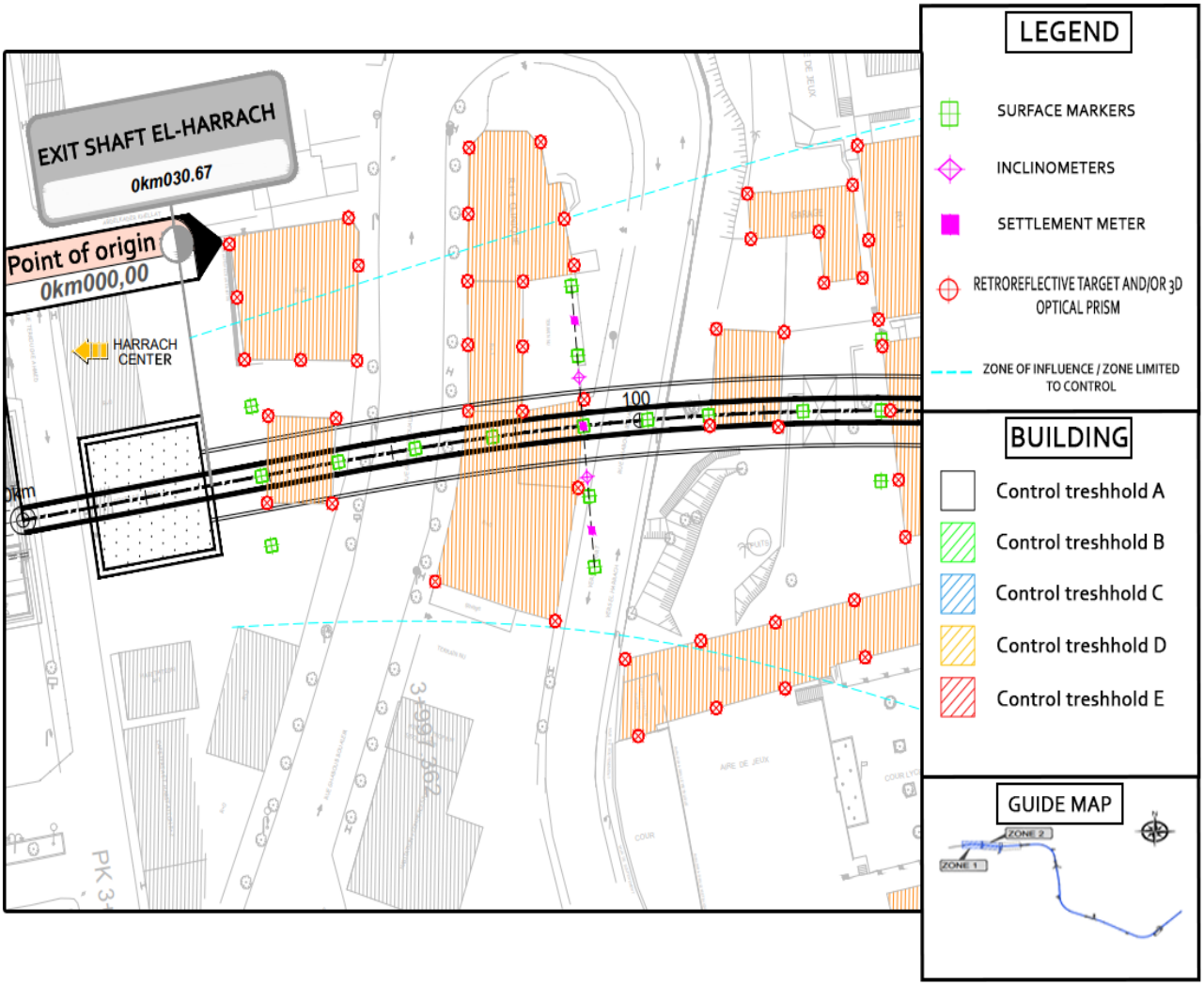

Figure 2.19: Instrument distribution plan at tunnel section 1 pk0+000,0 to pk0+150,00. (Appendix B)

The highlighted buildings in Figure 2.19 represents the control threshold for additional admissible movements according to classification (Figure 2.19), in Tunnel section 1 (El-harrach to Hasan Badi) the sensibility levels are devised into 3 types (Figure 2.20)

Figure 2.20: Identification of sensitivity types along Tunnel section 1.

Table 2.5: Allowable Settlement Limits Based on Structural Sensitivity and Control Thresholds

Parameter		Allowable settlement (mm)		
Control threshold		GREEN	YELLOW	RED
Type A	- Areas without buildings - Streets with vehicular roads	<30	30-50	>50
Type D	- Surface-foundation buildings - Surface damage - No apparent damage	<10	10-15	>15
Type E	- Buildings with damaged surface foundations or monumental buildings	<5	5-10	>10

2.5 Extraction and Analysis of Ground Surface Settlements

The primary objective of the measurements with settlement markers is to measure maximum surface settlements above the tunnel centerline (Figure 2.21).

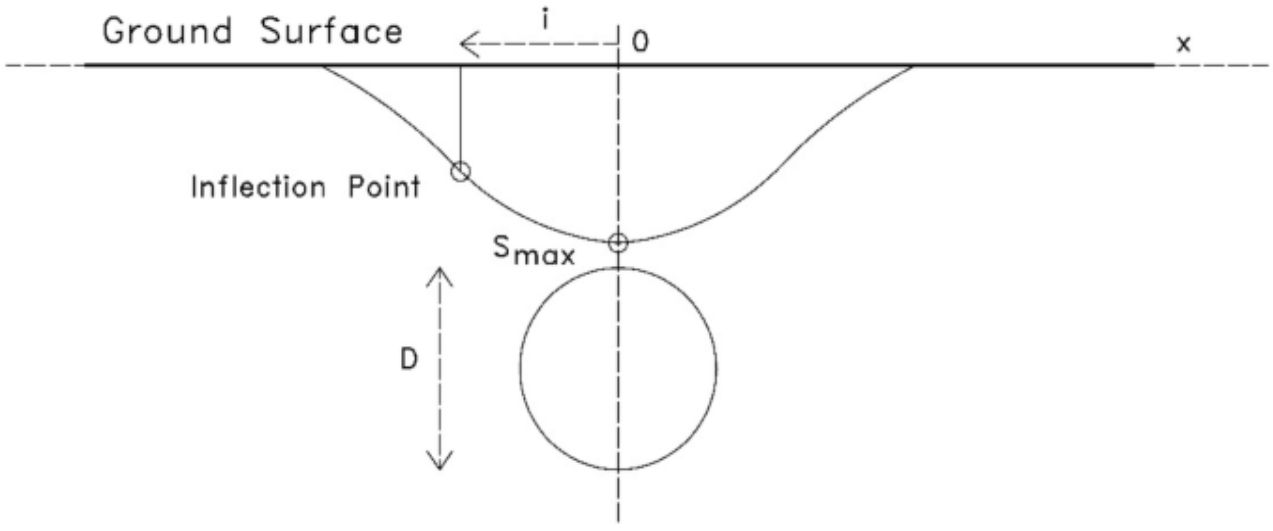

Figure 2.21: Maximum surface settlement [12].

Additionally, readings were taken every day before and after shield passing but increased to higher frequency (i.e., every 2–4 h) during shield passing in order to capture the development of surface settlements. Surface settlement markers also allow the observation of longitudinal surface settlement profiles (Figure 2.22) which tend to reach a maximum after the shield's passing then stabilize. It is at that moment where the maximum GSS is extracted.

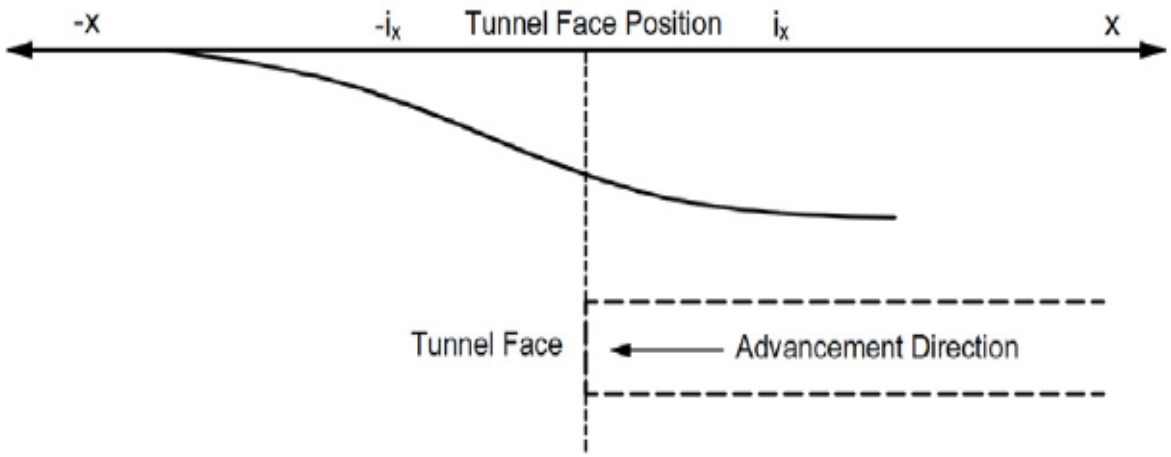

Figure 2.22: Longitudinal settlement trough [13].

Figure 2.23 shows examples of settlement recordings using different instruments mentioned above, we can clearly see resemblance of the longitudinal settlement trough and the stabilization of settlement after the shields passing.

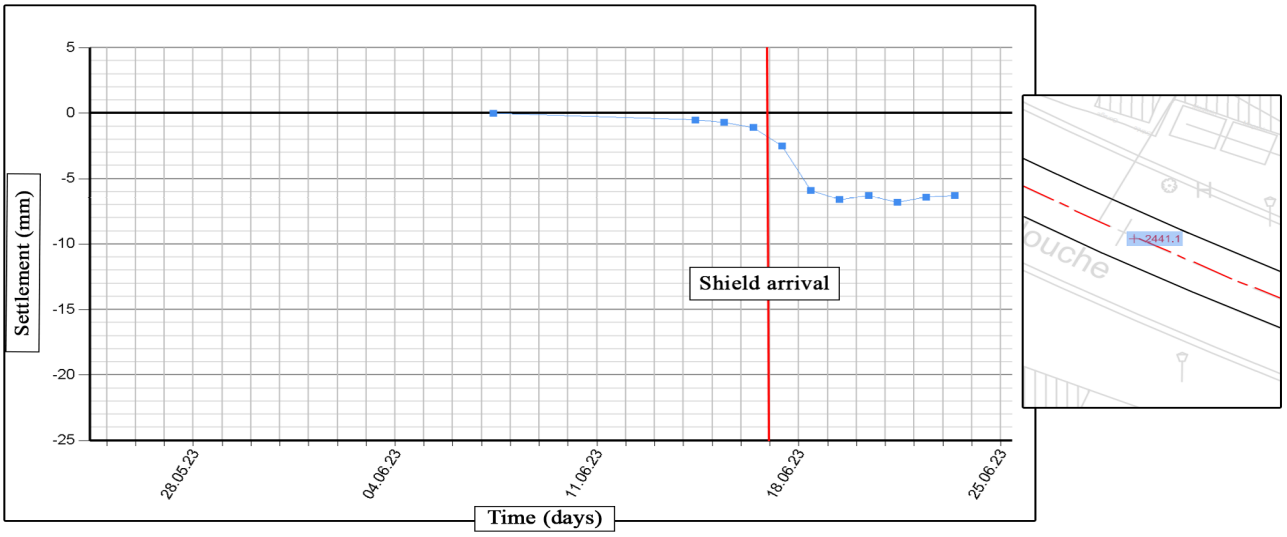

(a) Recording of a surface marker at pk 2+441,00.

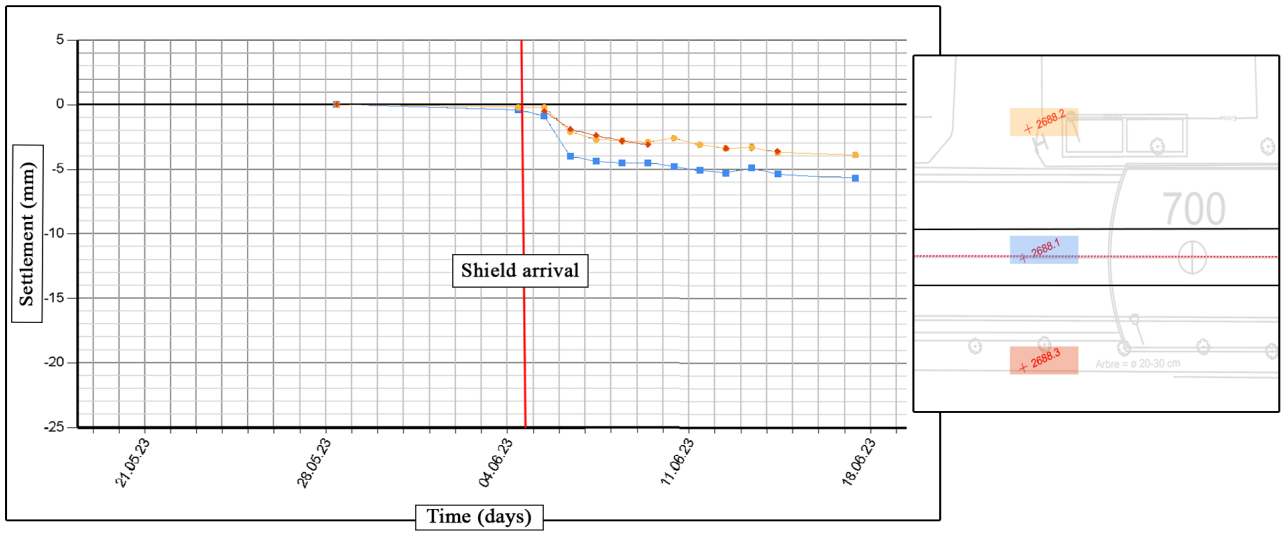

(b) Recording of an array of surface markers at pk 2+688,00.

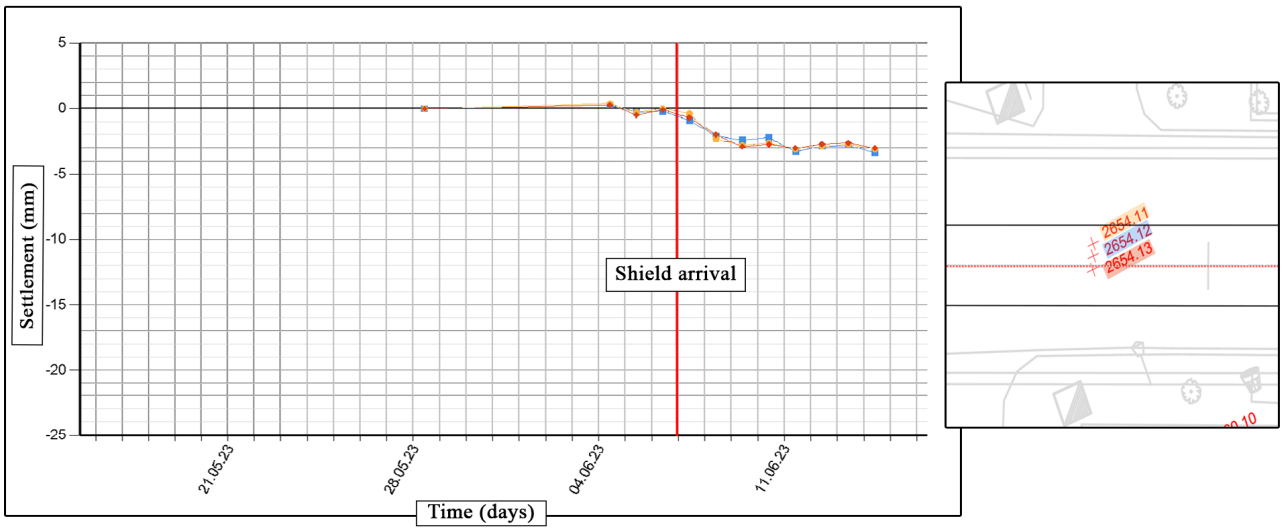

(c) Settlement meter (Extensometer) recordings at pk 2+654,00.

Figure 2.23: Examples of settlement recordings using surface markers and extensometers.

Figure 2.24 shows the evolution of ground settlement as a function of the horizontal distance from the tunnel axis, at section pk2+688,00 m. The graph indicates that the maximum settlement consistently occurs at the centerline of the tunnel, where the settlement curve typically takes the shape of a trough. Settlement increases progressively in depth while also spreading laterally, affecting areas to the left and right of the axis, although to a lesser extent.

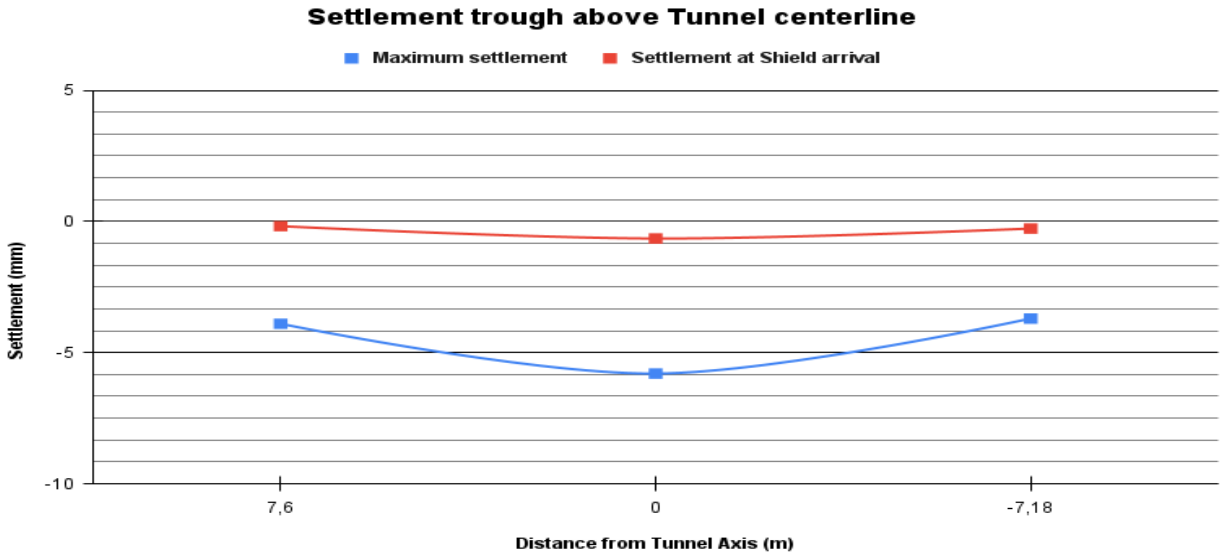

Figure 2.24: The settlement profile trough at section pk2+688,00.

It is clearly observed that this curve exhibits a shape similar to the Gaussian curve, as demonstrated by Peck. In 1969, he furthered his research and showed that a Gaussian curve effectively models the ground settlement induced by tunnel excavation. Based on data from various sites and projects he studied, he concluded that the settlement curve, in cross-section, is generally symmetrical with respect to the tunnel's central axis. He proposed specific equations to calculate the settlement at any point along the cross-sectional profile.

The following equation is identified among these:

$$S_v = S_{\max} \cdot \exp\left(\frac{-Y^2}{2i^2}\right)$$

Where:

- Sv: is the vertical surface settlement at the Y distance from tunnel centerline.
- $Smax$: is the maximum ground surface settlement that usually occurs above tunnel centerline.
- i: is horizontal distance from tunnel centre to point of inflection of the settlement trough.

2.6 Conclusion

This chapter examined the phenomenon of ground surface settlement, particularly in the context of EPB-TBM tunneling. The analysis focused on three main categories of influencing parameters: geometric, geological, and TBM operational.

Among geometric parameters, only cover depth and distance from the launching shaft were retained as significant. The geological parameters discussed such as cohesion, permeability, and water table level were also identified as key factors in the settlement process. Regarding TBM operational parameters, all were found to be effective contributors, either directly or through interdependent mechanisms such as mass loss or face instability.

The chapter also presented the instrumentation used to monitor ground deformation, including surface markers, inclinometers, and settlement meters. Measurement frequency increased during shield passage to better capture settlement evolution. Surface marker data enabled the observation of longitudinal and transverse settlement profiles, which stabilized after shield advance. The settlement curves typically formed a symmetrical trough, with maximum displacement at the tunnel centerline This profile guided the extraction of maximum ground surface settlement (GSS), to be used in the predictive modeling that follows.

Chapter 3

Overview of Artificial Neural Networks

3.1 Introduction

To effectively apply Artificial Neural Networks (ANNs) in this study, it is essential to understand their core components namely the network architecture, activation functions, and supervised learning algorithms that enable training. This chapter begins with a brief overview of their biological inspiration and historical development, followed by a detailed explanation of the key technical concepts relevant to their implementation as predictive models.

3.2 Origins and inspiration

The concept of artificial neural networks is inspired by biological neural networks, which are part of the human nervous system. These networks consist of a large number of interconnected neurons (nerve cells) that generate electrical signals known as action potentials. These signals enable the rapid transmission of information over long distances within the body.

These neurons perform these key functions:

- Receive signals from outside through structures called dendrites.
- Processes the incoming signals in the cell body, determining whether the signal should be transmitted further
- Communicate signals to target cells which might be other neurons or muscles or glands via the axon through a junction called the synapse, which connects the axon with other neurons (Figure3.1) [14].

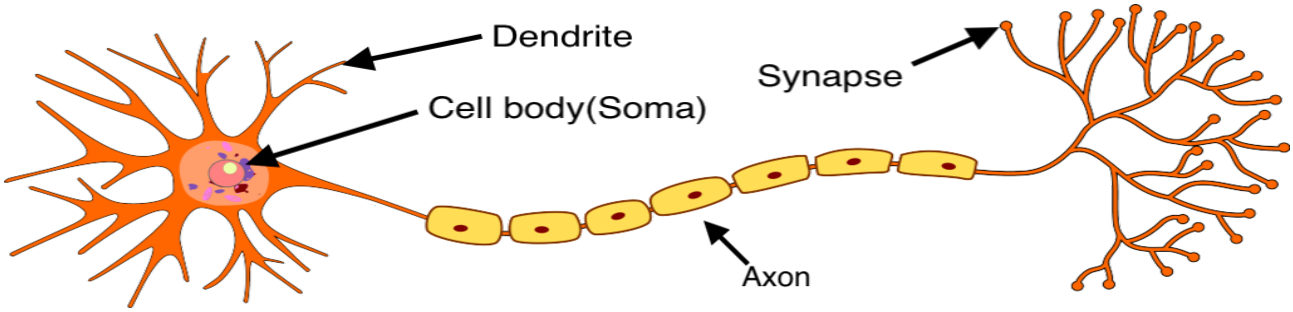

Figure 3.1: Biological Neural Network (Modified from [14]).

3.3 Artificial neurons (perceptrons)

The artificial neuron, also known as a perceptron, is the fundamental building block of a neural network. Conceptually, it is a mathematical model inspired by the structure and function of biological neurons. Functionally, it can be viewed as a simple logic gate that produces binary outputs based on weighted inputs and a threshold function [14]. The perceptron model typically comprises four main components:

Input values

Similarly to a dendrite in biological neurons, input values are passed to the neuron using this layer. These inputs can be a simple array of values, representing features of the data, which are then passed to the artificial neuron for further processing.

Weights and Bias

Weights are a set of numerical values associated with each input, used to determine the importance of each feature. Each input value is multiplied by its corresponding weight, and the results are summed together to produce a weighted sum.

A fixed number known as bias then added to this weighted sum, this bias helps the model make better predictions by allowing it to shift the activation function, improving flexibility.

Activation function

The final result (weighted sum + bias) is passed through an activation function. This function determines whether the neuron should be "activated" by producing an output based on that value. In a basic perceptron, the activation function is typically a step function [32] that outputs binary values (such as 0 or 1), allowing the model to make make binary decisions.

Output Layer

The output layer provides the final output of a neuron. This output can either be passed on to other neurons in deeper layers of the network or used directly as the model's final prediction in shallow ANNs.

Figure 3.2 describes a general model of an artificial neuron or a simple perceptron, where x_i is the input, w_i is the weight, $\sum$ denotes summation, and f is the activation (or transformation) function.

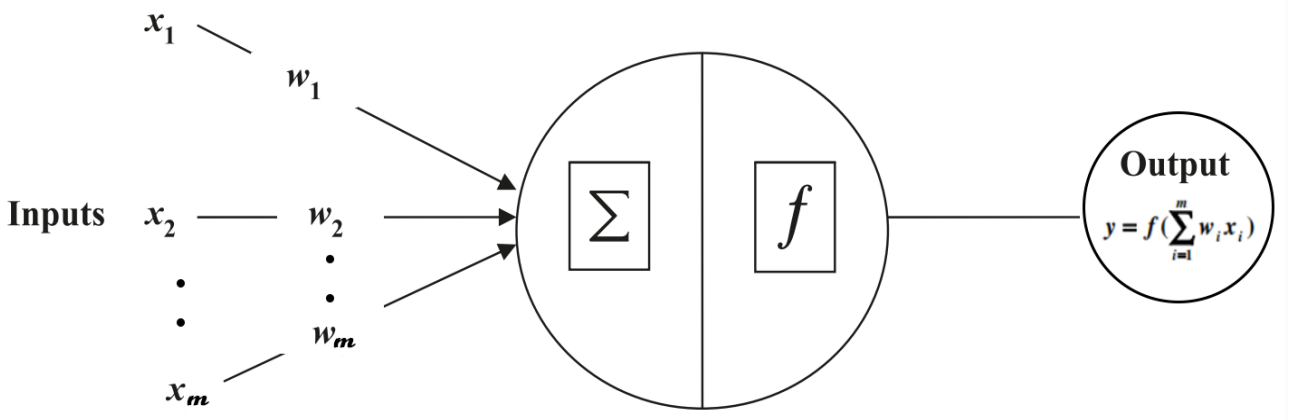

Figure 3.2: Simple perceptron (Modified from [15]).

3.4 Evolution of the ANN

McCulloch and Pitts' pioneering work in the 1940s is widely recognized as the foundation of artificial neural networks (ANNs). They introduced the first computational model of artificial neurons using electrical circuits, demonstrating that such networks could perform logical operations similar to those of Turing machines.

In the late 1950s, Frank Rosenblatt developed the perceptron and its related learning rule marking the first practical implementation of neural networks. However, the basic perceptron was limited in its capabilities, as it could only solve linearly separable problems [33].

During the 1970s, Marvin Minsky and Seymour Papert published *Perceptrons*, a critical analysis of the perceptron model. They emphasized its inability to solve non-linear problems such as XOR, which led to skepticism, reduced research funding, and a decline in interest in neural networks, an era later termed the "AI Winter" [34].

Interest in neural networks resurged in the late 1980s, largely due to the work of David Rumelhart, Geoffrey Hinton, and Ronald Williams. Their introduction of the backpropagation algorithm enabled the efficient training of multi-layer networks, addressing earlier limitations and revitalizing ANN research.

3.5 Artificial Neural Network (ANN)

An ANN is an information-processing system whose principal applications are optimization, classification, and prediction [15]. It consists of a number of interconnected processing elements, commonly referred to as neurons or perceptrons. These neurons or perceptrons are logically arranged into two or more layers in parallel, and interact with each other via weighted connections. Each neuron is connected to all the neurons in the next layer. There is an input layer where data is presented to the ANN, and an output layer that holds the response of the network to the input. It is the intermediate layers, also known as hidden layers, which enable these networks to represent and compute complicated associations between patterns. [35]

3.5.1 Layers of the ANN

Neural networks have evolved from simple to increasingly complex architectures. Initially, they consisted of only an input and an output layer, forming what is known as a single-layer neural network. The introduction of one or more hidden layers between the input and output transformed them into multi-layer neural networks. A typical multi-layer neural network thus comprises an input layer, one or more hidden layers, and an output layer.

The neural network that has a single hidden layer is called a shallow neural network or a vanilla neural network. A multi-layer neural network that contains two or more hidden layers is called a deep neural network. Most of the modern neural networks used in practical applications are deep neural networks [36]. The following table summarizes the branches of the neural network depending on the layer architecture.

Table 3.1: Types of Neural Network Architectures Based on Layer Depth

Single-layer Neural network		Input layer – Output layer
Multi-layer Neural network	Shallow neural network	Input layer – Hidden layer – Output layer
	Deep neural network	Input layer – Hidden layers – Output layer

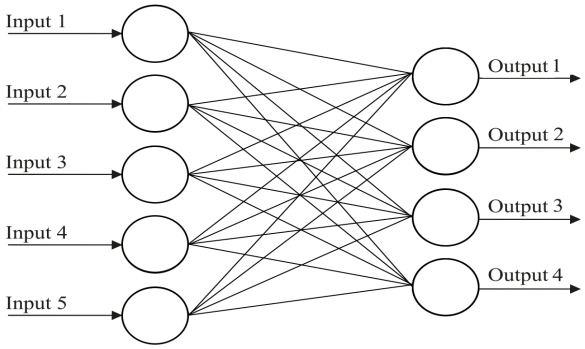

Figure 3.3: Single-layer ANN

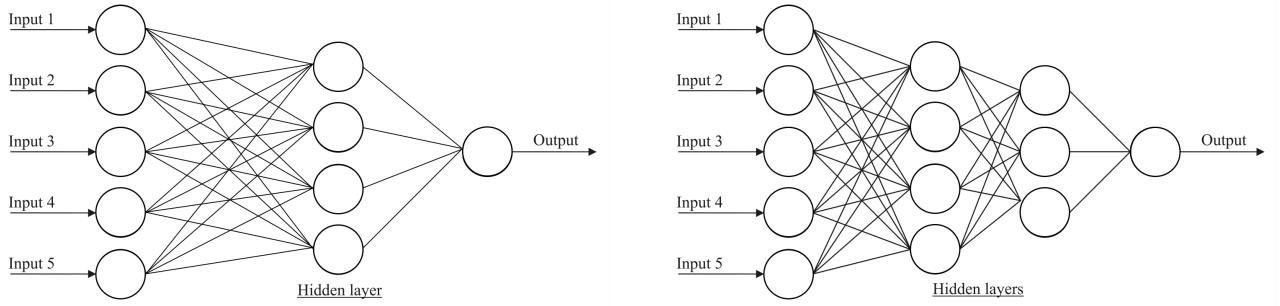

(a) Shallow multilayer ANN

(b) Deep multilayer ANN

Figure 3.4: Multi-layer ANN's.

3.6 Supervised Learning of a Neural Network

After understanding the structure of artificial neurons and how they form layers in an ANN, it becomes essential to look into how these networks actually learn and make predictions.

This learning process is commonly achieved through a process called supervised learning, this process can be summarized in the following steps:

- The weights are initialized with adequate values.
- The network is provided with input data from the training set, structured as pairs of input- expected output. The input is processed by the network to produce an output, which is then compared to the expected output in order to calculate the error.
- The weights are adjusted based on the calculated error.

- Steps 2 and 3 are repeated for all samples in the training dataset. This iterative process continues until the network's performance reaches an acceptable level.

3.6.1 Training of a Single-Layer Neural Network

The Delta Rule is the representative learning rule used in the training of single-layer neural networks [36]. It is a type of numerical method called gradient descent. provides an algorithm for updating the weights of the network based on the observed error that insights:

"If an input node contributes to the error of the output node, the weight between the two nodes is adjusted in proportion to the input value x_j, and the output error e_i ."

The training process using the delta rule for the single-layer neural network is summarized by the following steps:

1. The weights are initialized with adequate values.
2. The input from the training dataset, structured as pairs of input-desired output, is fed into the neural network. The output error e_i for each output node is computed by subtracting the actual output from the desired output:

$$e_i = d_i - y_i$$

3. The weight update is calculated using the Delta Rule as follows:

$$\Delta w_{ij} = \alpha \, e_i x_j$$

   where α is the learning rate, e_i is the output error, and x_j is the input value.

4. The weights are then adjusted by adding the computed change:

$$w_{ij} \leftarrow w_{ij} + \Delta w_{ij}$$

5. Steps 2–4 are performed for all examples in the training dataset.
6. Steps 2–5 are repeated iteratively until the total error falls below a predefined tolerance threshold.

The learning rate α determines how much the weight is changed per time. If this value is too high, the output wanders around the solution and fails to converge. In contrast, if it is too low, the calculation reaches the solution too slowly

These steps are almost identical to that of the process for the supervised learning in the "Supervised Learning of a Neural Network" section. The only difference is the addition of Step 6 states that the whole training process is repeated.

The single-layer neural network is limited in its applicability, as it can only solve problems that are linearly separable [36]. Consequently, its usage is restricted to relatively simple tasks, and it lacks the capacity to model complex, non-linear relationships.

3.6.2 Training of Multi-Layer Neural Network

In an effort to overcome the practical limitations of single-layer neural networks, the architecture evolved into a multi-layer structure. However, the previously introduced delta rule becomes ineffective in training such networks. This is because the error, the essential element for applying the delta rule for training, is not directly defined for the hidden layers. Training data only provides target outputs for the output layer, making it impossible to compute the error at hidden nodes using the same method (the difference between predicted and actual outputs) [36].

That's how the back-propagation algorithm, the representative learning rule of the multi-layer neural network was formulated in 1986. It provided a systematic method to determine the error of the hidden nodes. Once the hidden layer errors are determined, the delta rule is applied to adjust the weights.

3.6.2.1 Backpropagation Algorithm

The backpropagation algorithm operates in two main phases:

- **Forward pass :** The input data is propagated through the network to compute the output, the weighted sum of inputs is passed through an activation function to produce an output value.
- **Backward pass (Backpropagation) :** The error between the network's predicted output and the actual output (target) is calculated using a loss function. This error is then propagated backward from the output layer to the hidden layers, computing the gradient of the loss with respect to each weight. The weights are updated accordingly using this formula:

$$w_{ij}^{(t+1)} = w_{ij}^{(t)} - \alpha \frac{\partial E}{\partial w_{ij}} \tag{3.1}$$

where:

- $w_{ij}^{(t)}$ is the weight between neuron i and neuron j at iteration t,
- α is the learning rate,
- $\frac{\partial E}{\partial w_{ij}}$ is the partial derivative of the error E with respect to the weight w_{ij}.

This iterative process continues until the network converges to a solution where the total error is minimized across the training set.

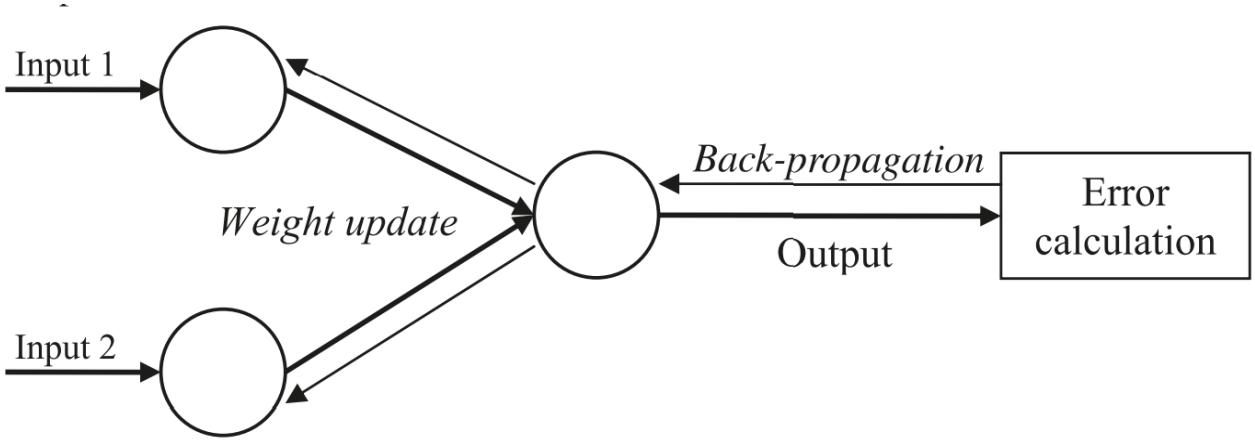

Figure 3.5: Backpropagation Principle (Modified from [15]).

3.7 Feedforward back-propagation neural networks

The feedforward neural network (FNN) is among the most widely used neural network architectures, particularly for structured data such as tabular datasets [37], and for supervised learning tasks including regression and classification. The neurons are generally grouped into layers. Signals flow from the input layer to the output layer via connections, the neurons being connected from one layer to the next, but not within the same layer. A feedforward network can be viewed as a graphical representation of a parametric function which takes a set of input values and maps them to a corresponding set of output values. Figure 3.6 shows an example of a multi-layer feedforward network of a kind that is widely used in practical applications [24].

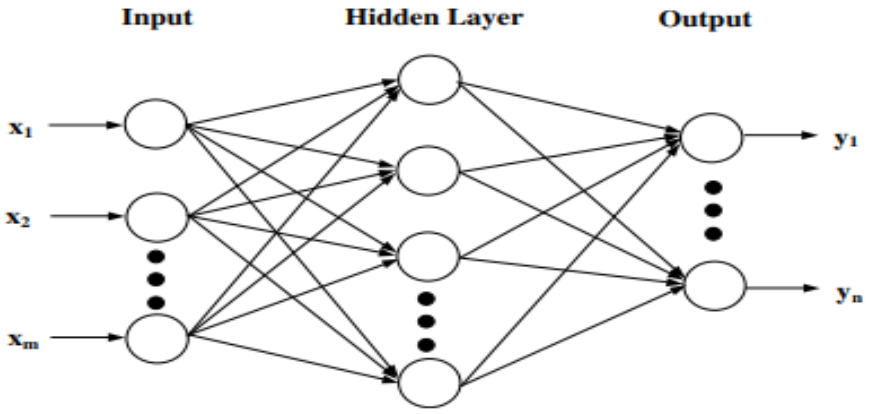

Figure 3.6: Basic Multi-layer feedforward ANN

As shown in Figure 3.7, a problem is presented to the network as an array of input values x_i. The input neurons transmit these values across the links to the second layer (hidden layer) of neurons. Each link has a weight w_{ij} used to multiply transmitted values.

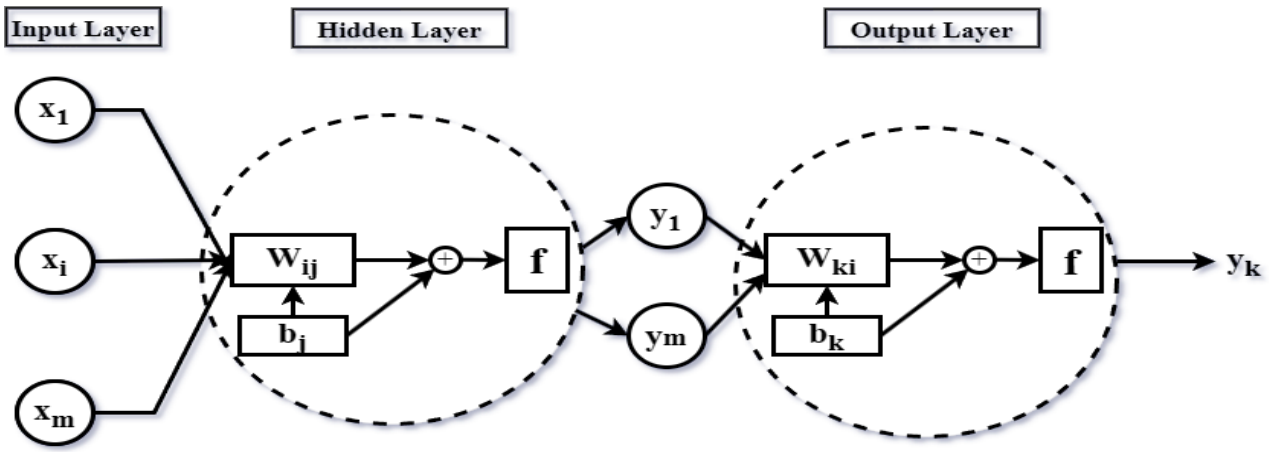

Figure 3.7: Working principle of a feedforward backpropagation ANN

The weighted values converging at a neuron in the hidden layer are summed along with a bias b_j associated with that neuron. The result is then put through a transformation function f .

To generate a signal result for the neuron. The results of the hidden neurons are then transmitted across their outgoing links to the neurons in the output layer. As before, these values are weighted w_kj and biased b_k during transmission across the links, then summed at the output neuron and put through a transformation function.

Expressions (1) and (2) below represent these processes. The function signal generated at the output neuron(s) is the network's solution or output y_k to the problem presented at the inputs.

All neurons within a layer in this type of network operate synchronously in the sense that, at any point in time, they will be at the same stage in processing.

$$y_j = f\left(\sum_{i=1}^{m}(w_{ji} \cdot x_i + b_j)\right) \tag{1}$$

$$y_k = f\left(\sum_{j=1}^{m}(w_{ki} \cdot y_j + b_k)\right) \tag{2}$$

Where:

- x_i: Input value.
- y_j: Output from hidden node j.
- y_k: Final output from output node k.
- w_{ji}, w_{kj}: Weights between the respective layers.
- b_j, b_k: Bias terms for the neurons.
- $f(\cdot)$: Transfer function (Activation Function).

After computing the final output y_k (Equation 2), the network evaluates the prediction error using a loss function (Section 3.7.1).

This error is then propagated backward through the layers using the backpropagation algorithm (Section 3.6.2.1), which computes the gradient of the error with respect to each weight.

The weights are updated iteratively via the rule in Equation 3.1, guiding the network toward minimizing the total error.

3.7.1 Loss Functions

A loss function measures the error between a predicted output and its actual target, typically at the level of a single data point. When averaged over the entire training set, it becomes the cost function, which guides the network's learning via optimization algorithms like gradient descent. The choice of loss (and cost) function depends on the task type.

For regression problems, the most commonly employed loss functions include:

- **Mean Squared Error (MSE)**: This function calculates the average of the squared differences between predicted and actual values. It heavily penalizes larger errors and is defined as:

$$\text{MSE} = \frac{1}{n}\sum_{i=1}^{n}(y_i - \hat{y}_i)^2 \tag{3.2}$$

  where y_i is the true target value, $\hat{y}_i$ the predicted output, and n the number of observations.

- **Mean Absolute Error (MAE)**: MAE computes the average of the absolute differences between predicted and actual values. Compared to MSE, it penalizes errors linearly and is less sensitive to outliers:

$$\text{MAE} = \frac{1}{n}\sum_{i=1}^{n}|y_i - \hat{y}_i| \tag{3.3}$$

For classification problems, other types of loss functions are typically used, such as:

- **Binary Cross-Entropy**, commonly used for binary classification tasks.
- **Categorical Cross-Entropy**, suited for multi-class classification.

3.7.2 Transfer Functions

Transfer functions, also known as activation functions, are essential components of ANNs that introduce non-linearity into the model, enabling it to capture complex patterns in the data. The most commonly used activation functions in regression-based ANNs are described below.

Sigmoid function: The sigmoid function is a classical activation function used primarily in the output layer when the output values are normalized between 0 and 1. It is differentiable, which facilitates backpropagation. It is defined by:

$$\alpha(x) = \frac{1}{1+e^{-x}} \quad \forall x \in \mathbb{R} \tag{3.4}$$

Its characteristic "S"-shaped curve maps any real-valued input into a range between 0 and 1.

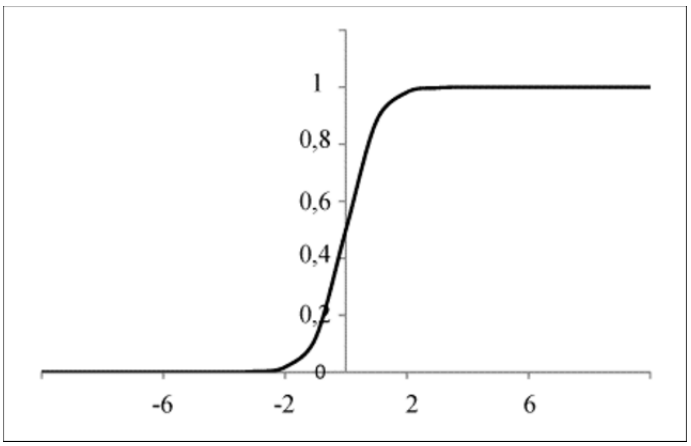

Figure 3.8: Sigmoid activation function

Hyperbolic tangent (tanh) function: The `tanh` function is widely used in hidden layers of ANNs. Unlike the sigmoid, it maps input values to a range between –1 and 1, which makes it zero-centered and generally helps training converge faster. It is defined by:

$$\tanh(x) = \frac{\sinh(x)}{\cosh(x)} = \frac{e^x - e^{-x}}{e^x + e^{-x}} \tag{3.5}$$

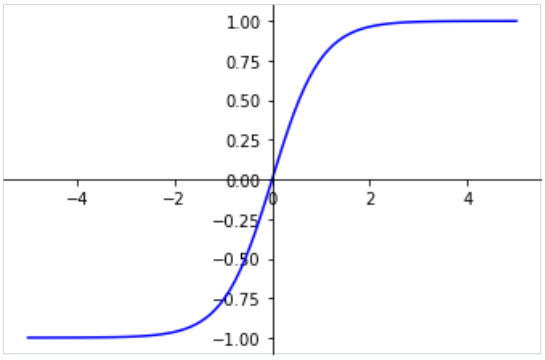

Figure 3.9: tanh activation function

Rectified Linear Unit (ReLU) function: Though more commonly used in deep learning models, ReLU can also be used in ANNs for its computational simplicity and effectiveness. It outputs zero for all negative values and the input itself for positive values. ReLU introduces sparsity and helps avoid the vanishing gradient problem to some extent. It is defined as:

$$G(E) = \max(0, E) = \begin{cases} E & \text{if} \quad E \geq 0 \\ 0 & \text{otherwise} \end{cases} \tag{3.6}$$

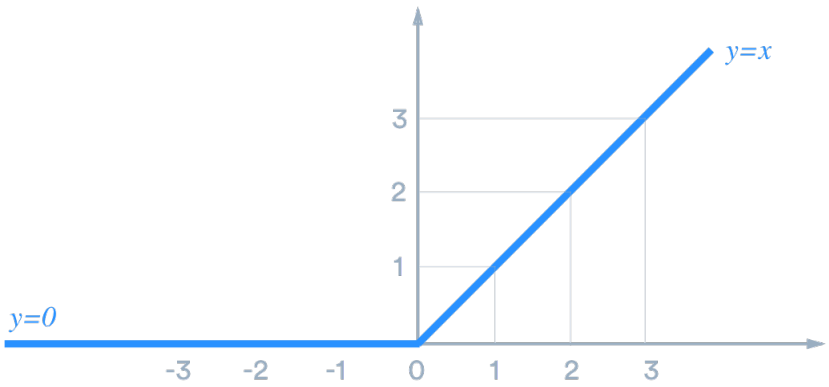

Figure 3.10: ReLU activation function

3.8 Conclusion

In conclusion, this chapter provided a comprehensive overview of Artificial Neural Networks (ANNs), tracing their development from biologically inspired models to their implementation as powerful computational tools. It covered the essential building blocks of ANNs including input layers, weights, biases, and activation functions, highlighting their roles in enabling complex, nonlinear decision-making. Various network architectures and training methods, such as the Delta Rule and backpropagation, were discussed, illustrating how ANNs have evolved from simple perceptrons to deep learning frameworks. The chapter also emphasized the role of loss and cost functions in quantifying prediction errors and guiding the optimization process, as well as the pivotal role of activation functions in allowing networks to approximate intricate relationships. Overall, ANNs have emerged as indispensable components in modern machine learning, with wide-ranging applications in classification, prediction, and optimization.

Chapter 4

Data Construction and Data Preprocessing

4.1 Introduction

After identifying in Chapter 2 the factors affecting ground surface settlement, it is indispensable to create a dataset to serve as the input source for the Artificial Neural Network. In this chapter, we outline the input parameters, describe their sources, and explain the extraction process. Finally, we detail the preprocessing steps applied to prepare the data for training.

4.2 Factors Affecting Settlement

All the factors considered in this study are referred to as "Features". Table 4.1 summarizes the source, unit, and relevant notes for each feature.

Table 4.1: Summary of Features sources

Feature	**Source**	**Unit**	**Notes**
Penetration rate	TBM mining parameter report/Excavation data analysis logs.	mm/min	Extracted/calculated per ring.
Face pressure	TBM mining parameter report/Excavation data analysis logs.	bar	Extracted and averaged per ring.
Thrust	TBM mining parameter report/Excavation data analysis logs.	KN	Extracted per ring.

Grout volume	TBM mining parameter report/Excavation data analysis logs.	m^3	Extracted per ring.
Mass loss	TBM mining parameter report/Excavation data analysis logs.	%	Extracted per ring.
Equivalent cover-depth	Geology/Geotechnics – Plan and longitudinal profile.	m	Calculated per Settlement point.
Distance from Station	Geology/Geotechnics – Plan and longitudinal profile.	m	Calculated per Settlement point.
Groundwater Head	Geology/Geotechnics – Plan and longitudinal profile.	m	Calculated per Settlement point.
E_M/Pl	Geotechnical Investigation reports.	/	Calculated per Settlement points.

4.3 Data Acquisition and Computation

In this section, we will present, as an example only settlement points at sections “pk6+417,00” and “pk6+180,00” will be representing Zone 1 (As described in section 1.3.4). And settlement point at section “pk3+591,00” representing Zone 2.

4.3.1 TBM Operation parameters

All TBM operational parameters will be extracted on a per-ring basis, which means we must first identify the ring number corresponding to the 3 sections mentioned above. This can be done by consulting the **"TBM Mining Parameter report"** files (Figure 4.1 and Appendix C for details).

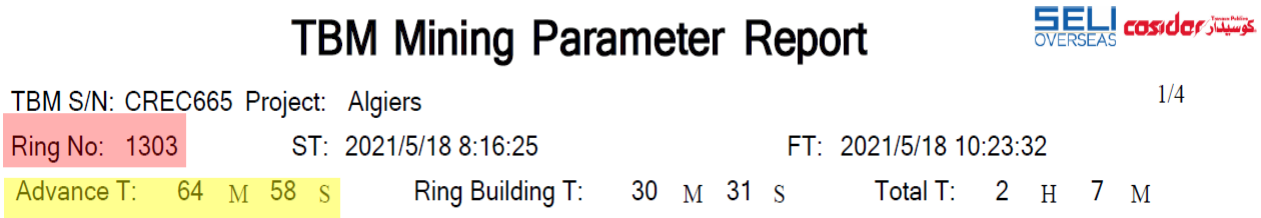
TBM Mining Parameter Report

SELI OVERSEAS cosider

TBM S/N: CREC665 Project: Algiers 1/4

Ring No: 1303 ST: 2021/5/18 8:16:25 FT: 2021/5/18 10:23:32

Advance T: 64 M 58 S Ring Building T: 30 M 31 S Total T: 2 H 7 M

Figure 4.1: Example showcasing the ring number for section pk6+417,00.

4.3.1.1 Thrust and Penetration-rate

- **Zone 1**: This Zone can be divided into 2 sections:

  - **Section 1 (pk3+904.00 to pk6+180.00):** In this section, the **"TBM Mining Parameter report"** files do not provide the penetration rate directly; instead, they include the advance step and the corresponding advance time. Therefore, the penetration rate is calculated as follows:

$$\text{Penetration rate} = \frac{\text{Advance step}}{\text{Advance time}} \tag{4.1}$$

  For instance, in section PK 6+180.00, the recorded advance time is 1:10:33, which is equivalent to 70.55 minutes. (Figure 4.2)

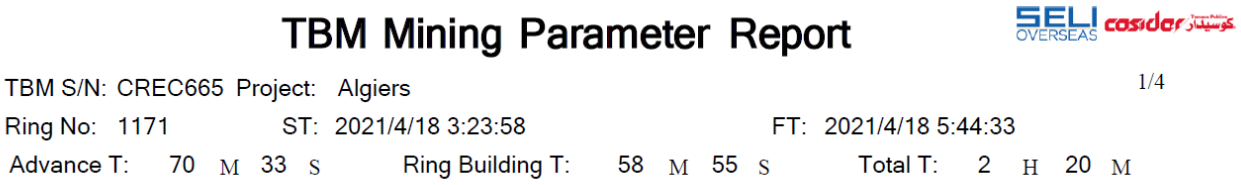
TBM Mining Parameter Report

SELI OVERSEAS casider

1/4

TBM S/N: CREC665 Project: Algiers

Ring No: 1171 ST: 2021/4/18 3:23:58 FT: 2021/4/18 5:44:33

Advance T: 70 M 33 S Ring Building T: 58 M 55 S Total T: 2 H 20 M

Figure 4.2: Parameter report for section pk6+180.00

To determine the penetration rate, the corresponding advance step interval that includes this chainage is first selected. As illustrated in Figure 4.3 the value of (1.784 meters) represents the length of the advance step between chainage PK 6+179.431 and pk6+181.215

PK	Pas d'avancement (m)
6179,431	0
6181,215	1,784

Figure 4.3: Advance step for section pk6+180.00

After converting this distance to millimeters, the penetration rate for this section is calculated as 25.38 mm/min. As for the **thrust** data across the entirely zone 1, it is directly extracted from the logging files.

  - **Section 2 (pk6+180.00 to pk8+8853.00):** In this section, the two operational parameters are directly extracted from the corresponding **"TBM Mining Parameter report"** files. (Figure 4.4)

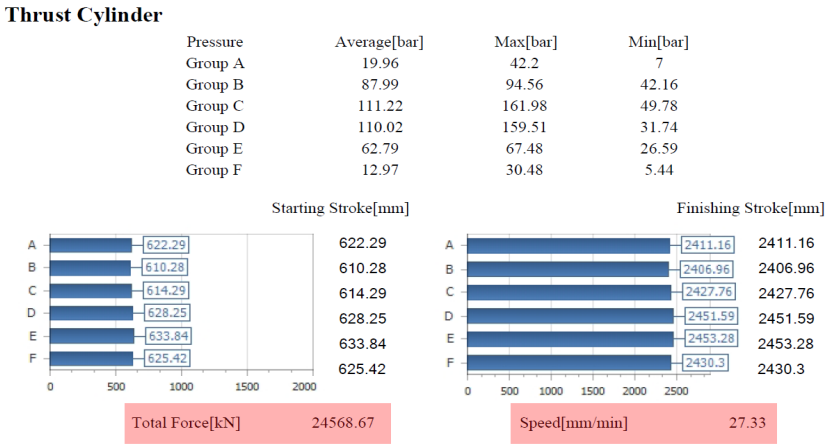

Figure 4.4: Thrust and Penetration-rate Logging

- **Zone 2**: The procedure for calculating the penetration rate is the same as in Zone 1. The only difference lies in the source of the advance time, which, in this zone, is extracted from the **"Excavation Data Analysis Logs"** (Figure 4.5). Furthermore, the thrust force is also directly obtained from the same logging file.

Time		11:54:14	Chainage			Propulsion		1,79		
Ring number		2968		3599,884	3591,085	Pump1:168,75	2730,53	Rotat ccw :0m0s	2500	50m	28018,79
Start ex	13/3/2023	Ring	Total t			Propulsion				
advance t	45m33s	54m9s		38h42m		Pump2:151,36		Rotat cw:50m38s		

Figure 4.5: Excavation Data Analysis Logs. (Appendix D)

4.3.1.2 Face pressure (Earth pressure)

A total of 11 sensors are installed inside the muck chamber in a clockwise arrangement, primarily to measure and record the internal muck chamber pressure. For the purposes of this study, only the three sensors positioned around the ring vault are considered (Figure 4.6).

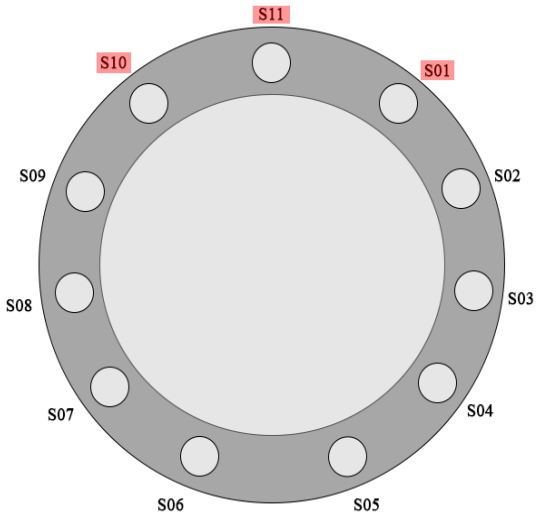

Figure 4.6: Disposition of Earth Pressure sensors in the Muck chamber

- **Zone 1**: The face pressure values recorded for section pk6+417.00 are the following: S01=0.27 bar, S11=0.62 bar, and S10=0.62 bar.

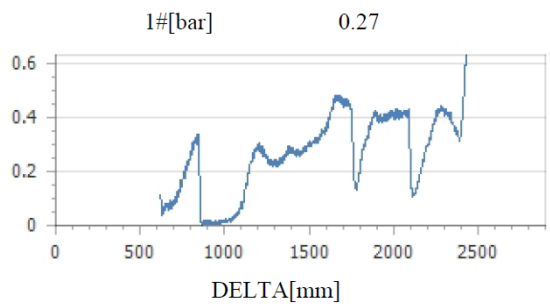

(a) Sensor 01

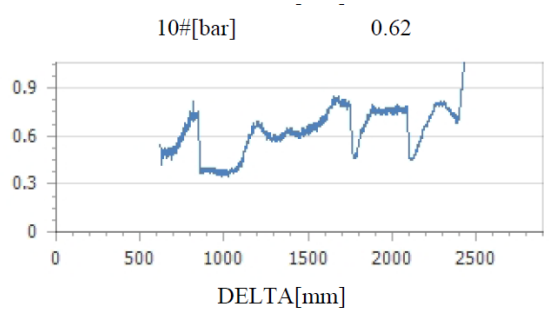

(b) Sensor 10

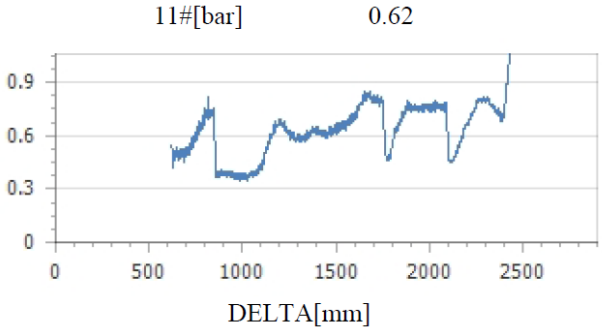

(c) Sensor 11

Figure 4.7: Earth Pressure recorded for Vault sensors

- **Zone 2**: For section pk3+591.00, Earth Pressure is extracted from **"Excavation Data Analysis Logs"**, are the following: S01=1.49 bar, S10=1.80 bar and S11=1.30 bar.

Earth pressure										
S01	S02	S03	S04	S05	S06	S07	S08	S09	S10	S11
1,49	1,38	1,44	1,92	2,28	2,72	2,66	2,49	2,12	1,8	1,3

Figure 4.8: Earth Pressure for section pk3+591.00

4.3.1.3 Mass loss

Mass loss is calculated using the following formula:

$$\text{Mass Loss} = \frac{\text{Theoretical mass} - \text{Excavated mass}}{\text{Theoretical mass}} \tag{4.2}$$

The theoretical mass is obtained from **"Excavation Data Analysis Logs"**, while the excavated mass is derived from the **"TBM Mining Parameter report"** files. In this context, Weight 1 corresponds to the muck weight measured as it falls onto the conveyor belt, accounting for gravitational force, whereas Weight 2 represents the weight of the muck as it is conveyed along the belt.

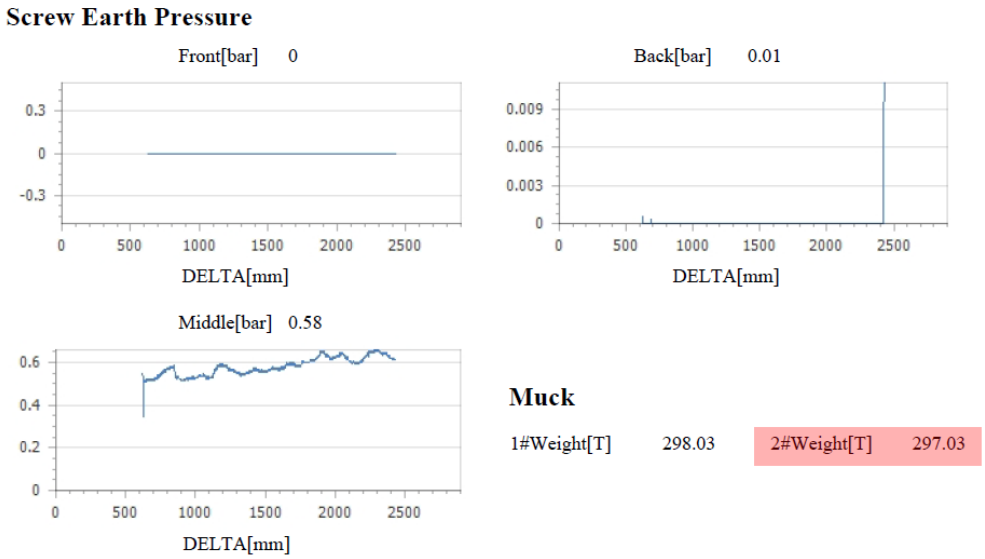

Figure 4.9: Screw Earth Pressure Logs for section pk6+417,00

Mass loss was directly obtained from the Excavation Data analysis Logs for both Zone 1 and Zone 2.

4.3.1.4 Grouting volume

As mentioned in Section 1.3.3, Tail void Gouting is bicomponent. Therefore we will be using the sum of two liquids volumes as a single grouting volume.

- **Zone 1:** The two volumes are highlighted in Figure 4.10

TBM Mining Parameter Report

4/4

Grouting Volume	Liquid A	Liquid B
Grouting 6[m³]	0	0
Grouting 5[m³]	0	0
Grouting 4[m³]	0	0
Grouting 3[m³]	0	0
Grouting 2[m³]	5.08	0.36
Grouting 1[m³]	3.48	0.25
	Σ 8.56	Σ 0.61

Figure 4.10: Grout Volume Logs for section pk6+417,00

For Zone 1, the data is extracted from the **"TBM Mining Parameter report"** files and

subsequently summed.

- **Zone 2:** The same approach is applied for Zone 2.

	Grouting	
8	0	0
8	0	0
52	0	0
5	4,38	4,79
4	6,74	1,75

Figure 4.11: Grout Volume Logs for section pk3+591.00

4.3.2 Geometric parameters

4.3.2.1 Equivalent cover-depth

To account for the varying geotechnical conditions along the tunnel alignment, we employed the concept of equivalent cover depth, which provides a more realistic representation of the vertical stress acting at the tunnel crown. Unlike simple geometric cover depth, this approach incorporates the influence of different soil layers and their respective humid unit weights. The calculation method, detailed below, ensures that both material heterogeneity and hydrostatic effects are properly considered when assessing face stability and support requirements.

The equation is the following:

$$\mathrm{ECV}_i = \frac{\sum(\gamma_i \cdot h_i)}{\gamma_{\mathrm{crown}}} \tag{4.3}$$

Where:

- ECV_i : Equivalent cover depth at section i.
- γ_i : Humid unit weight of each layer i overlying the tunnel.
- h_i : Thickness of each layer.
- γ_{crown} : Humid unit weight at the tunnel crown.

The humid unit weight values used to calculate the equivalent cover depth are listed in table 4.2 for each unit and section.

Table 4.2: The humid unit weight values for each unit, depending on the section.

Geotechnical unit	Re	Qa	Qs	QM	QMSG	QMS	Ts	TM	QG
T1	20	20	21	21	21	20	21	21	/
T2	20	20	21	21	21	/	21.5	21	/
T3	20	21	21	21	20	21	21	/	20
T4	20	20	21	21	21	20	/	/	/
T5	20	21	21	20	21	/	/	/	/
T6	20	21	21	21	21	/	/	/	/
T7	20	21	21	21	/	20	/	/	/
T8	20	20	21	21	/	/	/	/	/
T9	20	20	21	21	21	20	/	/	20

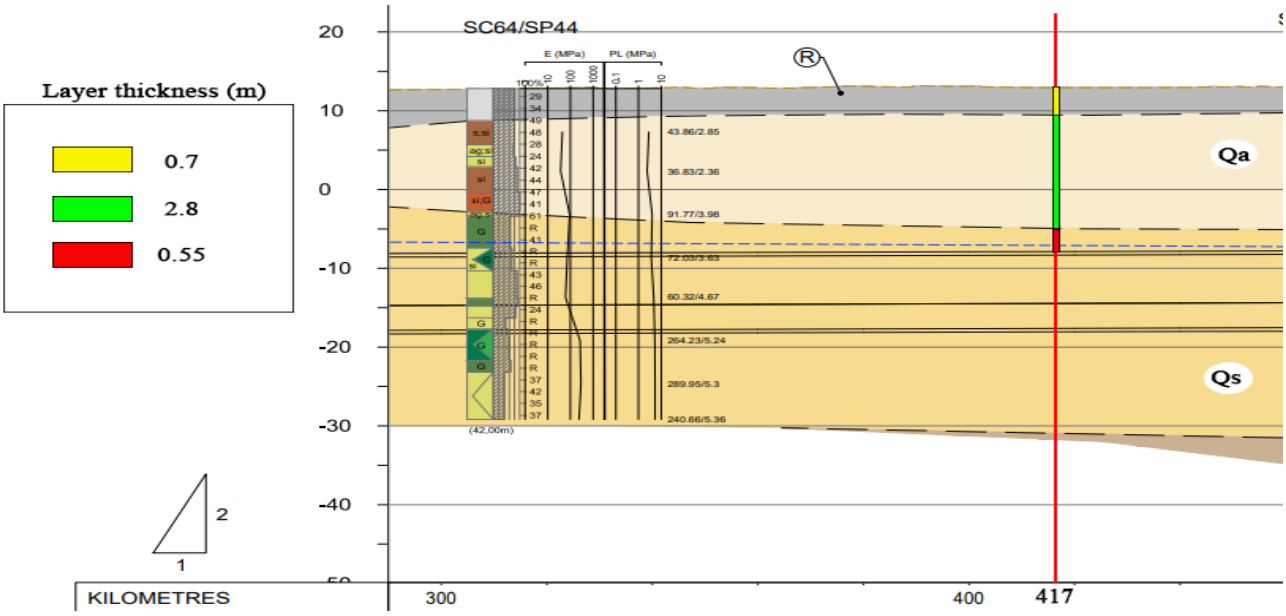

Figure 4.12: Example illustrating layer thickness assessment for cross section at pk pk6+417,00.

4.3.2.2 Distance from Station

It represents the horizontal distance of tunnel front position to the nearest station in the direction of tunnel advancement.

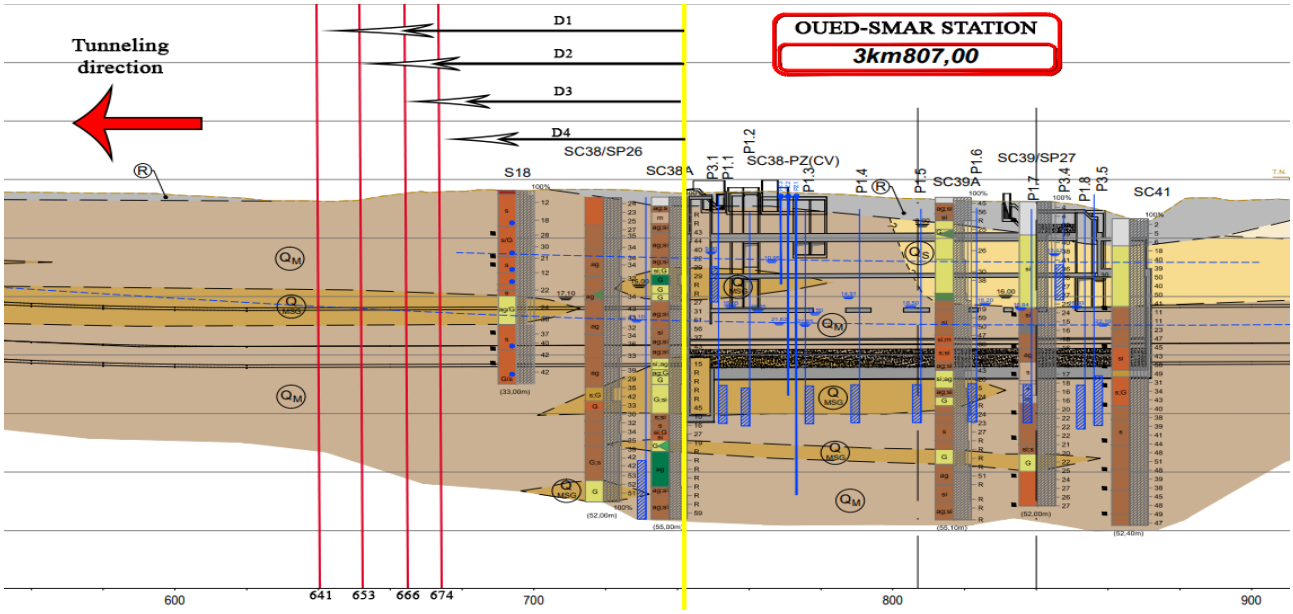

Figure 4.13: Illustration of Distances From Station assessment For different tunnel front positions.

4.3.3 Geotechnical parameters

4.3.3.1 Groundwater Head

To determine the Groundwater head at the tunnel level, we calculated the vertical distance between the piezometric surface and the tunnel invert. In tunneling and geotechnics, this value is commonly used to estimate the hydrostatic pressure acting on the tunnel face or lining, as it represents the height of the water column above the tunnel. For this purpose, we referred to the file entitled **"Geology/Geotechnics – Plan and Longitudinal Profile"** (Appendix A) which includes the tunnel alignment along with relevant geological and hydrogeological information. Figure 4.14 illustrates the position of the piezometric surface to the tunnels invert from which the groundwater head values were derived.

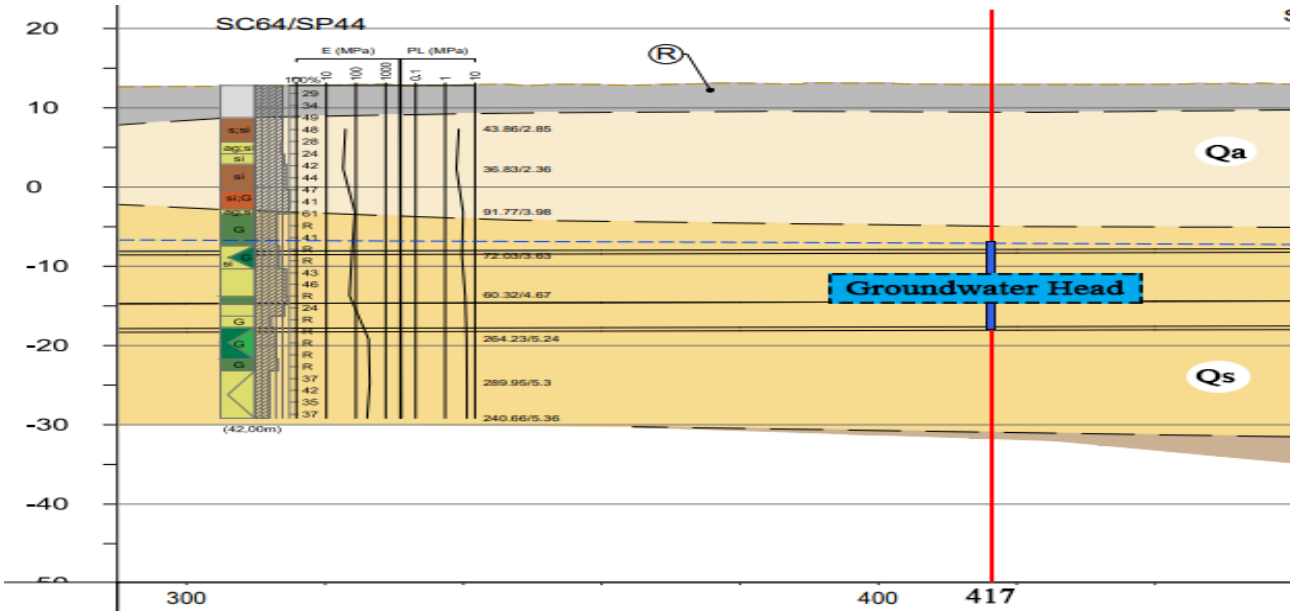

Figure 4.14: Illustration of Groundwater Head assessment at cross section pk pk6+417,00.

4.3.3.2 The Menard Modulus-Limit Pressure ratio $\frac{E_M}{pl}$

The $\frac{E_M}{pl}$ ratio, defined as the ratio between the Menard modulus of elasticity (E_M) and the limit pressure (pl), serves as a practical indicator of the soil's deformability under loading conditions. The Menard modulus (E_M) reflects the soil's elastic response during a pressuremeter test, while the limit pressure (pl) represents the pressure at which the soil yields or fails. A low $\frac{E_M}{pl}$ ratio typically indicates highly deformable soils, such as soft clays or loose sands, where the elastic stiffness is relatively low compared to the failure threshold. Conversely, a high $\frac{E_M}{pl}$ ratio suggests stiffer, less deformable soils.

In the context of the present study and given the geotechincal investogation reports, this ratio was the only parameter available that could meaningfully capture soil deformability across the project area. Given the limitations of the geotechnical dataset, it offered a consistent and interpretable means of assessing ground behavior. Its integration into our database was key to evaluating settlement risk and refining our interpretation of face stability, particularly in zones lacking detailed laboratory data.

Since the tunnel face may include several soil types, an equivalent E_M and an equivalent Pl are first calculated by taking into account the proportion of each soil type present at the tunnel face, and the $\frac{E_M}{pl}$ ratio was then computed accordingly using the following equation:

$$\frac{E_M}{pl} = \frac{\sum_{i=1}^{n} \alpha_i E_{Mi}}{\sum_{i=1}^{n} \alpha_i pl_i}$$

α_i : ratio (expressed as a percentage) of the thickness of soil i present in the face to the tunnel diameter.

The values of E_{Mi} and pl_i are extracted from **Geotechnical Investigation reports**. (Figure 4.15 as an Example) (Appendix E for selected results)

Phase	Unité	Sondage		E_M	Pl	Pf	E_M/P_l
		Code	Profondeur				
			(m)	MPa	MPa	MPa	--
	QM	SP13	4,50	26,57	2,04	1,42	13,00
	QM	SP13	9,00	81,69	4,95	4,95	16,50
	QM	SP13	13,50	97,29	5,55	3,34	17,53
	QM	SP13	18,00	123,88	5,50	3,63	22,54
	QM	SP13	22,50	146,36	5,11	5,11	28,65
	QM	SP13	27,00	36,02	3,01	2,28	11,98
	TS	SP13	31,50	66,45	4,21	4,21	15,78
	TS	SP13	36,00	41,17	2,86	1,88	14,39
	QA	SP14	4,50	14,49	0,67	0,47	21,72

Figure 4.15: Example of Pressuremeter test Results

4.4 Data Preprocessing

After assembling all feature data into a single dataset, preprocessing is essential, as Artificial Neural Network training is highly sensitive to data quality. This step ensures the model learns from meaningful patterns rather than noise or errors. Quality control involved verifying the absence of missing values, data duplicate entries and data outliers. Preprocessing was carried out in two main phases: data cleaning and data normalization.

4.4.1 Data Cleaning

This phase aimed to ensure a reliable dataset by addressing missing values and duplicates and outliers.

- **Missing Data**

The first step was to check for missing values (e.g., NaN, Null). A Python script confirmed the dataset contained none. Figure 4.16 illustrates the result.

```
Missing values per column:
 Settlement (mm)              0
Penetration rate (mm/min)     0
Groundwater Head (m)          0
Mass loss (%)                 0
Thrust (KN)                   0
ECV (m)                       0
Face Pressure (bar)           0
Grout volume (m3)             0
Distance from Station (m)     0
EM/PL                         0
dtype: int64
```

Figure 4.16: Data Analysis for Missing data

- **Detecting and eliminating duplicate entries**

The dataset was also checked for duplicate records, which were removed if found, as they may bias the model by reinforcing certain patterns and reducing generalization. Figure 4.17 presents the analysis results.

```
Index: []
Total number of duplicated rows: 0
```

Figure 4.17: Data Analysis for Duplicated Values

- **Outliers**

All Data was carefully reviewed, and none were identified as outliers. Therefore, the complete dataset was retained for analysis.

4.4.2 Data Distribution Analysis

This analysis provides insight into the distribution characteristics, the degree of skewness, for each feature.

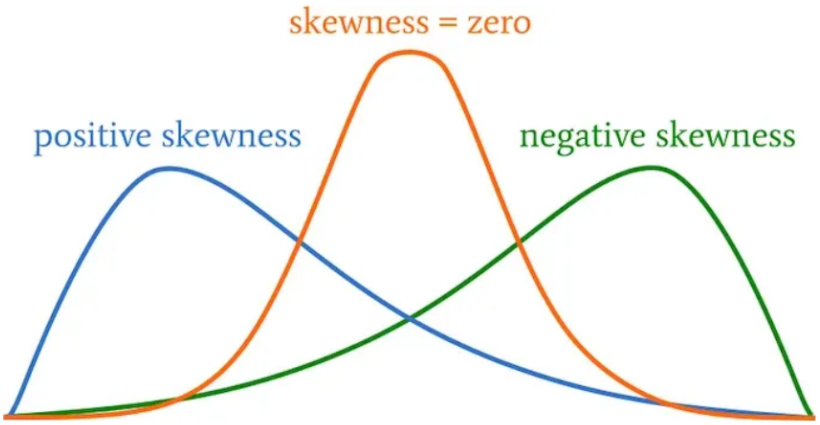

Figure 4.18: Illustration of Skewness degree [16].

- **Settlement (Target Variable)**

Figure 4.19 illustrates the distribution of values for Settlement.

The settlement distribution peaks at minor displacements (0 to -10 mm), indicating predominantly stable ground conditions. Significant right-skewness reveals infrequent severe subsidence events (down to -80 mm), highlighting localized geotechnical vulnerabilities.

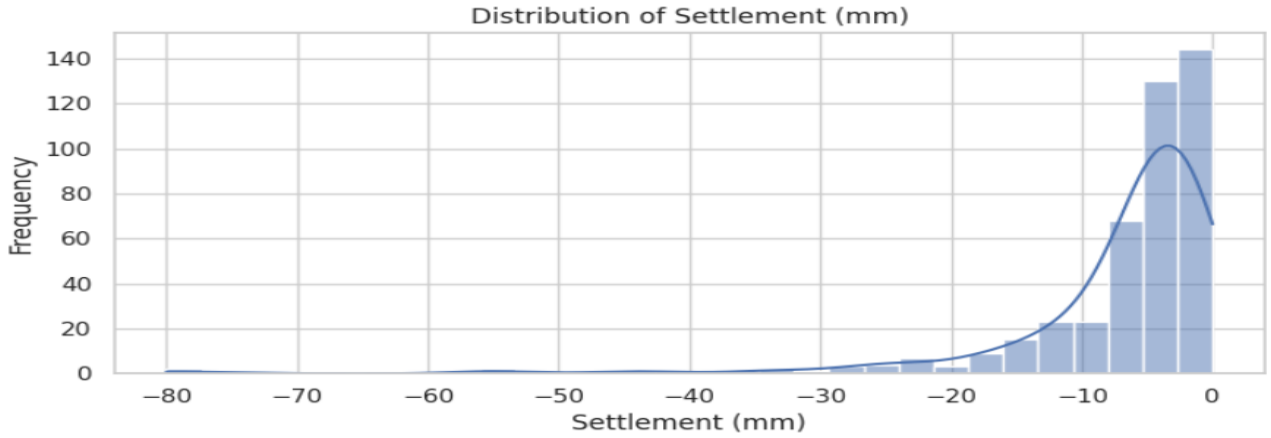

Figure 4.19: Histogram representing Settlement Distribution

- Distribution: Asymmetric Peaking at (0 to -10 mm).
- Skewness: Negative-skewed tail toward more severe/more negative settlements on the left.

- **Penetration rate**

Figure 4.20 illustrates the distribution of values for Penetration rate.

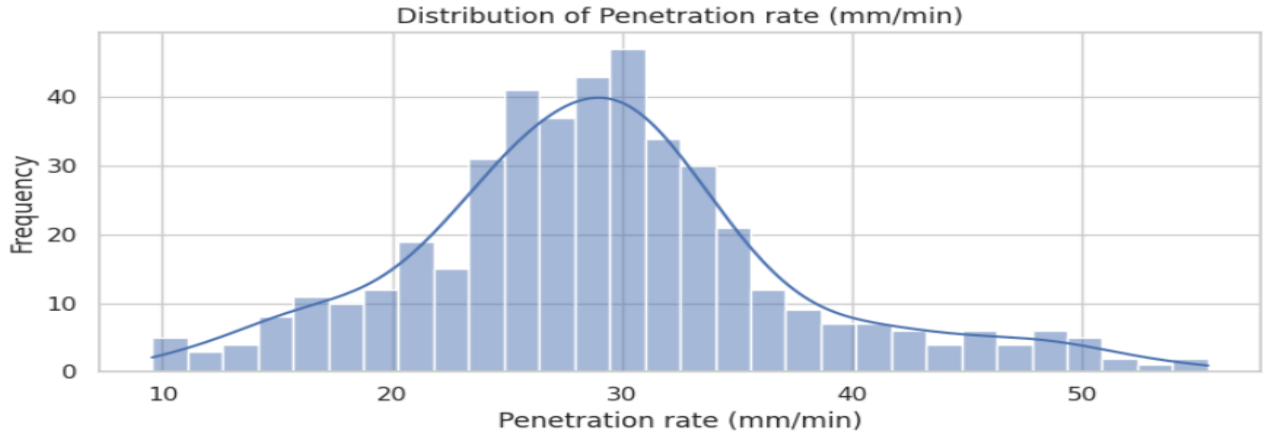

Figure 4.20: Histogram representing Penetration-rate Distribution

- Distribution: Symmetric (peaks at 30 mm/min).
- Skewness: Negligible skew (zero).

Optimal TBM advancement rates; symmetry suggests consistent machine-soil interaction.

- **Groundwater head**

Figure 4.21 illustrates the distribution of values for Groundwater Head.

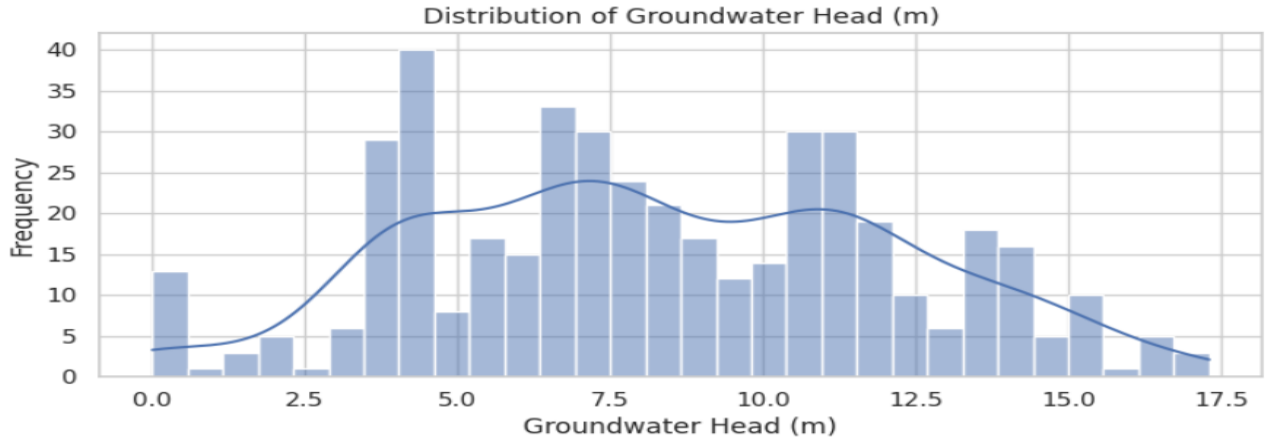

Figure 4.21: Histogram representing GroundWater Head Distribution

- Distribution: Asymmetric (peaks at 5–10m, rare high heads).
- Skewness: Positive-skewed (tail toward high heads on the right).

Moderate groundwater levels dominate;the multimodel distribution observed reflects Groundwater Head variations due to geological conditions.

- **Mass loss**

Figure 4.22 illustrates the distribution of values for Mass Loss.

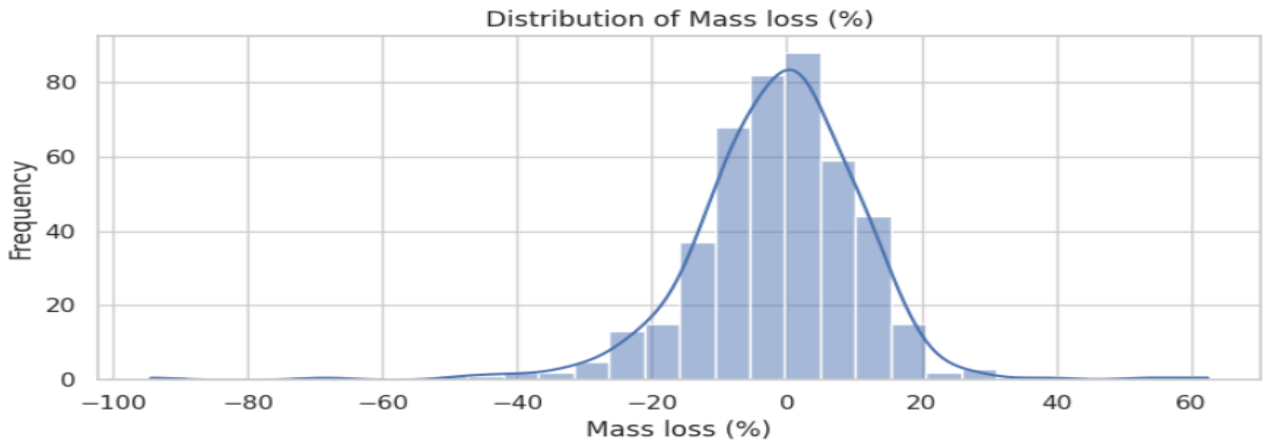

Figure 4.22: Histogram representing Mass Loss Distribution

- Distribution: Symmetric (centered around 0).
- Skewness: Negligible skew (Zero).

- **Thrust**

Figure 4.23 illustrates the distribution of values for Thrust.

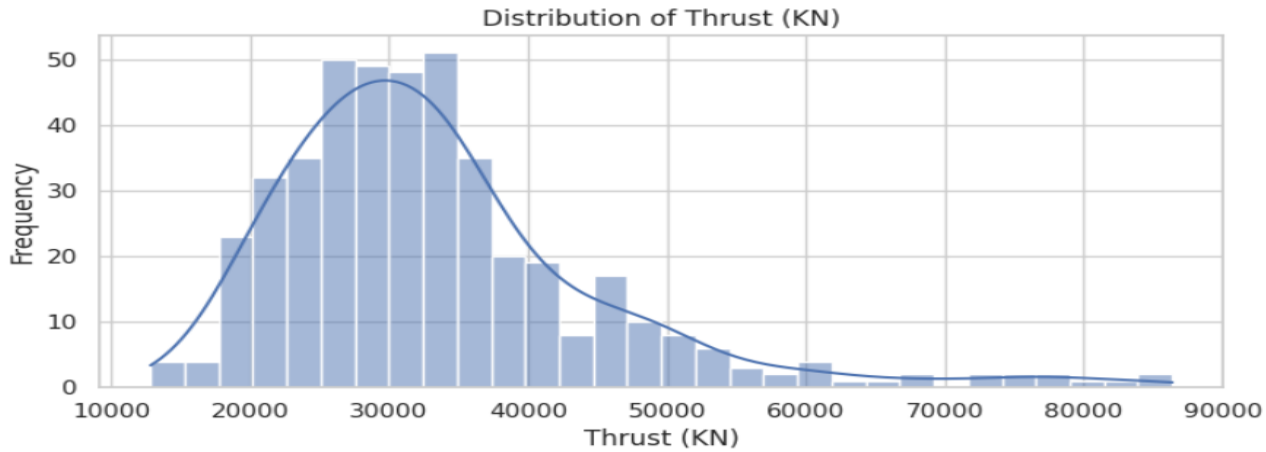

Figure 4.23: Histogram representing Thrust Distribution

- Distribution: Symmetric (peaks at 50,000 KN).
- Skewness: Near-zero (balanced distribution).

- **Equivalent Cover-Depth**

Figure 4.24 illustrates the distribution of values for Equivalent Cover-depth.

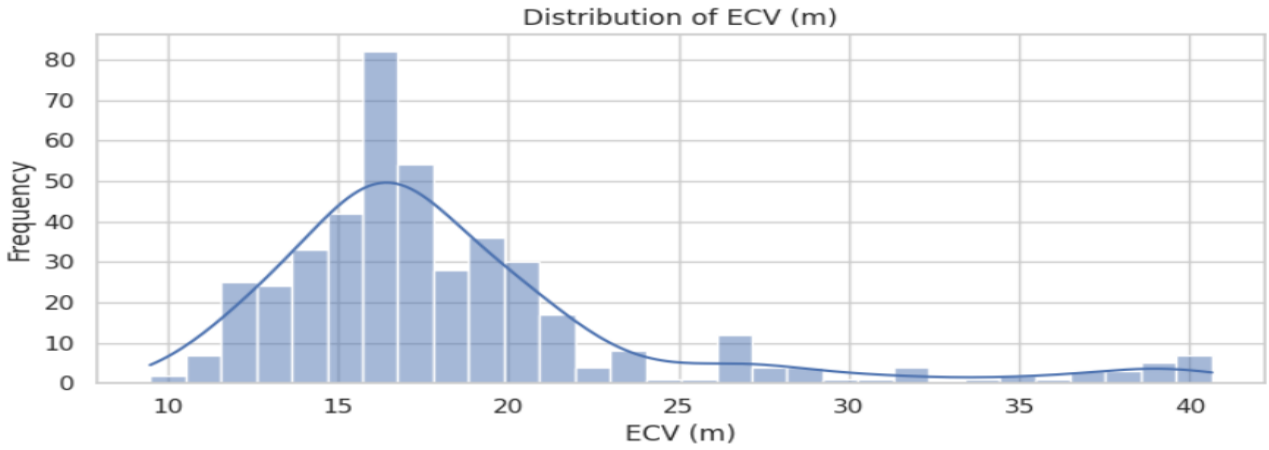

Figure 4.24: Histogram representing Equivalent Cover-Depth Distribution

- The distribution is of a Multimodal structure: two distinct parts can be identified. Part 1, with cover depths ranging from 10 to 25 meters, corresponds to the tunnel sections between Hasan Badi and Airport stations , is symmetrically distributed. Part 2, with depths from 26 to 41 meters, represents the restricted zone of tunnel section 1.

- **Face pressure**

Figure 4.25 illustrates the distribution of values for Face pressure.

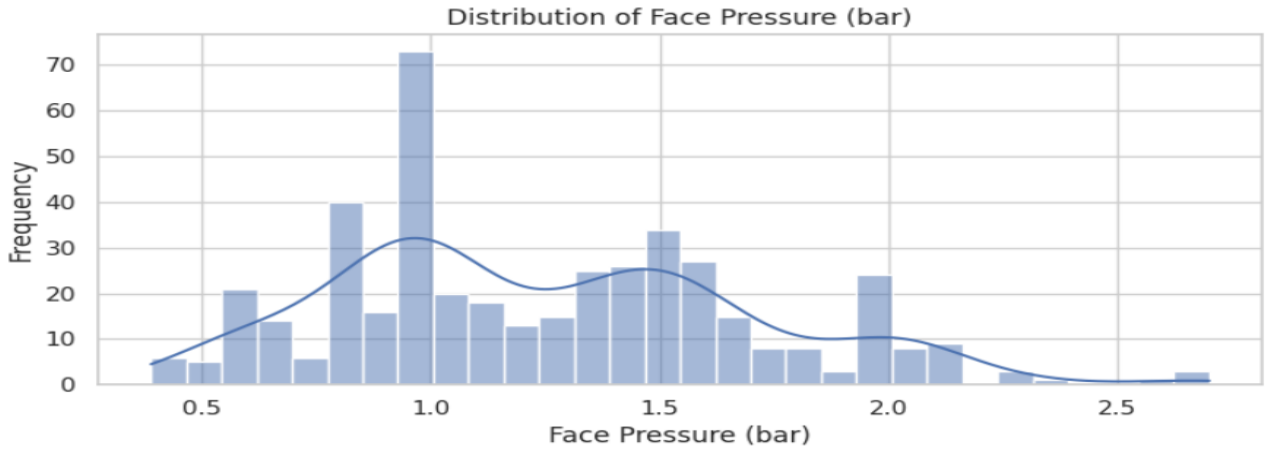

Figure 4.25: Histogram representing Face Pressure Distribution

  - The distribution is Multimodal due to varying geological conditions encountered along the tunnel alignment.

- **Tail Void Grout**

Figure 4.26 illustrates the distribution of values for Tail void grout.

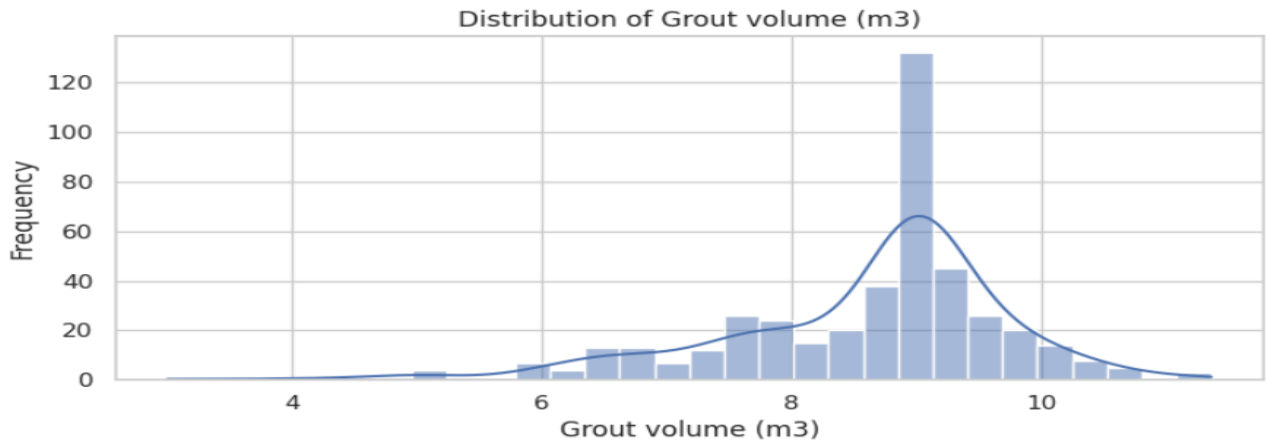

Figure 4.26: Histogram representing Tail void Grout Volume Distribution

- Distribution: Near-symmetric.
- The histogram is slightly negatively skewed, which can be attributed to changes in the nature of the soil along the tunnel alignment.

- **Distance from station**

Figure 4.27 illustrates the distribution of values for Distance from station.

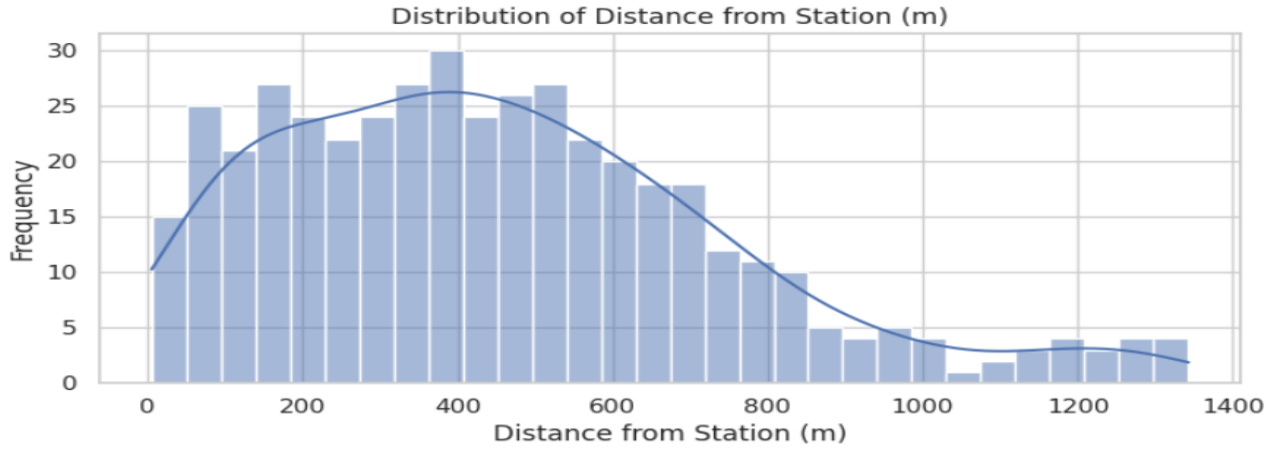

Figure 4.27: Histogram representing Distance from Station Distribution

- Distribution: Asymmetric.
- Skewness: Positively skewed, with a longer tail extending toward higher distances on the right, since most of the distances from the station are less than 800 meters..

- **The Menard Modulus-Limit Pressure ratio $\frac{E_M}{p_l}$**

Figure 4.28 illustrates the distribution of values for $\frac{E_M}{p_l}$.

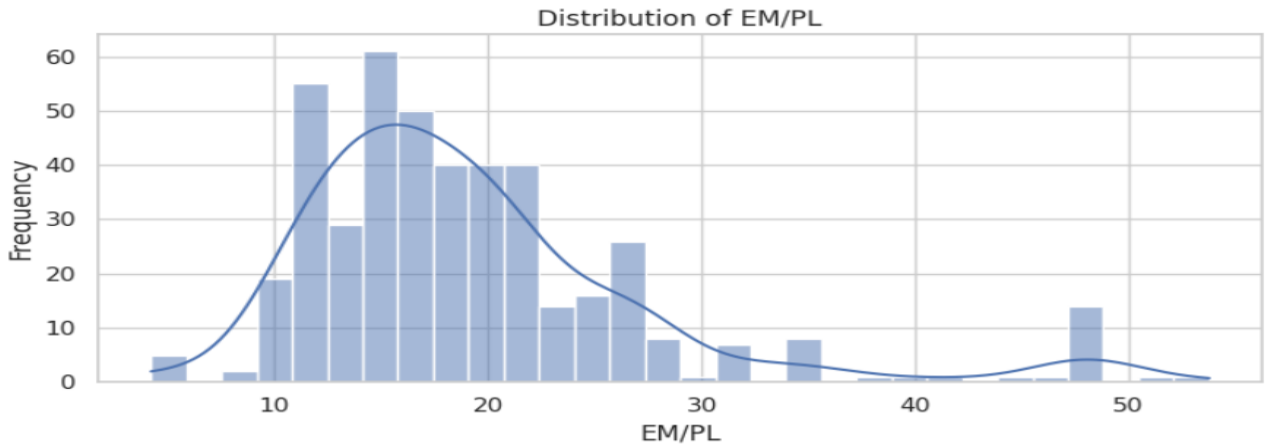

Figure 4.28: Histogram representing $\frac{E_M}{p_l}$ Distribution

- The distribution is Multimodal due to varying geological conditions encountered along the tunnel alignment.

A summary of descriptive statistics of considered features are presented in Table 4.3.

Table 4.3: Descriptive Statistics of Considered features.

Feature	Type	Data (442 samples)				
		Minimum	Maximum	Mean	Standard Deviation	Coefficient of Variation
Penetration rate (mm/min)	Input	9.56	55,45	29,14441	8,17605	0,28054
Groundwater head (m)		0	17.3	8,32429	3,86505	0,46431
Mass loss (%)		-94.3	62,44	-1,36681	13,21872	9,67122
Thrust (KN)		12833,69	86378,78	33408,00835	11854,12791	0,35483
Equivalent CD (m)		9,48	40,65	18,46077	5,93975	0,32175
Face pressure (bar)		0,39	2,7	1,25052	0,45359	0,36272
Grout volume (m^3)		3	11,36	8,58183	1,18081	0,13759
Distance from Station (m)		5	1343	454,45226	291,2336	0,64085
$\frac{E_M}{Pl}$		4.23	53.76	19,29792	8,42018	0,43633
Settlement (mm)	Target	-80	0	-7,03767	9,82042	1,39541

4.4.3 Data Normalization

After verifying that the dataset contained no missing or duplicated values, the next crucial step was data normalization, which involves appropriately scaling the input features.

Data normalization serves several important purposes:

- **Improved model convergence**: Scaling the data helps the model converge more efficiently during training by ensuring all features contribute proportionally.
- **Reduced risk of overfitting**: When features have widely different value ranges, the model may assign disproportionate importance to those with larger magnitudes. Normalization mitigates this bias, helping the model generalize more effectively.
- **Accelerated training**: Normalized data enables faster convergence toward an optimal solution.
- **Better compatibility with activation functions**: Activation functions such as sigmoid or hyperbolic tangent are sensitive to input scale. Feeding unnormalized data into the network may result in slower learning and less accurate predictions. Normalization stabilizes the training process and enhances model performance.

Several data normalization methods exist, including:

- Logarithmic transformation,
- Min-Max scaling,
- Standardization (which centers the data around zero),
- Decimal scaling normalization,
- etc.

In the present case, we used the Min-Max normalization method, defined by the following formula:

$$x_{\text{norm}} = -1 + \frac{(x - x_{\min}) \times 2}{x_{\max} - x_{\min}}$$

where:

- x :is the original value,
- $x_{\min}$ and $x_{\max}$ are the minimum and maximum values of the variable, respectively,
- x_{norm} :is the normalized value ranging between -1 and 1.

The choice of normalization to the range $(-1, 1)$ offers several advantages for handling the diverse distribution shapes and ranges in the dataset:

- **Skewed Distributions:**
  - **Positively skewed** ($\frac{E_M}{p_l}$, Face Pressure, Thrust, ECV, Groundwater Head): These variables exhibit long right tails due to rare extreme values. Scaling to $(-1, 1)$

reduces their influence while preserving the relationships between common observations. This helps avoid biases and issues that standardization might introduce in such cases.

- **Negatively skewed** (Settlement, Tail void Grout Volume):
  Min-max scaling constrains rare negative outliers (possible measurement errors), reducing their destabilizing effect during training.

- **Symmetric or Near-Normal Distributions** (Mass Loss, Penetration Rate):
  Scaling these variables to $(-1, 1)$ maintains their balanced shape and symmetry, ensuring consistent gradient updates without introducing skew.

4.5 Conclusion

This chapter provided an overview of the data assembly and preprocessing phase, a necessary step for building a predictive model based on Artificial Neural Networks (ANNs). It detailed the source of the data and described the extraction of relevant tunneling and geotechnical parameters from Earth Pressure Balance Tunnel Boring Machine (EPB-TBM) project records.

Subsequently, several preprocessing steps were undertaken to ensure the quality and consistency of the dataset:

- The dataset was found to be complete and consistent, with no missing values or duplicate records, thereby ensuring data integrity for the training process.

- Although certain data points may be viewed as statistical outliers, all samples were retained. This decision was based on the recognition that these values stem from actual field measurements and may capture meaningful behavior patterns essential to accurate settlement prediction.

- To ensure numerical stability and enhance training performance, all features were normalized using Min-Max scaling within the range $(-1, 1)$. This approach was chosen with regard to the distribution characteristics of the input variables and the mathematical properties of the activation functions employed in the ANN.

The preprocessed dataset, consisting of 442 samples (Appendix F), is thus considered suitable for model development.

Chapter 5

Artificial Neural Network Modeling and Performance Analysis

5.1 Introduction

With Data Preprocessing completed, this chapter presents the development and evaluation of an Artificial Neural Network (ANN) designed to predict surface settlements induced by EPB-TBM tunneling. We begin with a general overview of ANN principles and key parameters, followed by considerations related to the overall design and performance of the model. These concepts are then applied in the implementation section, where the network is configured, trained, tested, and evaluated, followed by a sensitivity analysis to assess the impact of each input parameter on the predictions.

5.2 ANN Model Configuration and Design Process

Artificial Neural Networks (ANNs) are defined by a set of interconnected components and tunable parameters that directly influence their learning capacity and generalization performance. Selecting appropriate values for these parameters is essential for building an effective and robust model. Table 5.1 summarizes the key architectural, functional, and training-related parameters commonly considered when configuring an ANN.

Table 5.1: Summary of neural network configuration parameters

Neural network model	- Feedforward backpropagation Neural Network - Convolutional Neural Network - Recurrent Neural Network
Input nodes	Number of features fed into the network
Hidden layer	Single or multiple hidden layers
Hidden layer neurons	Number of neurons in the hidden layer(s)
Output layer neurons	Number of outputs the model predicts
Training network algorithm	- Levenberg-Marquardt - Gradient Descent - Bayesian Regularization
Training percentage	Percentage of total data used for training
Testing percentage	Percentage of total data used to evaluate model generalization
Validation percentage	Percentage of total data used to monitor overfitting during training
Transfer function hidden layer	- Tansig (Hyperbolic-tangent Sigmoid) - Logsig (Log-Sigmoid) - ReLU (Rectified Linear Unit)
Transfer function output layer	- Purelin - Logsig
Data division	- Random division - Sequential split - User-defined indices
No. of epochs	Maximum number of training iterations
Validation checks (iterations)	Number of validation failures allowed before early stopping

Performance	- Mean Squared Error (MSE) - Root Mean Squared Error (RMSE) - Regression coefficient R^2

5.2.1 Design of the optimum artificial neural networks

The determination of the optimal network architecture, particularly the number of neurons in the hidden layers, is a crucial step in the modeling process. In feedforward backpropagation neural networks, this aspect has been extensively studied, and two principal methodological strategies have emerged: **constructive approaches** and **pruning strategies**.

- **Constructive approaches**, such as the Cascade-Correlation algorithm, begin with a minimal architecture and incrementally add neurons based on improvements in performance, typically evaluated on a validation set. This method allows the network to adaptively grow in complexity, enhancing learning capacity while maintaining generalization and reducing the risk of overfitting [38].

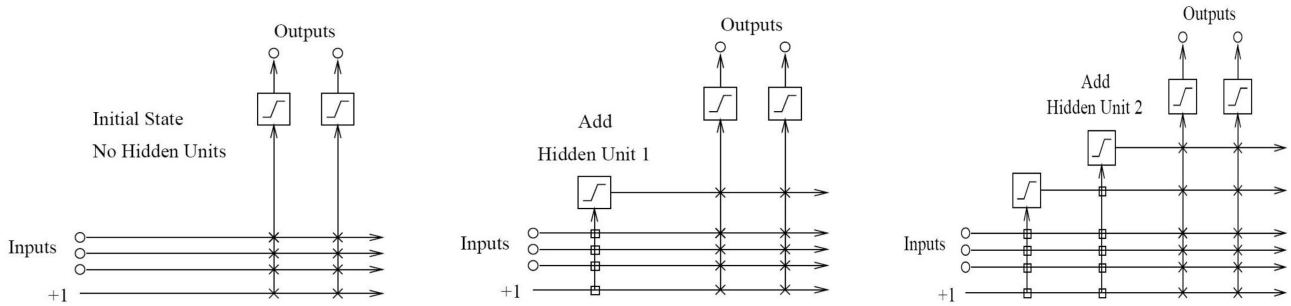

(a) No hidden units (b) One hidden unit added (c) Two hidden units added

Figure 5.1: Illustration of the constructive strategy: incremental addition of hidden neurons during training [17].

- **Pruning strategies** start from an over-parameterized network and remove neurons or weights that contribute little to the overall predictive performance. These removals are guided by sensitivity analyses or the magnitude of weights, ultimately resulting in a more compact, computationally efficient network without a significant loss in accuracy [39, 40].

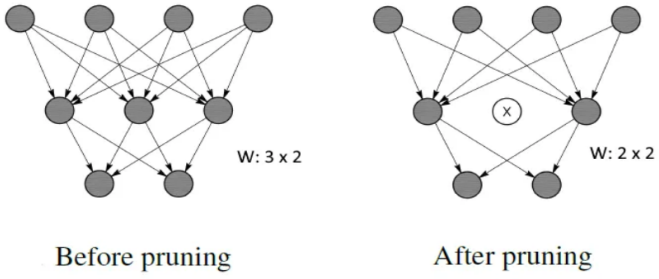

Figure 5.2: Illustration of the pruning strategy: reducing an over-parameterized network to a simpler one [18].

In the present study, a constructive approach was adopted using a trial-and-error methodology, where various configurations of hidden neurons were tested iteratively by incrementally adding neurons to the hidden layer. Each configuration is trained using a pre-defined data divison, and its performance is evaluated to determine which network structure best balances accuracy and model simplicity.

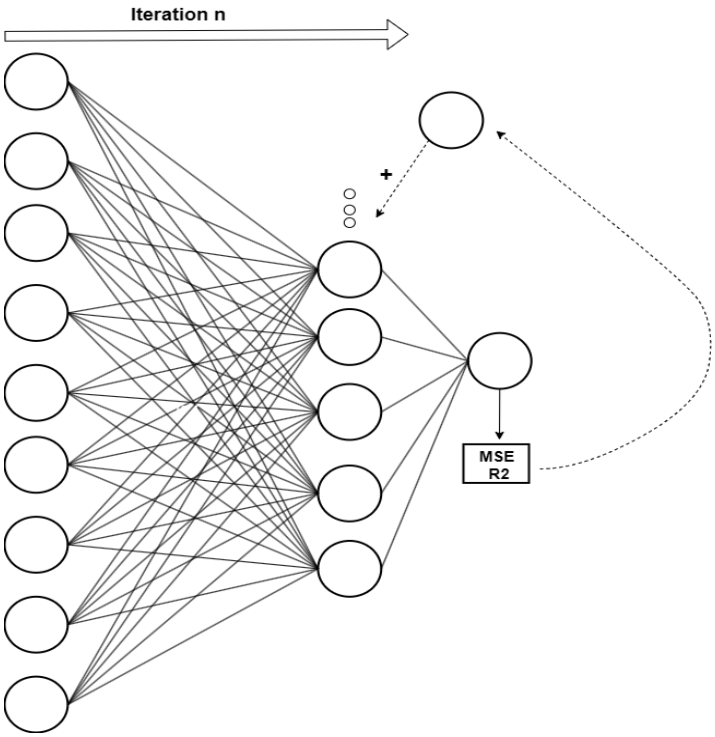

Figure 5.3: Constructive strategy adopte using a Trial-and-error methodology

In addition, several empirical formulas have been proposed in the literature to estimate a suitable number of hidden neurons in a feedforward neural network [41]. While these formulas do not guarantee optimality, they offer a practical starting point when designing network architectures. One such expression for determining the hidden layer size in a backpropagation ANN that demonstrated consistently lower prediction errors,is given by:

$$N_h = \frac{4n^2 + 3}{n^2 - 8} \tag{5.1}$$

where N_h represents the number of hidden neurons and n is the number of input neurons.

5.2.2 Performance Analysis

Following the selection of the network architecture, each neural network configuration is evaluated using two key statistical indicators: the Root Mean Squared Error (RMSE) and the coefficient of determination (R^2).

- **Root Mean Squared Error (RMSE)**: RMSE is derived from the Mean Squared Error (MSE), previously defined in Section 3.7.1. It provides an error metric in the same unit as the output variable, making it more interpretable. It is computed as:

$$\text{RMSE} = \sqrt{\frac{1}{n}\sum_{i=1}^{n}(a_i - p_i)^2}$$

- **Coefficient of Determination (R^2)**: This indicator evaluates the proportion of variance in the observed data that is predictable from the model. Values closer to 1.0 reflect stronger predictive power and better generalization. The formula is:

$$R^2 = 1 - \frac{\sum_{i=1}^{n}(a_i - p_i)^2}{\sum_{i=1}^{n}(a_i - \bar{a})^2}$$

  where:

  - a_i is the actual (measured) value of settlement at observation i,
  - p_i is the predicted value of settlement at observation i,
  - $\bar{a}$ is the mean of all actual settlement values.

Together, RMSE and R^2 provide a comprehensive evaluation of model accuracy and reliability, guiding the selection of the most suitable ANN configuration.

5.2.3 Overview of Sensitivity Analysis Approaches

While Artificial Neural Networks (ANNs) are powerful tools for modeling complex, nonlinear systems, they are often criticized for their lack of interpretability a limitation commonly referred to as the "black-box" problem. This issue becomes particularly critical in engineering applications such as tunneling-induced ground settlement, where understanding the relationship between input parameters and predicted outcomes is just as important as achieving high predictive accuracy.

This interpretability step is crucial. While accurate predictions can support general forecasting, they are not sufficient for practical engineering decision-making. Engineers must identify which input parameters most influence settlement to inform design choices, monitoring strategies, and risk mitigation efforts. For this reason, a sensitivity analysis will be introduced as a post-implementation step, to assess the relative importance of each input variable and provide insights into the physical mechanisms captured by the ANN.

In the ANN literature, sensitivity analysis techniques are commonly categorized into two main approaches: Perturbation-based and Weight-based methods.

5.2.3.1 Perturbation-based Sensitivity Analysis

Perturbation-based approaches assess the influence of individual input variables by systematically altering one feature at a time and observing the resulting change in the model's output. These techniques are intuitive and model-agnostic, as they do not rely on the internal structure of the network. They are particularly useful for examining the local behavior of the model and for quantifying how sensitive the output is to small variations in input values.

In the context of this study, perturbation-based sensitivity analysis proves particularly valuable, as the input parameters span three distinct categories: controllable TBM operational factors,

uncontrollable geotechnical conditions, and fixed geometric parameters. By systematically isolating and modifying each input, this method yields practical insights into which operational settings can be optimized to reduce settlement, while also identifying geotechnical factors that present elevated risk but lie beyond direct control. Additionally, it allows for assessing the influence of geometric parameters established during the design phase.

Algorithm Overview

The following procedure was implemented to evaluate the relative importance of each input variable in the trained neural network model:

1. **Dataset Definition:** The initial dataset, denoted by $\mathbf{x}_0$, is an $N \times d$ matrix, where N is the number of samples and d is the number of input features.

2. **Perturbation of Input Variables:** For each input variable x_j, with $j = 1, \ldots, d$, two perturbed versions of each sample i are generated:

   - $\mathbf{x}_{\text{plus}}^{(i,j)}$, in which the value of x_j is increased by a factor $(1 + \varepsilon)$

   $$x_{\text{plus}}^{(i,j)} = x_j^{(i)} \cdot (1 + \varepsilon)$$

   - $\mathbf{x}_{\text{minus}}^{(i,j)}$, in which the value of x_j is decreased by a factor $(1 - \varepsilon)$

   $$x_{\text{minus}}^{(i,j)} = x_j^{(i)} \cdot (1 - \varepsilon)$$

   The value of ε is a small perturbation factor, typically ranging between 0 and 1.

3. **Model Prediction and Output Variation:** The trained model is used to predict the outputs corresponding to each perturbed input:

   $$y_+^{(i)} = f(\mathbf{x}_{\text{plus}}^{(i,j)}), \quad y_-^{(i)} = f(\mathbf{x}_{\text{minus}}^{(i,j)})$$

   Here, $f(\cdot)$ denotes the trained ANN function.

   The absolute variation in output for each sample is then computed as:

   $$\Delta y_i^{(j)} = \frac{\left| y_+^{(i)} - y_-^{(i)} \right|}{2\varepsilon}$$

4. **Aggregation of Variations:** The average variation for each input variable x_j is calculated across all samples:

   $$S_j = \frac{1}{N} \sum_{i=1}^{N} \Delta y_i^{(j)}$$

5. **Normalization:** The relative importance of each variable is expressed as a percentage of the total sensitivity:

   $$\text{Relative Importance}_j = \frac{S_j}{\sum_{k=1}^{d} S_k} \times 100$$

5.2.3.2 Weight-based Sensitivity Analysis

Weight-based methods analyze the internal structure of the trained Artificial Neural Network (ANN), focusing on the synaptic weights that connect the input, hidden, and output layers. By examining the magnitude and distribution of these weights, these methods estimate the relative contribution of each input variable to the model's output. This approach provides a global overview of how the network prioritizes different features during the training process. It helps identify which parameters had the strongest influence on the model's learning behavior, offering valuable insights into the internal logic captured by the ANN.

In this study, the Milne method was adopted as a weight-based sensitivity analysis technique to evaluate the relative importance of each input parameter.

Mathematical Formulation

Let:

- n: number of input variables
- h: number of hidden neurons
- w_{ji}: weight connecting input neuron i to hidden neuron j
- w_{oj}: weight connecting hidden neuron j to the output neuron

$$IIF_i = \frac{\sum_{j=1}^{h} \left(\frac{w_{ji}}{\sum_{l=1}^{h} |w_{jl}|} w_{oj} \right)}{\sum_{k=1}^{n} \left| \sum_{j=1}^{h} \left(\frac{w_{jk}}{\sum_{l=1}^{h} |w_{jl}|} w_{oj} \right) \right|} \tag{5.2}$$

Where:

- $\frac{w_{ji}}{\sum_{l=1}^{h} |w_{jl}|}$: normalizes the weight of input i to hidden neuron j, ensuring that the contributions of all inputs to a given hidden neuron are evaluated on a consistent scale.
- w_{oj}: represents the weight connecting hidden neuron j to the output, indicating the contribution of that hidden neuron to the final output.
- The numerator: quantifies the total weighted influence of input i on the output neuron through all hidden neurons.
- The denominator: aggregates the influence of all inputs to normalize the result, allowing the importance values to be expressed as relative contributions.

Algorithm Overview

1. **Initialization of Raw Influence Scores**

   Define an initial influence score vector $\text{IIF}_i^{\text{raw}} \leftarrow 0$ for all $i = 1$ to n, where n is the number of input neurons.

2. **Iterative Computation Across Hidden Neurons**

   For each hidden neuron $j = 1$ to h, where h is the total number of hidden neurons:

   - Compute the normalization factor for the weights entering hidden neuron j:

$$S_j = \sum_{l=1}^{n} |w_{jl}|$$

   - For each input neuron $i = 1$ to n:

     a. Calculate the normalized weight contribution from input i to hidden neuron j:

$$\hat{w}_{ji} = \frac{w_{ji}}{S_j}$$

     b. Compute the weighted contribution of input i to the output through hidden neuron j:

$$C_{ji} = \hat{w}_{ji} \cdot w_{oj}$$

     c. Accumulate the influence of input i across hidden neurons:

$$\text{IIF}_i^{\text{raw}} \leftarrow \text{IIF}_i^{\text{raw}} + C_{ji}$$

3. **Conversion to Absolute Influence Scores**

   The raw influence values are converted to absolute form to quantify magnitude:

$$\text{IIF}_i^{\text{abs}} = |\text{IIF}_i^{\text{raw}}| \quad \text{for all } i = 1 \text{ to } n$$

4. **Normalization to Relative Importance**

   The absolute influence scores are normalized to obtain relative percentage contributions:

$$\text{IIF}_i = \frac{\text{IIF}_i^{\text{abs}}}{\sum_{k=1}^{n} \text{IIF}_k^{\text{abs}}} \times 100$$

5. **Final Output**

   Return the resulting vector of relative influence for all inputs: $[\text{IIF}_1, \text{IIF}_2, \ldots, \text{IIF}_n]$

5.3 Implementation

5.3.1 Computational Environment

MATLAB was employed as the main computational platform for developing, training, and simulating the Artificial Neural Network (ANN) model, primarily due to its dedicated Neural Network Toolbox and optimized training functions. Although Python was also used extensively during the preprocessing and exploratory phases particularly for data cleaning, normalization, and visualization. The final model development and sensitivity analyses were conducted in MATLAB.

As a starting point, we utilized the fitnet configuration provided by MATLAB's Neural Network Fitting Tool, which is specifically designed for function approximation problems using feedforward neural networks.The default configuration of fitnet includes the following key characteristics:

Table 5.2: Default fitnet Configuration in MATLAB

Neural network model	Feedforward backpropagation Neural network
Hidden layer	Single hidden layer
Training network algorithm	Levenberg-Marquardt
Transfer function hidden layer	`tansig`
Transfer function output layer	`purelin`
No. of epochs	1000
Validation checks (iterations)	6
Performance	MSE and R2

5.3.2 Neural Network Training Procedure

To develop an effective neural network model for predicting ground surface settlement, a full-scale training phase is conducted using the entire dataset, with appropriate data partitioning to ensure robust model evaluation. In this phase, the data set is divided into three subsets: 70% for training (310 samples), 15% for validation (66 samples), and 15% for testing (66 samples). This approach enables both model learning and independent performance assessment while avoiding data leakage. In the present case, a Feedforward Backpropagation Neural Network (FF-BP-ANN) is employed, with an input layer consisting of 9 neurons corresponding to the 9 selected input features (Figure 5.4). Various hidden layer configurations are systematically tested to identify the network architecture that yields the best generalization performance. Once the optimal configuration is determined, it is evaluated on the test set to assess its predictive capability on unseen data.

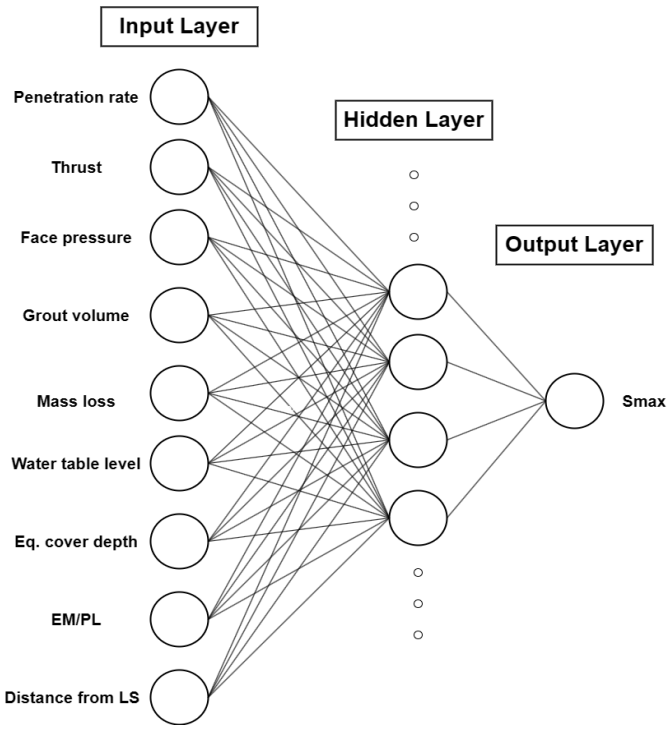

Figure 5.4: Neural Network Input Configuration

Utilizing Equation 5.1, and considering that the model includes nine input features, the estimated starting number of neurons in the hidden layer was calculated to be approximately 4,48. This theoretical value was rounded to 5, which served as the baseline for network design.

To systematically evaluate the influence of hidden layer size on the prediction performance of the neural network, the number of neurons was gradually increased from 5 to 40, in increments of 2. This design was motivated by both theoretical considerations starting from the estimate obtained using Equation 5.1 and the need to explore how increasing model complexity impacts generalization. The goal was to identify the optimal number of neurons that offers a balance between predictive power and robustness without causing overfitting or underfitting.

In total, 16 configurations with different number of neurons in one hidden layer were tested. For each configuration, the network was trained 15 times, allowing for slight variations due to random initialization and data shuffling. From these repetitions, the best performing result based on the highest validation and test R^2-was retained to represent each configuration. This repetitive training ensured that the evaluation of each architecture was not biased by outliers or unstable initial conditions, and that the peak performance for each structure was reliably captured.

The results visualized in Figure 5.5 present the regression coefficients (R^2) for training, validation, testing, and overall data across all configurations. The graph clearly shows that performance initially improves as the number of neurons increases. The optimal performance was achieved with 8 neurons, where the model attained R^2 values close to 0.94 for all three phases.

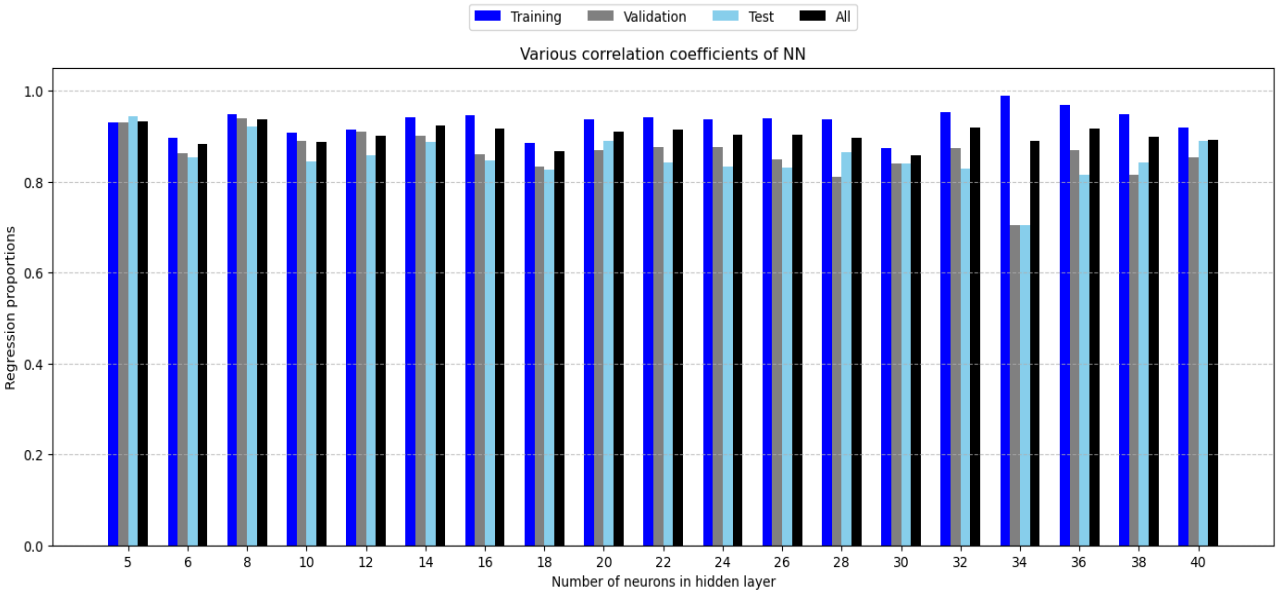

Figure 5.5: Regression Coefficients (R^2) Across Neuron Configurations

Beyond 10 neurons, although the training R^2 remained high or increased which suggests a tighter fit to the training data, the validation and test R^2 values began to decline in many configurations. This divergence reflects signs of overfitting, where the model becomes too specialized to the training data and loses its ability to generalize.

Another evaluation step in the pre-assessment of networks is illustrated in Figure 5.6, which presents the RMSE values of all generated networks on the test dataset. The 9-8-1 architecture achieved the lowest RMSE, with a value of 4.16 mm, indicating strong performance. This result supports the relevance of Equation 5.1 as a useful criterion for determining the optimal number of hidden neurons in BP-ANN models. In contrast, the 9-34-1 network exhibited the highest RMSE, reaching 9.77 mm.

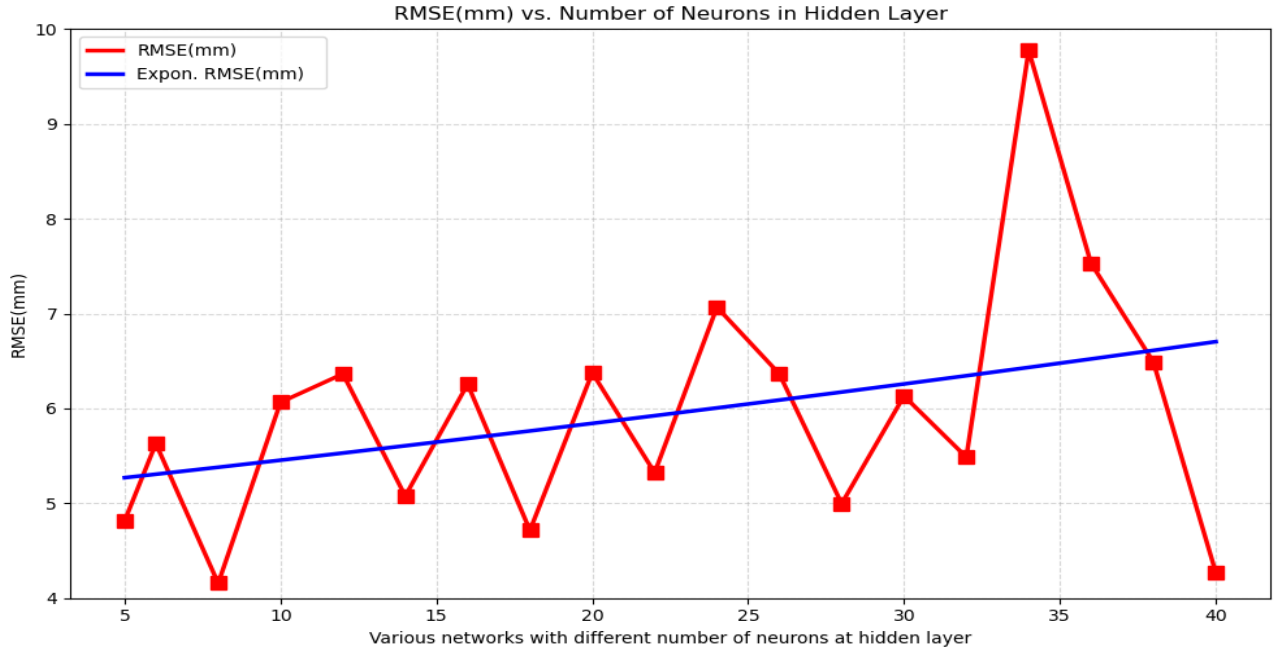

Figure 5.6: RMSE for Different NN in Hidden Layer

The curve labeled Expon (Performance(RMSE)) represents an exponential fit applied to the data in order to model the overall trend of *RMSE* evolution as the number of neurons in the hidden layer increases.

5.3.3 Prediction of Maximum Settlement Using the Most Accurate Neural Network

In this study, several neural network architectures were designed and evaluated to predict surface settlements induced by excavation using an Earth Pressure Balance Tunnel Boring Machine (EPB-TBM). After a series of tests, the NN 9-8-1 model was identified as the most effective due to its high accuracy and stability throughout the different phases of training.

The results obtained, presented in Figure 5.7 , show a very good agreement between the predicted values and the measured settlements, with correlation coefficients of R^2=0.949 for training, R^2=0.94 for validation, and R^2=0.92 for testing, all exceeding 0.90.

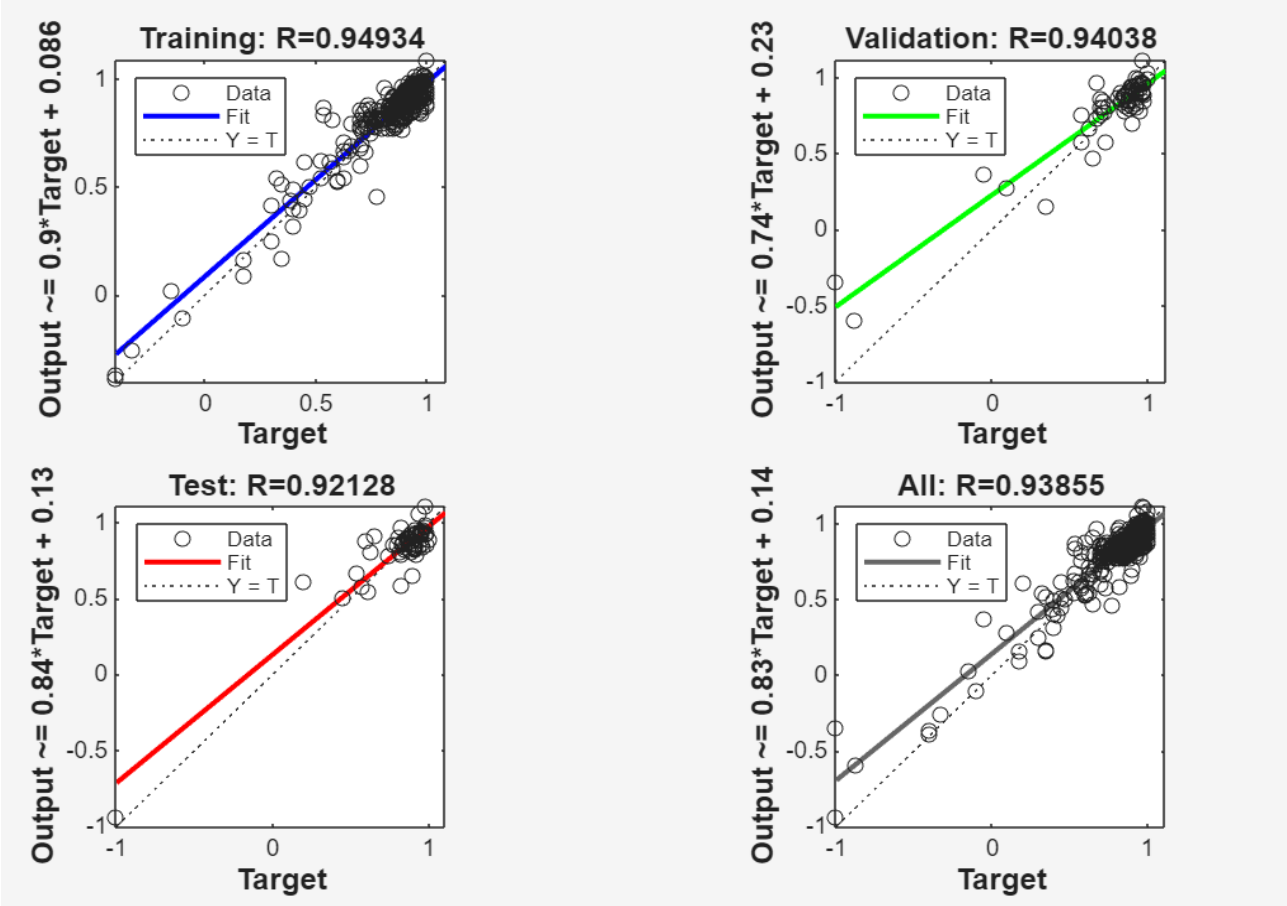

Figure 5.7: Regression Plots for Training, Validation, Testing, and Overall

Figure 5.8 presents a comparison between the normalized measured settlements (in red) and the normalized predicted settlements (in blue) for the Test Dataset. The close agreement between the two curves across most of the test sample range reflects the model's ability to accurately reproduce the overall settlement trend.

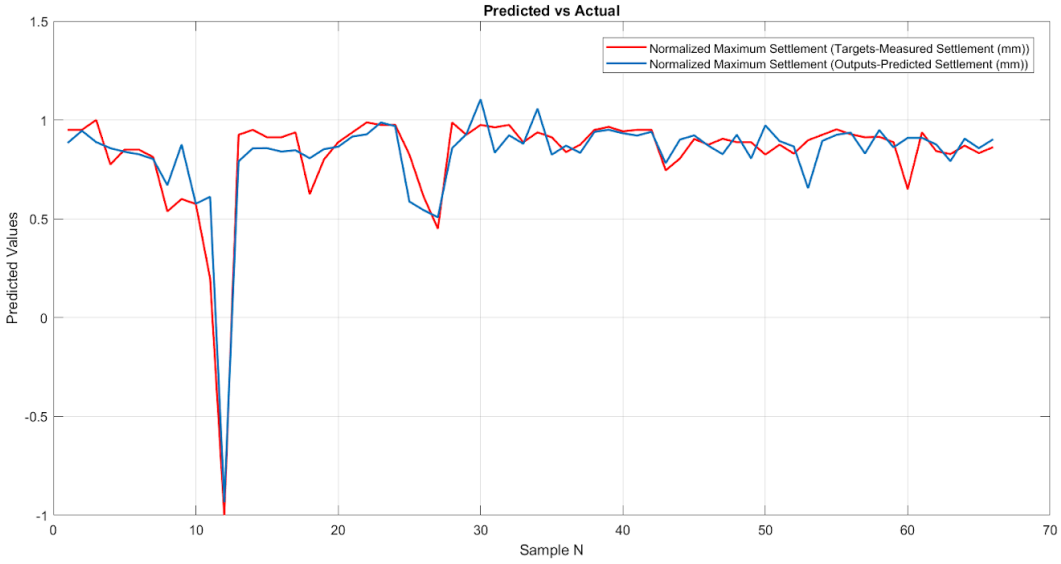

Figure 5.8: Predicted Settlement vs Actual Settlement for the Test Dataset

Figure 5.9 displays the residual error plot, which illustrates the difference between the measured and predicted settlement values across all monitoring points along the tunnel alignment. Each blue dot represents the residual error at a given location, while the red line indicates the zero-error reference. The residuals appear to be symmetrically distributed around zero.

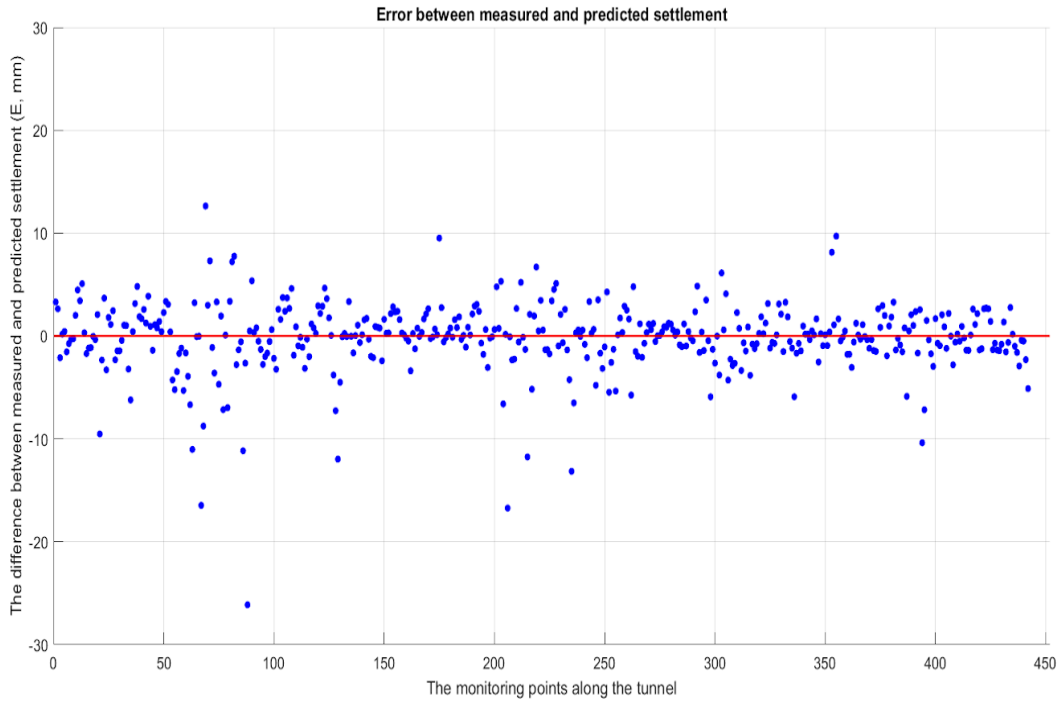

Figure 5.9: Residual Error Distribution of Predicted vs Measured Settlements Along the Tunnel Alignment

5.4 Sensitivity Analysis

After evaluating the performance of the selected neural network architecture (9-8-1) on the test dataset and confirming its high predictive accuracy and low error metrics, it is appropriate to proceed with a sensitivity analysis.

5.4.1 Perturbation Sensitivity Analysis

The figure below presents the results of the perturbation-based sensitivity analysis performed on the test dataset. Three different perturbation magnitudes 10%, 15% , and 20% were systematically applied to each input feature.The corresponding changes in the predicted maximum surface settlement were recorded to evaluate the relative sensitivity of the model to each parameter.

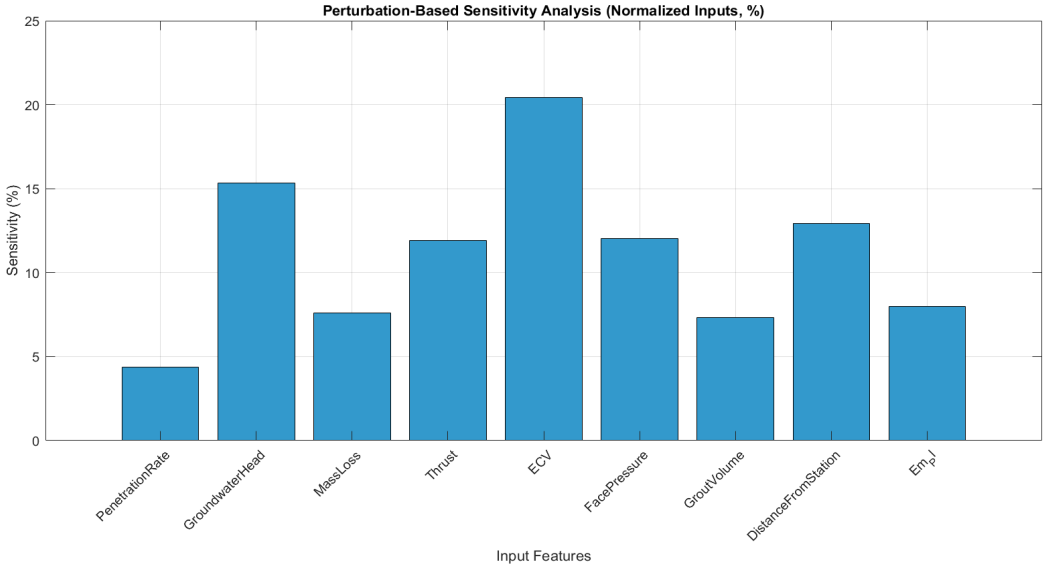

Figure 5.10: Perturbation-based sensitivity analysis with a 10% input variation.

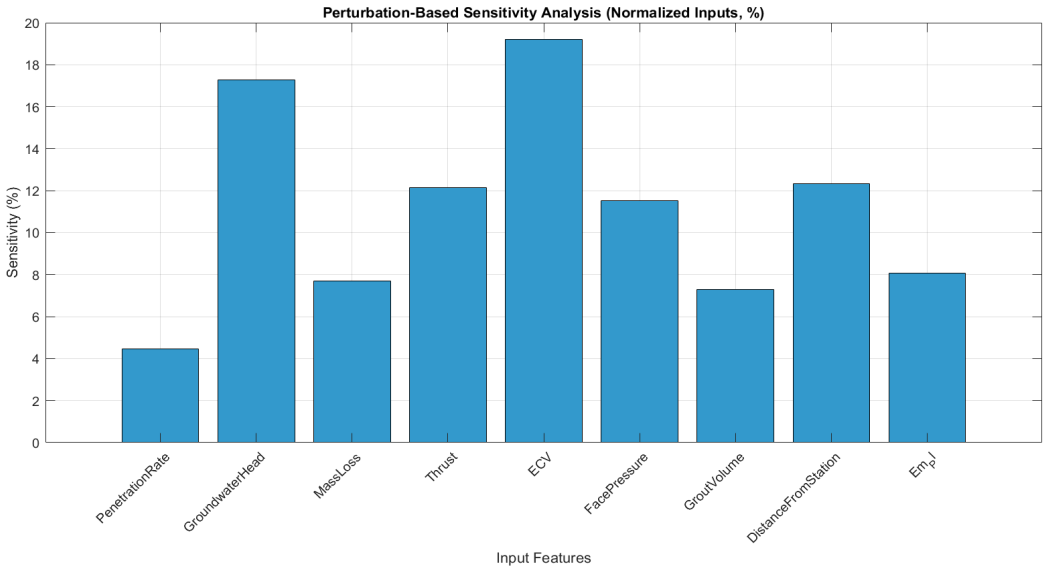

Figure 5.11: Perturbation-based sensitivity analysis with a 15% input variation.

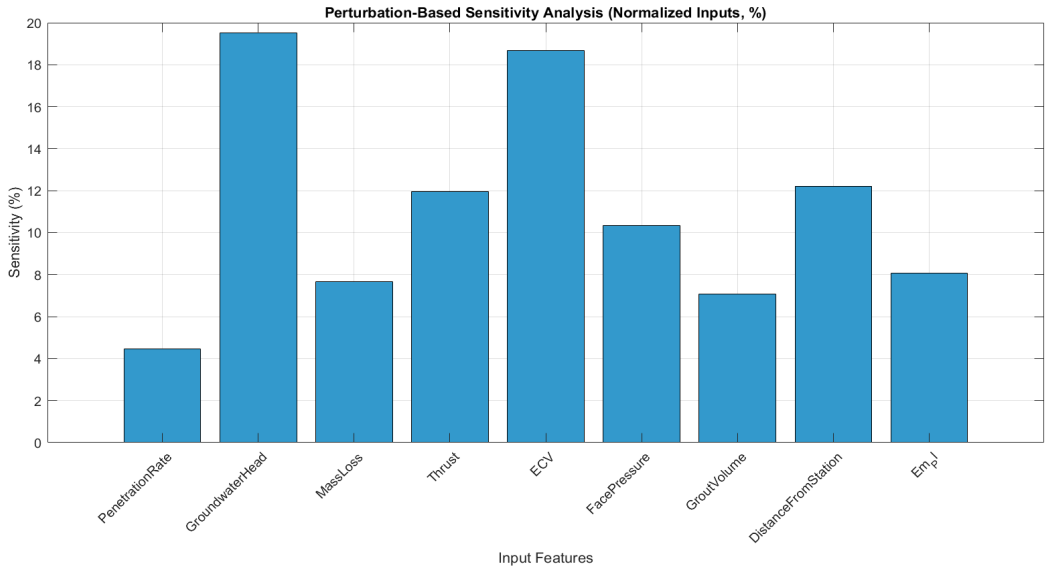

Figure 5.12: Perturbation-based sensitivity analysis with a 20% input variation.

5.4.1.1 Results Analysis

The results obtained for the three levels of perturbation show that, for the first two successive values of ±10% and ±15%, the three most influential parameters on the prediction results are, in order: Equivalent Cover Depth, Groundwater Head, and Distance from Station.

However, for the ±20% variation, a change is observed in the ranking of these three most influential parameters.This finding suggests that the model exhibits strongly nonlinear behavior or some instability when the perturbation amplitude becomes significant.

In the present case, A decision to retain the results obtained with a ±15% perturbation was made based on two main reasons:

- It reflects a realistic range of variability for geotechnical and operational parameters, ensuring the analysis remains relevant to practical engineering conditions.
- It is sufficiently pronounced to capture potential nonlinear interactions within the model, without introducing excessive distortions in the output.

5.4.2 Weight-based Sensitivity Analysis

The analysis was conducted by extracting and evaluating the synaptic weights connecting the input, hidden, and output layers, as shown in Table 5.3.

Table 5.3: Synaptic Weights Connecting the Input, Hidden, and Output Layers of the Trained ANN

	Inputs										Target
	TBM params				Geology		Geotechnical parameters	Geometry	Settlement		
	Penetration rate	Thrust	Face pressure	Grout volume	Mass loss	Ground water head	Equivalent Cover depth	EM/PL	Distance from Station		
Hidden neurons	Penrate variable weights	TH variable weights	FP variable weights	GV variable weights	ML variable weights	WTL variable weights	ECD variable weights	EM/PL variable weights	DS variable weights	Smax variable weights	
1	0.12914	-0.38366	1.16181	-0.03607	1.22441	6.54519	-4.39802	0.17999	3.78295	-3.95595	
2	0.75635	0.63084	-1.59512	-0.31161	-0.18384	-0.08581	-2.11306	-1.01983	0.98319	-2.31137	
3	-0.91774	-0.98713	2.85070	0.42518	0.04268	-0.00837	3.87149	0.86859	-1.34541	-1.74814	
4	0.04452	-0.42354	-0.48498	-0.06413	-1.07588	-6.41319	4.94460	-0.04235	-3.32660	-3.92278	
5	0.04578	0.65607	0.33131	-2.60266	-1.68915	1.36805	2.06010	-0.84492	-0.13516	0.38029	
6	-0.40639	0.66091	0.45652	-3.38484	3.08497	2.54837	0.12188	2.82609	-3.41657	0.17907	
7	-0.06273	-0.41411	-0.49601	2.06026	0.69205	-1.11673	-1.65835	-0.05515	0.73264	0.56747	
8	0.43403	0.01190	-5.14714	0.66119	0.12270	0.79422	-8.26129	1.57529	0.63891	-0.58807	

After carrying out the necessary computations to calculate the Individual Input Factor IIF_i for each input parameter using the Milne method, as defined in Equation 5.2, the resulting sensitivity values are presented in Figure 5.13.

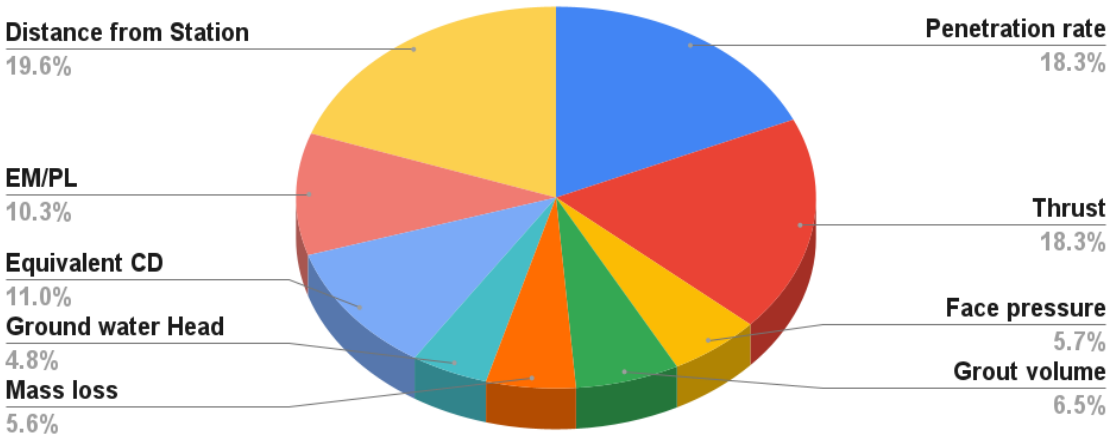

Figure 5.13: Weight-based Sensitivity Analysis result

5.5 Discussion

Following the application of both Perturbation-based and Weight-based (Milne) sensitivity analyses, several important insights emerged regarding the influence of each input parameter on the predicted ground surface settlement. Although both approaches aim to assess variable importance, they provide distinct yet complementary insights revealing both converging and differing patterns that enhance the interpretation of the ANN's internal logic and its representation of the underlying physical phenomena.

The perturbation-based analysis, which quantified the effect of ±15% variations in each input on the model's output, identified the most sensitive parameters as shown in Table 5.4 .

Table 5.4: Results of the perturbation-based sensitivity analysis

Input Parameter	**Relative Influence (%)**
Equivalent Cover Depth (ECV)	19.1
Groundwater Head (Water Table Level)	17.3
Distance from Station (DistS)	12.2
Thrust	12.2
Face Pressure	11.5
E_M/p_l	8.3
Mass Loss	7.6
Grouting Volume	7.2
Penetration Rate	4.7

These findings underscore the strong influence of geometric and hydrogeological conditions on ground surface settlement. This aligns with fundamental geomechanical principles: greater overburden increases vertical stress at tunnel vault depth, amplifying the potential for downward soil movement toward the tunnel face. If this displacement is not properly controlled, it can propagate upward and manifest as surface settlement. However, the ability of the ground to resist such deformation is strongly linked to the cover depth through the arching effect, whereby greater depth provides sufficient confinement for the soil to laterally redirect vertical stresses around the tunnel, limiting deformation above the crown and reducing surface settlement. This phenomenon is clearly illustrated in Figures 2.4 and 2.5 which shows significantly lower displacement values above the tunnel crown as the cover depth increases. Conversely, the Algiers Metro tunnel characterized by predominantly shallow equivalent cover depths (13–25 m) demonstrates insignificant arching effect, resulting in a greater vulnerability to surface settlement. As also depicted in Figure 2.4, displacement becomes notably more pronounced above the tunnel crown at a shallow cover depth of 20 m. Similarly, elevated groundwater levels reduce effective stress and may lead to soil softening, increasing susceptibility to deformation. Prior research on tunneling through water-rich or soft soils supports this, often showing a near-linear relationship between groundwater fluctuations and surface settlement magnitude [42].

In contrast, the Milne weight-based analysis, which evaluates the contribution of each input based on the magnitude of normalized weight paths within the network, highlighted a greater emphasis on parameters associated with machine operation such as thrust and penetration rate. This suggests that the network, during training, structurally relied on these variables, even if the predicted output does not strongly react to small perturbations in their values.

A particularly noteworthy outcome is the consistent prominence of Distance from Station in both analyses. This parameter likely captures a positional or temporal trend: sections closer to stations are encountered during early tunneling stages, when the TBM may not yet be fully stabilized. In these zones, machine parameters like thrust and penetration rate may exhibit more variability, increasing the likelihood of surface disturbance. The ANN appears to have learned this implicit condition, associating early-stage tunneling operations with increased settlement risk.

Thrust and Face Pressure emerged as key operational parameters influencing surface settlement, each playing a distinct but interconnected role in TBM performance. Thrust directly governs the forward advance of the machine and contributes significantly to face stability. The sensitivity analysis confirmed its strong influence, with high scores in both perturbation- and weight-based methods. Face Pressure, while showing only moderate sensitivity (5.7% structural importance), is critical in counteracting earth and water pressures at the tunnel face especially in weak soils or under high groundwater conditions.These two parameters are highly interdependent in practice. An increase in thrust, if not balanced by adequate face pressure, can destabilize the face and induce excessive ground deformation. Conversely, excessive face pressure with insufficient thrust can reduce advance efficiency or cause blowouts. The ANN likely captured this dynamic, assigning importance to both features while moderating their standalone sensitivity based on how they vary together in the dataset.

Penetration Rate further reinforces this interdependency. Although it received the second highest structural importance in the Milne weight-based analysis (18.3%), it showed the lowest perturbation sensitivity. This discrepancy suggests that Penetration Rate's influence is conditional meaning it only significantly impacts settlement when combined with specific thrust and face pressure conditions. This is supported by its statistical distribution: being approximately normal and centered around 30 mm/min, small perturbations often remain within operationally stable limits. Therefore, while Penetration Rate alone may not trigger large prediction changes,

it acts as an informative indicator of how thrust and face pressure interact, reflecting the efficiency of TBM advance and stress transmission to the ground.

The $\frac{E_M}{pl}$ ratio showed a measurable and consistent influence on predicted settlement, indicating that the ANN captured the link between soil deformability and ground response. Lower values, reflecting more compressible soils, were associated with increased settlement under TBM-induced loading.

Grouting Volume and Mass Loss exhibited low but non-negligible importance across both analyses. Although consistently ranked near the bottom, perturbation results show they can influence settlement predictions under specific conditions. Their limited but measurable effect suggests that while not primary drivers, they may contribute in context-dependent scenarios.

Conclusion

This study successfully developed an Artificial Neural Network (ANN) model to predict maximum ground surface settlement induced by EPB-TBM tunneling in the Algiers Metro project. The research integrated machine learning with geotechnical engineering, yielding a robust predictive tool while also providing interpretable insights into the key factors influencing settlement.

Key Findings

- **Optimal ANN Architecture** :

    - A feedforward backpropagation ANN (9-8-1) with 8 hidden neurons achieved the best performance, yielding R^2 values above 0.92 across all datasets and maintaining a low prediction error with an RMSE of 4.16 mm.

    - Levenberg-Marquardt optimization algorithm and tanh/purelin activation functions proved effective in modeling the nonlinear relationships between TBM operations and settlement.

- **Sensitivity Analysis Insights** :

    - Perturbation-based analysis ($\pm 15\%$ variation) revealed that Equivalent Cover Depth (ECV) and Groundwater Head were the most influential factors, followed by Distance from Station (DistS) and Thrust/Face Pressures.

    - Weight-based analysis (Milne method) highlighted Thrust and Penetration Rate as structurally significant, despite their lower perturbation sensitivity.

    - Differences between analysis methods reveal that parameters like Penetration Rate, while structurally important to the ANN, exert their influence primarily through interactions with other key variables, rather than in isolation.

- **Geotechnical and Operational Implications** :

    - Shallow Equivalent Cover Depth (ECV) and elevated groundwater levels were identified as key contributors to surface settlement. Reduced cover depth diminishes the arching effect that normally shield the ground surface, while high groundwater lowers effective stress and softens the soil, increasing susceptibility to deformation during excavation.

    - Early-stage tunneling at low Distance from Station was associated with increased settlement risk, likely due to transitional TBM behavior before reaching operational stability.

- Penetration Rate serves as an indirect indicator of TBM–ground interaction dynamics. While relatively insensitive to small input variations, it reflects the coordinated effect of thrust and face pressure, making it a valuable parameter for assessing excavation efficiency across varying ground conditions.
- Grouting Volume demonstrated low sensitivity across both analysis methods, suggesting a minor overall role in predicting settlement. However, its consistent presence points to potential influence in specific contexts particularly where proper compensation of the annular void is essential to maintain ground stability, such as in loose or low-cohesion soils. In such cases, inadequate grouting may allow void migration or relaxation, subtly contributing to deformation.
- Mass Loss also showed consistently low sensitivity across both methods, reinforcing its limited general impact on settlement prediction. Nevertheless, under certain conditions such as weak confinement or face instability it may indirectly contribute to ground deformation. These scenarios often involve over-excavation or insufficient face pressure control, where even small mass losses can lead to stress redistribution and local soil loosening.

Practical Recommendations

- **Design Phase**
  - Adequate cover depth should be prioritized during route selection and profile optimization. Where shallow cover cannot be avoided, mitigation should focus first on adjusting TBM operating parameters such as optimizing face pressure and regulating advance rate to maintain face stability, with targeted ground treatment or localized support measures reserved only for critical locations.
  - In sections with elevated groundwater levels, pre-excavation dewatering systems (e.g., deep wells, vacuum wells) should be employed to maintain ground strength.
  - Pre-excavation ground treatment such as jet grouting should be considered near stations or launching shafts to improve initial TBM face stability and minimize early-stage ground deformation.
- **Construction Phase**
  - Key TBM operational parameters particularly ones that have strong interactions with the critical soil conditions along the tunnel alignment should be closely monitored and controlled.
  - Conduct ground response monitoring (e.g., extensometers, settlement markers) above critical structures to detect surface movement early and allow for intervention.
- **Model Deployment**
  - Translate model predictions into recommended adjustments that can be presented to operators in real time.
  - Integrate real-time sensor data to refine predictions dynamically.
  - Deploy warning thresholds in the model output to alert operators of potentially unsafe trends in settlement behavior.

Constraints and Future Work

Some Constraints in data availability and quality had to be addressed during the Database construction and preprocessing:

- **Geomechanical Parameters**

  Classical soil parameters such as cohesion and friction angle were not available, as they were either untested or likely derived through empirical correlations rather than direct measurements. To maintain consistency with field-based input data, the model used the E_M/pl ratio obtained from pressuremeter tests as a proxy for soil deformability.

- **Operational Parameters**

  Several TBM operation variables were either missing or incomplete. Grouting volume was not recorded for some tunnel sections, so estimated values provided by the construction company were used instead. In Zone 1, penetration rate was not logged directly and was therefore calculated from raw-Data as the ratio of advancement distance to excavation time.

- **Settlement Assessment in Zone 1**

  The maximum surface settlements for Zone 1 were manually extracted from monitoring data provided by the surveying company VBSS, as explicit maximum values were not directly recorded. This procedure preserved data continuity for model training, though it may have introduced minor variability due to the interpretive nature of manually identifying maximum values.

- **Face Pressure Assessment**

  As mentioned in Section 4.3.1.2, face pressure (or earth pressure) was measured using 11 sensors arranged in a clockwise configuration. The three sensors located near the crown were selected for analysis due to their higher reliability, as other sensors were more prone to malfunction or data distortion caused by soil adhesion or blockage.

For future work we recommend Including direct measurements of key geotechnical parameters, such as cohesion (c) and friction angle (ϕ), to improve soil characterization.

Final Remarks

This research highlights the capability of Artificial Neural Networks to predict tunneling-induced settlement with high accuracy. When paired with robust sensitivity analyses, the dual approach combining perturbation-based and weight-based methods bridges the 'black-box' gap by revealing both the model's internal structure and its real-world responsiveness. The findings contribute actionable guidance for future urban tunneling operations, especially in soft ground contexts like the Algiers Metro. Moving forward, real-time adaptive learning and sensor integration offer promising avenues to enhance predictive accuracy and risk management in mechanized tunneling.

Bibliography

[1] D. Vizzino, G. Raimondo, and P. Felici. Algiers metro, el harrach centre / airport project, extension e. In *ITA-AITES World Tunnel Congress, WTC2022 and 48th General Assembly*, pages 1–15, 2022.

[2] Metro-Eldjazair. Station place des martyrs, 2018.

[3] Candaş Topal and Yılmaz Mahmutoğlu. Assessment of surface settlement induced by tunnel excavations for the esenler–başakşehir (istanbul, turkey) subway line. *Environmental Earth Sciences*, 80(5):188, 2021.

[4] Yang Zhao, Weiguo Gong, Yi Jiang, and Xuexue Liu. A hybrid algorithm of artificial neural network and simulated annealing for prediction of ground surface settlement caused by epb shield tunneling. *Engineering with Computers*, 35(4):1323–1336, 2019.

[5] Wikipedia. List of algiers metro stations, 2025.

[6] China Railway Construction Equipment Group (CRECG). Field machines and backup equipment, 2025.

[7] Ryan Rakhmat. Introduction to tunnel boring machine (tbm) – part 1, 2022.

[8] Master Builders Solutions. Earth pressure balance - epb technology for tunnel boring machines, 2023.

[9] Dream civil. Settlement in foundation, 2023.

[10] Ghorban Khandouzi and Mohammad Hossein Khosravi. Prediction of ground settlements induced by shield tunneling using a hybrid particle swarm optimization–support vector machine model. *Tunnelling and Underground Space Technology*, 139:105347, 2023.

[11] FERCONSULT, CENOR, DONGMYEONG, Euroestudios, SAETI, and COSIDER Travaux Publics. Hypothèses géotechniques pour le tunnel : Pk 0+000,00 – pk 9+575,00. Document technique interne L1B1-GCG-COSM28-3000-A10-40-002-A, Projet Métro d'Alger, Alger, Algérie, 2016.

[12] Vahed Ghiasi and Mehdi Koushki. Numerical and artificial neural network analyses of ground surface settlement of tunnel in saturated soil. *SN Applied Sciences*, 2(5):939, 2020.

[13] Gang Niu, Xuzhen He, Haoding Xu, and Shaoheng Dai. Tunnelling-induced ground surface settlement: A comprehensive review with particular attention to artificial intelligence technologies. *Natural Hazards Research*, 4(1):148–168, 2024.

[14] Saurabh Mhatre. What is the relation between artificial and biological neuron?, June 2020.

[15] Fabrice Emeriault Rim Boubou and Richard Kastner. Artificial neural network application for the prediction of ground surface movements induced by shield tunnelling. *NRC Research Press*, pages 1215–1233, 2010.

[16] Tarun @ DataMantra. Skewness: “unpacking the distribution shape to know the direction of outliers”, August 2024.

[17] DTREG. Cascade correlation neural network. DTREG technical documentation, 2025.

[18] Poh Soon Chang. Network trimming, 2021.

[19] bridgetomoscow. Moscow subway, 2022.

[20] Forest glen station, 2024.

[21] The New Arab. Algiers commutes back in time with metro station museum, 2018.

[22] Emilios M. Comodromos, Mello C. Papadopoulou, and Georgios K. Konstantinidis. Numerical assessment of subsidence and adjacent building movements induced by tbm-epb tunneling. *Journal of Geotechnical and Geoenvironmental Engineering*, 140(11), 2014.

[23] Ke Wu et al. Mechanical aspects of construction of new tbm tunnel under existing structures. 2021. Large-scale 3D simulations to study TBM–ground interaction mechanisms.

[24] Suchatvee Suwansawat and Harry H. Einstein. Artificial neural networks for predicting the maximum surface settlement caused by epb shield tunneling. *Tunnelling and Underground Space Technology*, 21(4):445–458, 2006.

[25] Martin Herrenknecht and Ulrich Rehm. Earth pressure balanced shield technology. Technical report, Herrenknecht AG, 2001. Technical presentation, available online.

[26] Hyobum Lee, Dae Young Kim, Dahan Shin, Jaehyun Oh, and Hangseok Choi. Effect of foam conditioning on performance of epb shield tunnelling through laboratory excavation test. *Transportation Geotechnics*, 32:100692, 2022.

[27] Karl Terzaghi. *Theoretical Soil Mechanics*. Wiley, 1943.

[28] Md Shariful Islam and Magued Iskander. Effect of geometric parameters and construction sequence on ground settlement of offset arrangement twin tunnels. *Geosciences*, 12(1):41, 2022.

[29] International Tunneling and Underground Space Association (ITA). Guidelines for mechanized tunnelling – ita working group 14. Technical report, ITA-AITES, 2019.

[30] Pietro Lunardi. *Design and Construction of Tunnels: Analysis of Controlled Deformations in Rocks and Soils (ADECO-RS)*. Springer, Berlin, Heidelberg, 2008.

[31] Kenichi Soga, Robert J. Mair, and Malcolm D. Bolton. Instrumentation for monitoring around tunnels. *Proceedings of the ICE - Geotechnical Engineering*, 149(1):17–25, 2001.

[32] Wikipedia contributors. Perceptron — wikipedia, the free encyclopedia, 2024.

[33] Yu-Lung Lai, Tsung-Han Yu, Sheng-Fu Liang, and Hong-Han Chang. A brief survey of artificial neural network models and their applications. *Proceedings of the 2016 International Conference on Machine Learning and Cybernetics (ICMLC)*, pages 173–178, 2016.

[34] Marvin Minsky and Seymour Papert. *Perceptrons*. MIT Press, 1969.

[35] Chungen Yin, Lasse Rosendahl, and Zhongyang Luo. Methods to improve prediction performance of ann models. *Energy Conversion and Management*, 44(11):1781–1799, 2003.

[36] Phil Kim. *MATLAB Deep Learning: With Machine Learning, Neural Networks and Artificial Intelligence*. Apress, Berkeley, CA, 2017.

[37] Aurélien Géron. *Hands-On Machine Learning with Scikit-Learn, Keras, and TensorFlow*. O'Reilly Media, 2nd edition, 2019.

[38] Scott E. Fahlman and Christian Lebiere. The cascade-correlation learning architecture. In *Advances in Neural Information Processing Systems (NeurIPS)*, volume 2, pages 524–532. Morgan Kaufmann, 1990.

[39] Yann LeCun, John S. Denker, and Sara A. Solla. Optimal brain damage. In *Advances in Neural Information Processing Systems (NeurIPS)*, volume 2, pages 598–605. Morgan Kaufmann, 1990.

[40] Russell Reed. Pruning algorithms—a survey. *IEEE Transactions on Neural Networks*, 4(5):740–747, 1993.

[41] K. Gnana Sheela and S. N. Deepa. Review on methods to fix number of hidden neurons in neural networks. *The Scientific World Journal*, 2013:1–11, 2013.

[42] Chungsik Yoo. Ground settlement during tunneling in groundwater drawdown environment – influencing factors. *Underground Space*, 1(1):20–29, 2016.

Appendices

A

Geology / Geotechnical – Plan and Longitudinal Profile (PK 0+000 to PK 0+700)

B

Monitoring of Tunnel Section (750.33 m) from PK 0+030.67 to PK 0+781.00

C

TBM Mining Parameter Report

D

SELI Monitoring Files

E

SUMMARY OF IN-SITU TEST RESULTS – PRESSIOMETER TESTS

F

Subset of the database